UNIVERSITÉ DU QUÉBEC EN OUTAOUAIS

PARTICLE SWARM OPTIMIZATION BASED MODELING AND ANALYSIS OF PHOTOVOLTAIC MODULE CHARACTERISTICS IN SNOWY CONDITIONS

By

Mohammad Khenar Malek Kheili

Thesis Presented to

Département d'informatique et d'ingénierie

In partial fulfillment of the requirements for the degree of doctor of philosophy Ph.D.

ABSTRACT

Photovoltaic (PV) technologies are emerging as a significant solution in energy systems around the world not only to address the climate change target, but also to reduce electricity generation costs. Substantial deployments of solar installations as renewable, not contaminating, and inexhaustible sources of energy are gaining popularity in cold geographical locations with considerable snowfall. Similar to other electrical devices, solar systems can also operate efficiently in cold climates, but the accumulation of snow and ice on the surface of PV panels can reduce their performance. The variation of atmospheric conditions caused by snow is an important factor to consider in the research and development of PV technologies in order to reach a highly efficient and highly-reliable integration of solar energy into a power grid. The latter can be achieved by an appropriate design and analysis of snow shaded PV systems based on accurate models.

The main goal of this thesis is to bring contributions for enhancing the knowledge about the use of PV systems in cold climate regions, and to present a modeling toolbox that can help PV developers and researchers to characterize the real field behaviour of PV systems under snowy conditions. In this context, the innovative contributions of this thesis are: 1) development of an optimized modeling method for characterizing the performance of PV modules under uniform snow coverage, 2) development of a novel modeling technique for PV modules subjected to the nonuniform snow coverage, 3) study of the effect of PV panels layout and snow patterns on their electrical characteristics, and 4) development of a prediction model based on real field data coming from different PV technologies to estimate the maximum power production of snow-covered PV modules.

Regarding to the first contribution, an improved procedure for the modeling of PV modules is presented based on the single-diode model and capitalizing on the Giddings-LaChapelle theory to accurately estimate the irradiation intensity received on the surface of uniform snow-covered PV modules. Moreover, the particle-swarm optimization (PSO) algorithm is employed to determine and update instantaneous values of electrical model parameters of PV modules as per variable snow conditions. Furthermore, an empirical equation of snow power losses as a function of snow depth is proposed. With respect to the second contribution, the first modeling algorithm was modified to propose a comprehensive

approach and a universal algorithm to model the PV systems covered with different snow patterns. This modeling algorithm brings contributions through a novel multi-zone contour-based approach of modeling that separates nonlinear PV characteristics of partial shaded modules into the multiple linear ones. Furthermore, the adaptation of a variant of a PSO-based algorithm is utilized in this model to instantaneously update and evaluate the output characteristics of PV modules. A power loss equation validated using data collected through real field tests is also proposed. Related to the third contribution, the effect of PV panels' layout on the performance of snow shaded PV modules is investigated through three different positions, namely horizontal, vertical and diagonal layouts. Different snow removal scenarios representing probable partial snow shading are tested on different technologies of PV modules (with or without bypass diode protection) to analyze their electrical characteristics and power losses for selecting appropriate panel layout as well as PV module technology in snowy regions. The final contribution of this research aims is the development of an improved prediction model for PV modules' energy production based on a combination of meteorological data and historical data during the cold months. The parameters such as irradiance, back-surface temperature of modules, ambient temperature, humidity, pressure, UV index, and wind speed are employed to implicitly predict the maximum output power of PV modules under different patterns of snow shading. Various prediction models based on different machine learning algorithms such as decision (regression) trees, gradient boosted trees, random forest, and artificial neural networks (ANN) are implemented and compared with the experimental results.

This research serves as a helpful reference in the development and appropriate selection of PV systems toward their application in cold weather regions.

RÉSUMÉ

La technologie photovoltaïque a connu un essor ces dernières décennies suite à la recherche des solutions énergétiques permettant de faire face aux défis majeurs tels que le changement climatique et l'économie des ressources énergétiques. Cette alternative a conduit à un intérêt grandissant de l'usage et du déploiement des panneaux solaires dans les régions du globe dotées d'un climat froid et connaissant de chutes de neige considérables. Un tel intérêt est dû au fait que l'énergie solaire s'avère non polluante et à coût moindre comparé aux énergies fossiles. À l'instar des différentes sources d'énergie électrique, les systèmes solaires sont de plus en plus utilisés dans des pays à climat froid. Les systèmes solaires peuvent fonctionner efficacement dans des régions du globe à climat froid, quoique leur rendement peut être affecté par les dépôts de neige et de glace sur leurs surfaces. De ce fait, la variation des conditions atmosphériques suite aux chutes de neige est un facteur essentiel à prendre en compte dans le domaine de recherche et développement des cellules photovoltaïques. Ce qui contribuera à la fabrication des panneaux solaires à grand rendement et d'une intégration à coût raisonnable. Ceci peut être accompli grâce à la conception et une analyse appropriée des systèmes photovoltaïques ombragés par la neige basée sur des modèles précis.

L'objectif fondamental de cette thèse est de contribuer à mettre au point des modèles permettant d'optimiser le rendement des panneaux solaires en région froide et de plus de mettre sur pied une application permettant d'assister les chercheurs et les industriels ayant un intérêt particulier relatif à ce champ de recherche prometteur afin de caractériser le comportement réel des systèmes photovoltaïques recouverts de neige. Dans ce contexte, les apports innovants de cette thèse sont : 1) le développement d'une méthode de modélisation optimisée pour caractériser la performance d'une cellule photovoltaïque (PV) sujette à un enneigement uniforme, 2) le développement d'un nouveau modèle de prédiction de la performance d'une cellule PV sujet à un enneigement non uniforme, 3) l'étude de l'effet de la disposition des panneaux photovoltaïques et d'un amas de neige recouvrant les cellules d'un panneau PV sur ses caractéristiques électriques et 4) le développement d'un modèle de prédiction portant sur des données de mesures prélevées sur différents sites utilisant des technologies PV spécifiques dans le but d'estimer la production en temps réel d'un module PV recouvert de neige.

En ce qui concerne la première contribution, une amélioration du modèle des cellules PV basée sur l'approche du modèle à diode unique portant sur la théorie de Giddings-LaChappelle a été considérée dans le but d'estimer de manière précise la densité d'irradiation reçue à la surface des modules PV uniformément recouverts de neige. De plus, l'algorithme d'essaims particulaires (EP) a été employé afin de déterminer et mettre à jour les valeurs instantanées des paramètres des modèles électriques des cellules PV en fonction des conditions d'enneigement. De même, un modèle empirique des pertes d'énergie dues à la neige en fonction de l'épaisseur de neige est proposé. Pour ce qui est du second objectif, il repose sur la modification de la première version du modèle dans le but de proposer une approche globale et un algorithme universel permettant la modélisation des systèmes photovoltaïques recouverts de différents motifs formés par les dépôts de neige. Cet algorithme correspond à une nouvelle approche de modélisation basée sur les contours multizones qui sépare les caractéristiques PV non linéaires des modules partiellement ombragés en plusieurs modules linéaires. En outre, l'adaptation d'une variante d'un algorithme basé sur l'EP a été utilisée dans ce modèle pour mettre à jour et évaluer instantanément les caractéristiques de sortie des modules PV. Une équation de perte de puissance validée à l'aide de données collectées par des tests réels sur le terrain a également été proposée. Concernant la troisième contribution, l'effet de la disposition des panneaux photovoltaïques sur les performances des modules photovoltaïques ombragés par la neige est étudié tenant compte de trois positions différentes, à savoir les dispositions horizontales, verticales et obliques. Différents scénarios de déneigement indiquant un ombrage partiel probable de la neige sont testés sur différentes technologies de modules PV (avec ou sans protection de diode de dérivation) pour analyser leurs caractéristiques électriques et leurs pertes de puissance afin de sélectionner la disposition des panneaux appropriée ainsi que la technologie des modules PV dans les régions enneigées. La contribution finale de cette recherche vise à développer un modèle de prédiction amélioré pour la production d'énergie à l'aide des modules PV basé sur une combinaison de données météorologiques et de données historiques de puissance de sortie pour un système PV susceptible d'être opérationnel pendant les mois froids. Les paramètres tels que l'irradiation solaire, la température de surface dorsale des modules, les températures ambiantes, l'humidité, la pression, l'indice UV et la vitesse du vent sont utilisés pour prédire implicitement la

puissance de sortie maximale des modules PV sous différents modèles d'ombrage de la neige. Divers modèles de prédiction portant sur des algorithmes d'apprentissage machine tels que les arbres de décision (régression), les arbres à gradient boosté, la forêt aléatoire et les réseaux de neurones artificiels (RNA) ont été mis au point et comparés aux résultats expérimentaux.

Cette recherche servira de référence utile pour le développement et le choix judicieux de critères de sélection des systèmes PV en vue de leurs applications dans des régions froides.

ACKNOWLEDGEMENT

This research project was done under the supervision of Prof. Shamsodin Taheri and co-supervision of Prof. Ana-Maria Cretu. First and foremost, I would like to express my sincere gratitude to my supervisors for the continuous support of my Ph.D study and related research, for their patience, motivation, and immense knowledge. Their guidance helped me in all the time of research as a real mentor. I could not have imagined traversing the way of this research without them.

I thank my fellow Dr. Seyed Kazem Hosseini for the stimulating discussions, for the sleepless nights we were working together before deadlines, and for all the fun we have had in the last four years. Also, it is my pleasure to express my appreciation to my friend Mr. Behzad Hashemi for his guidance, constructive suggestions, and countless hours of discussions.

My sincere thanks also go to Mr. Antoine Shaneen and Mr. Abdelkrim Chebihi, who have helped me undertake the laboratory and research facilities.

In particular, I am grateful to Dr. Hamed Taheri for enlightening me the first glance of research and for his technical guidance, encouragement and patience.

Last but not the least, I would like to thank my family: my parents and to my brother and sister for supporting me spiritually throughout my Ph.D. study and my life in general.

DEDICATION

This thesis is dedicated to *Iranian scientists who have been assassinated in the way of science.*

TABLE OF CONTENTS

LIST OF FIGURES

LIST OF TABLES

LIST OF ABBREVIATIONS

AC	Alternating Current
ABSO	Artificial bee swarm optimization
ABC	Artificial bee colony
AM	Air mass
ANN	Artificial Neural Network
ANFIS	Adaptive-neural fuzzy-inference system
AI	Artificial intelligence
BMO	Bird mating optimizer
I-V	Current-Voltage
CS	Cuckoo search
CPSO	Chaos particle swarm optimization
CNN	Convolutional neural network
DC	Direct Current
DE	Differential evolution
DT	Decision tree
DNN	Deep neural nets
GA	Genetic algorithm
GBDT	Gradient boosted tree
GASVM	Genetic algorithm-based support vector machine
GMPP	Global Maximum Power Point
GMPPT	Global Maximum Power Point Tracking
GW	Gigawatt
HS	Harmony search
LSA	lightning search algorithm
L–M	Levenberg–Marquardt
LSTM	Long short-term memory
MPP	Maximum Power Point
MPPT	Maximum Power Point Tracking
MW	Megawatt
OC	Open circuit
PS	Pattern search
PSO	Particle Swarm Optimization
PV	Photovoltaic
P-V	Power-Voltage
RMSE	Root mean square error
RF	Random forest
SA	Simulated annealing
STC	Standard Test Condition
SC	Soft computing
SC	Short circuit
SAM	System Advisor Model
SVM	Support Vector Machines
SVR	Support Vector Regression
TWh	Terawatt-hour

1 INTRODUCTION AND STATE OF THE ART

1.1 Overview

According to the recently published REN21's Renewables Global Status Report (GSR) 2019, 26% of global electricity production came from renewable energies [1]. Among the sustainable energy sources, solar photovoltaic (PV) systems are on the third place of the most important energy source after hydro- and wind power in terms of global installation capacity [2]. In recent years, applications of PV technologies have offered promising solutions not only to fulfil the climate change target, but also to reduce electricity generation costs. The maturity of solar photovoltaic technology is growing at an unprecedented rate. Solar systems are becoming financially competitive because the cost of solar electricity continues to decline [3]. The price of PV technologies has fallen to around one-hundredth per watt since 1977 [4]. In fact, a decrease in PV technologies' price, the noiseless operation, flexible scaling of installation and easy maintenance of solar systems keep it in close competition with hydro- and wind technologies. As per the International Energy Agency (IEA) report, global electricity production from PV will grow to 953 TWh by 2025, which represents more than 400% increase from 2014 [5]. The International Energy Agency (IEA) has estimated that the sun will be the world's largest source of electricity by 2050 [5].

The integration of PV systems into power grids has been also gaining popularity in climates with considerable snowfall. In 2009, nearly three-quarters of PV systems in the world were installed in countries such as Germany, Japan, Czech Republic and Canada that experience cold climate conditions [6]. For example, in Canada, the installed capacity of PV systems was around 1300 MW in 2013 with a growth of about 60% over the previous year. Moreover, estimates for the year 2020 predict an increase in the capacity of solar electricity to 6300 MW by producing nearly 1% of the total electricity generation of Canada [7].

Cold climate can improve solar panels' output since similar to most electronic devices, solar cells work efficiently in cold conditions. In addition, the white snow on the

ground reflects the sun's light and helps improve the PV performance. However, snow accumulating on PV panels can reduce their energy production capability during cold months. In other words, the amount of irradiance that penetrates the snow layer and reaches the PV module can be decreased, resulting in low or zero electricity generation. This phenomenon which is known as snow shading can result in an inability of PV technology to meet the power network requirements.

There are two important patterns of snow shading, i.e., uniform and nonuniform snow shading. The uniform snow shading happens when the whole surface of the PV panel is covered by a uniform snow layer. A nonuniform snow pattern creates partial shading conditions, in which some parts of the snow cover melt or slide down. Although there are other sources of shading such as passing clouds, soiling, and shadowing, snow shading is one of the most probable shading reasons that can hinder the reception of irradiance to the surface of PV panels in the regions with a considerable amount of precipitation. Hence, analysis of the solar systems performance under cold weather conditions plays a key role in clarifying their uncertainty and variability in electricity generation caused by this climatic phenomenon. To address this issue, an accurate model of a PV module capable of determining its instantaneous electrical characteristic taking into account the snow effect is necessary. Moreover, this online modeling method that is capable to resemble the PV generators' performance under the variation of environmental conditions can be interfaced with the PV converters and improves their maximum power point tracking (MPPT) controllers.

1.2 Targets of Thesis

In this context, this thesis aims, in an initial step, to propose a novel methodology of PV modeling to represent the instantaneous electrical characteristics of PV modules covered with uniform snow coverage. The attenuation of the transmitted solar radiation penetrating a layer of snow is rigorously estimated through an accurate theory describing the uniform snow coverage impact on the solar panels. In the next step, the effect of partial shading conditions due to nonuniform snow deposit on the PV panel is investigated through a comprehensive model. To this end, a novel universal multi-zone approach of photovoltaic

modeling is proposed to determine the electrical characteristics of PV modules covered with nonuniform snow patterns under partial shading conditions. In addition, the validity of the proposed model is investigated using real data obtained from the SCADA system of a 12-MW grid-connected PV farm. Finally, the effect of the PV panel layout on its electrical behavior under different snow deposit patterns is studied. This analysis is helpful for a proper installation of PV panels in cold climates, allowing to minimize power loss due to snow. In a broader perspective, the research work in this thesis can help interpret the performance of PV systems under snowy conditions and can be considered as a powerful tool for the design and selection of PV modules subjected to snow accretion.

1.3 State of the Art and Problem Formulation

PV systems have inherent intermittent characteristics which are negatively affected by weather conditions. Therefore, the integration of PV systems into the power grids brings challenges which impose undesirable impacts on the power grid operation. In cold climate regions, two important factors, i.e. ice and snow, increase considerably the uncertainty and variability of PV generation. Since PV systems are frequently installed in regions that experience unpredictable snow and icing conditions, attention to their electrical behavior becomes essentially important.

1.3.1 Impact of Snow on Solar Panels

Snow deposition is the most obvious manner by which the confluence of cold temperatures and moisture can obstruct the face of a PV array. Snow particles often bounce when they impact the glass face of a photovoltaic panel. The wind field plays a remarkable role in determining the relative velocity of a snow particle impacting the array, both on the first impact and on subsequent bounces [8]. After bouncing, a snow particle follows a trajectory determined by gravity, the wind field at the surface of the array, and the momentum of the particle immediately after its collision with the surface. The panel tilt angle is also significant in determining the tendency of a particle to stay at rest on the panel surface. For panel tilt angles less than 90º, the snow particle will probably return to the array surface, where there is an opportunity to bounce again. Snow particles withstand under the influence of different forces on the surface of the PV panel such as: wind (or air

resistance) force, normal and tangential component of the gravity force which are dependent on the weight, velocity and temperature of particles, panel tilt angle, surface irregularities and the friction force. Eventually, when the magnitude of the friction force exceeds the net force of the tangential components of the wind force and the gravity force, particles might decelerate and tend to come to rest [9].

The surface of PV panels can affect the ability of electricity production of a photovoltaic system during the cold months. Most obviously, the array will often be at a temperature different from the ambient air temperature. It is conceivable that the array will be above freezing when the ambient air temperature is well below freezing. The temperature of the array is influenced by radiation gains and losses to/from the environment and wind (convective cooling) [8].

Albedo which is defined as the ratio of the intensities of reflected radiation to incident radiation is calculated using radiation intensities averaged over the short-wave radiation spectrum. This important optical property of snow can be characterized as a reflective characteristic of light from snow accumulation on the surface and the surrounding snow-covered ground of PV panels. Tilted PV modules especially, in PV farms can typically collect more reflected radiation due to a larger view factor between the rear of the module and the snow-covered ground and array [6, 10].

The effect of installation parameters (e.g., tilt angle, height above ground, and albedo) on the bifacial gain and energy yield of three south-facing PV system configurations have been investigated using a set of measured data from Sandia National Laboratories, a bifacial PV test-bed [11]. The results of this experiment demonstrate that modules installed at the highest possible albedo with high enough height have higher production. Besides, the seasonal optimum tilt angles are usually higher for modules installed closer to the ground. The experimental report based on the full-year field study of two flat roofs PV sites located in Sweden with a low albedo of 0.05 is investigated for monofacial and bifacial modules with a 40° tilt facing south mounted in different orientation [12]. The Nordic conditions of this location show a higher albedo could be achieved on a sunny day with fresh snow for the bifacial modules.

1.3.2 Analysis and Accurate Modeling of Photovoltaic Module Under Uniform Snow Coverage

Over the years, several researchers have studied the effect of snow and ice on energy losses of PV systems. Investigations from the Natural Bridges National Monument, resulted in a daily loss prediction from 5% to 45% of system yield for two module angles of 30° and 40° depending on snow depth [13]. A study of PV losses due to snow shedding, performed in the Energy Diversification Research Laboratory, CANMET, analysed the effect of temperature and melting technology in reduction of some energy losses [14]. Marion et al. concluded that snowfall could be a serious threat to the failure of grid-connected photovoltaic systems in Arizona, U.S. which can affect the overall system losses [15]. A six year-data acquisition of a 28-degree roof mount PV system in Germany showed that the values of proportional annual yield reduction by snowfall losses range from 0.3 to 2.7% [16]. The authors of [17, 18] introduced a generalized monthly snow loss model taking into account the effect of insolation, humidity, temperature, ground interference, and tilt angle for two PV sites in Truckee, CA, U.S. Average annual losses of 6% - 26% for different tilt angles of 35°-0° were obtained. Other reported measurements have also indicated that a PV system can have annual snow losses as high as 12% for a series of six PV systems in Colorado [19], 3.5% for a PV system of 70 PV modules in Ontario [6], and 5-12% for seven PV modules in four tilt angles assessed in Calumet, MI, USA [20]. The model presented in [21] combined snow depth measurements with commonly available meteorological data of a 15-year continuous weather history in calculating PV outputs with and without snow to estimate the contribution of snow cover to PV power loss. In [22], a methodology that incorporates the Bouguer-Lambert Law [23] is proposed to estimate the transmitted level of insolation in deep layers of snow. However, it suffers from lack of accuracy to evaluate the diminished radiation intensity in light and medium snow coverage. Moreover, the parameters of the model for a particular environmental condition cannot be extracted simultaneously. The nonuniform distribution of solar irradiance on the backside of the bifacial PV modules was studied in [24]. A single diode-based model of the solar cell was used to characterize its current-voltage (I-V) curve and to calculate the micromismatch losses of the PV system as well [24]. These losses of the system were analyzed for surrounding ground of PV modules including grassland, cement floor, snowfield, with and

without a crossbeam. The snowfield demonstrates the highest micromismatch losses within 1%-3%. Table 1 summarizes the snow related research works on PV systems in recent years with their dataset, technology, method and application as follows:

Table 1. Snow related research works on PV systems in the literature.

Research	Dataset	PV technology and sites	Method	Application
[13] (B. L. Brench. 1979)	One winter season	Standard cell	Comparative	Daily snow loss
[14] (M. M. D. Ross. 1995)	30 Winter seasons	Polycrystalline silicon cells	Comparative	Overall snow losses
[15] (B. Marion et al.2005)	30 Winter seasons	18 Different grid-connected PV sites	Comparative	Overall snow losses
[16] (G. Becker, et al.2006)	Six winter seasons	Monocrystalline silicon	Correlation base	Overall snow losses
[17] (L. Powers, et al. 2010)	Two winter seasons	Two different sites	Analytical correlation base	Annual snow losses
[18] (T. Townsend and L. Powers. 2011)	Two winter seasons	Two different sites	Analytical correlation base	Annual snow losses
[19] (B. Marion, et al. 2013)	Two winter seasons	Polycrystalline and mono crystal silicon	Analytical Comparative	Annual snow losses
[6] (R. W. Andrews, et al. 2013)	Two winter seasons	Crystalline and Amorphous silicon	Correlation base	Annual snow losses
[20] (N. Heidari, et al . 2015)	One winter season	Polycrystalline silicon	Analytical Experimental	Annual snow losses
[21] (S. Pisklak. 2016)	10 – 15 Winter seasons	Three different sites	Comparative	Monthly and annual snow losses
[22] (S. Hosseini, et al. 2018)	One winter seasons	Thin film , monocrystalline and polycrystalline silicon	Numerical iteration	Circuit-based modeling and module snow losses
[24] (L. Wang, F. Li, et al.2019)	One winter season	Bifacial monocrystalline CZ silicon.	Analytical comparative	Micromismatch losses

In most of the previous work reported in the literature, energy losses due to snow have been addressed and calculated through a simple comparison between the expected energy and the measured output power of PV systems based on offline models. However, research has not yet adequately addressed the challenges associated with the penetration of solar radiation through snow pack to the surface of PV modules. Thus, such models exhibit serious deficiencies for describing the various physical processes that have an impact on the conversion of photo energy into electricity. Consequently, they cannot be employed to characterize accurately the PV modules covered with snow. To cope with these shortcomings, an electric model of a PV module in cold conditions could be a powerful tool not only for analyzing PV plant performance, but also for optimizing the power converter design and for studying the MPPT algorithms.

Furthermore, in order to obtain a good approximation of the measured data acquired from a true solar cell, a feasible optimization computational method should be employed to estimate the parameters of solar cell models [25]. Recently, various approaches have been presented for the extraction of the accurate parameters of solar cells models such as R_s and R_{sh} represent the series and shunt resistances respectively, I_{ph} defines the photo-generated current by the incidence of light, I_s is the diode's reverse saturation current, α_0 is the diode ideality factor. The results on the well-known solar cell diode-based model prove that most of the soft computing algorithms [26-29] have achieved better results than those achieved by analytical approaches [30, 31] or numerical methods [32, 33] due to their global search capability which can find the optimal solution for problems with multiple unknown parameters, especially for the models with nonlinear transcendental function. A transcendental function is an analytic function that does not satisfy a polynomial equation, in contrast to an algebraic function. Examples of transcendental functions include the exponential function, the logarithm, and the trigonometric functions.

In fact, the soft computing algorithms such as genetic algorithm (GA) [34, 35], particle swarm optimization (PSO) [36, 37], simulated annealing (SA) [27, 38], pattern search (PS) [39], cuckoo search (CS) [40], artificial bee swarm optimization (ABSO) [26], harmony search (HS) [25], differential evolution (DE) [31, 41, 42], artificial bee colony(ABC) [28], bird mating optimizer (BMO) [29, 43] and lightning search algorithm (LSA) [44] have been used for the extraction of parameters of solar cells in the literature.

Among the aforementioned soft computing algorithms, PSO has drawn the attention of many authors because of its specific features, namely the fact that the method can find with high probability the global optimal solution by tuning only a few parameters, it is easy to program by guiding particles to search the hyperspace without the need of transformation to binary encoding and of special genetic operators such as mutation and cross over, and has no limit of defining optimization objectives [45, 46]. Numerous authors developed and improved various versions of the PSO algorithm, each with its different advantages for different complex optimal problems of PV system parameter extraction [37, 47-50]. In [49], a PSO-based parameter extraction routine combined with an analytical algorithm is proposed to overcome the problem of encountering locally optimal solutions, in the three-diode lumped model. A PSO algorithm with time variation inertia weight and acceleration coefficient is developed in [48] for extracting solar cell parameters using a single diode model. The optimal parameters of silicon solar cell have been extracted and the results are compared with those of artificial bees swarm optimization (ABSO) [26], simulated annealing (SA) [38] and chaos particle swarm optimization (CPSO) [37]. The PSO algorithm is also attractive for the authors in the field of MPPT control, especially in finding the global maximum power point (GMPP) for the partially shaded PV modules [51-54]. Table 2 classifies the state-of the-art methods employed to extract the modeling parameters of PV modules in the recent years. It presents a comparison of methods in terms of circuit model, algorithm, PV technology, and accuracy. The accuracy of proposed methods in Table 2 is evaluated through different types of errors such as root mean square error (RMSE), sum square error (SSE), mean absolute error (MAE), normalized error, relative error, and graphical comparison. These errors are presented in [55] and the RMSE, as the selected error measure for the context of this work, is defined in detail in section 2.2.2.4. Although these modified variations of PSO improve the performance of the algorithm for finding the optimal model parameters, according to the best of our knowledge, the characteristics of snow-covered PV solar systems have not been modelled using PSO. Hence the work in this thesis is focused on the PSO- based modeling of PV modules under snowy conditions.

Table 2. Comparison of PV parameters extraction methods proposed in the literature.

Research work	Circuit model	PV technology	Algorithm	Accuracy
[33] (M. Chegaar, et al. 2001)	Single diode model	Polycrystalline and RTC France silicon	Optimized newton-based	Graphical comparison only
[34] (J. A. Jervase, et al. 2001)	Two-diode model	Silicon solar cell	Genetic algorithm (GA)	Relative error : varied from 2 to 36%
[36] (M. Ye, et al. 2009)	Both single and double diodes model	Silicon solar cell	Particle swarm optimization (PSO)	RMSE = 0.00014
[35] (M. Zagrouba, et al. 2010)	Single diode model	50 W PV module of ANIT-Italy	Numerical GA-based	SSE : varied from 0.0002 to 0.06
[37] (H. Wei, et al. 2011)	Single diode model	Silicon solar cell	Chaos particle swarm optimization (CPSO)	RMSE : varied from 0.265 to 0.6244
[41] (K. Ishaque, et al. 2011)	Single diode model	Multi-crystalline, mono-crystalline and thin-film	Differential evolution (DE)	Graphical comparison only
[25] (A. Askarzadeh, et al. 2012)	Both single and double diodes model	(R.T.C. France) silicon solar cell	Harmony search (HS)	RMSE = 0.00098
[31] (K. Ishaque, et al. 2012)	Two-diode model	Multi-crystalline, mono-crystalline and thin-film	Penalty based DE	Graphical comparison only
[38] (K. M. El-Naggar, et al. 2012)	Both single and double diodes model	Polycrystalline silicon	Simulated annealing (SA)	RMSE: varied from 0.0017 to 0.0027
[39] (M. AlHajri, et al. 2012)	Both single and double diodes model	Polycrystalline silicon	Pattern search (PS)	RMSE: varied from 0.0118 to 0.2863
[26] (A. Askarzadeh, et al. 2013)	Both single and double diodes model	RTC France silicon cell	Artificial bee swarm optimization (ABSO)	RMSE= 0.000983
[40] (J. Ma, et al. 2013)	Single diode model	Crystalline and amorphous silicon	Cuckoo search (CS)	RMSE = 0.0010

[48] (N. F. A. Hamid, et al. 2013)	Single diode model	RTC France silicon cell	PSO	RMSE= 0.000986
[30] (S.-x. Lun, et al. 2013)	Single diode model	Monocrystalline and polycrystalline silicon	Taylor's series	RMSE : varied from 0.0116 to 0.0065
[42] (W. Gong, et al. 2013)	Both single and double diodes model	Polycrystalline and RTC France silicon	Repaired adaptive DE	RMSE : Varied from 0.000986 to 0.002
[28] (D. Oliva, et al. 2014)	Both single and double diodes model	RTC France silicon	Artificial bee colony (ABC)	RMSE= 0.000986
[27] (F. Dkhichi, et al. 2014)	Single diode model	RTC France silicon	Levenberg–Marquardt (L-M)	RMSE= 0.000986
[32] (T. Ma, et al. 2014)	Single diode model	Crystalline silicon	analytical	Relative error = 0.5%
[29] (A. Askarzadeh, et al. 2015)	Single diode model	Amorphous silicon	Bird mating optimizer (BMO)	RMSE : varied from 0.0021 to 0.0071
[44] (R. Sirjani, et al. 2016)	Both single and double diodes model	Monocrystalline silicon	Lightning search algorithm (LSA)	SSE : varied from 0.00458 to 0.22640
[50] (A. Harrag, et al. 2017)	Both single and double diodes model	Not mentioned	PSO	Graphical comparison only -
[49] (T. Wei, et al. 2019)	Three-diode model	Organic solar cell (OSC)	PSO	Graphical comparison only -

1.3.3 Modeling of Photovoltaic Modules Covered with Nonuniform Snow Patterns

When some parts of snow on the surface of PV systems are melt or slide down, a nonuniform snow pattern can be created leading to a partial shading condition, in which the shaded sections of modules receive low or zero irradiation. Partial shading is also happening in lower scale levels and is known as a mismatch condition where, PV cells within the same installation receive different irradiance levels [56]. Although there are other mismatch conditions that can lead to an uneven irradiance such as soiling, shadowing, and cell damages, snow partial shading is the most remarkable factor of mismatching which can extremely decrease the efficiency of PV modules [57].

For the efficient utilization of the solar system in both commercial and research applications, the nonlinear electric behavior of PV modules should be properly characterized. This nonlinear behavior gets more complicated under partial shading conditions [58, 59]. Under this mismatch condition, with respect to the electrical properties and structure of PV modules, as well as the shading pattern and its intensity, the PV system characteristics deviate from their standard form bearing multiple peaks. Thus, the reliable modeling of the complex characteristics of PV systems due to nonuniform snow is a challenging issue that needs to be addressed.

Several research works have been conducted in the field of PV system modeling to address partial shading phenomena. The most popular PV models under snow-free conditions which utilize the concept of electrical equivalent circuit are commonly based on the single-diode model [60, 61] or on the two-diode model [62-64] which could include additional series and shunt resistances. Then, computational techniques are used for the modeling approach that can be classified into three main categories: analytical, numerical, and soft computing (SC) methods. In analytical methods, the mathematical formulation of the basic PV model is conducted by deriving the explicit equations, usually based on the three important operating points, namely maximum power point (MPP), short circuit (SC) and open circuit (OC) points, to completely avoid the iterative procedure for extracting the model parameters [65-68]. In numerical methods, the equations of the circuit-based model have been employed and directly implemented in suitable computational tools, such as MATLAB, to be solved numerically [69-72]. To this purpose, iterative solving procedures are mostly executed by the Newton-like methods [73]. SC techniques such as the Artificial Neural Network (ANN) can predict the PV characteristics based on trained data [74, 75]. This technique is considered by some authors as more suitable for theoretical investigation rather than practical implementation [76]. A comparison of research works on the modeling of PV systems under partial shading condition is listed in Table 3.

Table 3. Research works on the modeling of PV systems under partial shading condition.

Research	Method	Circuit Model	PV technology	Application	Accuracy
[77] (V. Quaschning, et al. 1996)	Newton-Raphson(numerical)	Double diodes	Monocrystalline silicon	Characterizing the I-V curve	Graphical comparison only
[71] (H. Kawamura et al.. 2003)	Newton–Raphson	Single diode	Not mentioned	Characterizing the I-V curve	Graphical comparison only
[70] (Y.-H. Ji, et al. 2009)	Numerical	Single diode	Simulink block of PV KPEMS150A72	MPPT	Graphical comparison only
[67] (Y.-J. Wang, et al. 2010)	Analytical	Single diode	Multicrystalline silicon	Effect of partial shading on PV characteristics	Graphical comparison only
[63] (K. Ishaque, et al. 2011)	Numerical-Analytical	Double diodes	Multicrystalline, monocrystalline, and thin-film	MPPT	Relative error : less than 10 %
[64] (K. Ishaque, et al. 2011)	Newton-Raphson	Double diodes	Multicrystalline, monocrystalline, and thin-film	MPPT	Relative error : less than 8 %
[78] (S. Moballegh, et al. 2013)	Analytical	Single diode	Crystalline silicon wafer surrounded by ultra-thin amorphous silicon	MPPT	Relative error : varied from 5-10%
[66] (M. Seyedmahmoudian, et al. 2013)	Analytical	Single diode	Multicrystalline silicon	Characterizing the P-V and I-V curves for MPPT	Graphical comparison only
[72] (Y. Mahmoud, et al. 2014)	Numerical	Single diode	Polycrystalline, monocrystalline, and thin-film	Characterizing the P-V and I-V	RMSE: varied from 0.55 to 1.92
[75] (H. Mekki, et al. 2016)	Artificial neural network (ANN)	Free	Multicrystalline silicon	Characterizing voltage and current based on time interval for Fault detection	mean absolute error (MAE) = 0.001
[61] (B. Meyers, et al. 2017)	Analytical	Both single and two diodes	Simulated module with 96 cells	Characterizing the P-V and I-V curves for MPP variation	Normalized error = 0.1

[56] (H. S. Moreira et al. 2018)	Analytical	Single diode	Monocrystalline Silicon	Characterizing the P-V and I-V curves for MPPT	RMSE: varied from 0.03 to 0.20
[73] (A. G. Peter, et al. 2019)	Numerical	Double diodes	Multicrystalline, monocrystalline, and thin-film	Characterizing the P-V and I-V curves	Relative error of model parameters: less than 0.1 %
[68] (P. Bharadwaj et al . 2019)	Analytical	Single diode	Polycrystalline silicon	Characterizing the I-V curve	Relative error = 5%

For the practical investigation of snow-covered PV modules, the physical and optical properties of snow need to be considered. Due to a higher albedo level of the snow-covered ground than that of snow-free surfaces, a portion of the reflected sunlight from surrounding areas could be absorbed by PV modules in snowy conditions. Furthermore, snow transfers heat in a more complex way than either other solids or fluids, and the insulating properties of snow/ice covering a PV module would influence the convective heat loss. Therefore, the existing models exhibit serious deficiencies to describe the various physical processes that influence the conversion of photo energy into electricity, and thus, cannot be used to characterize the PV modules covered with non-uniform snow.

Recently, two modeling approaches of PV modules covered with snow have been published to study the effect of snow on the PV characteristics. In [22], a snow modeling method based on the Newton-Raphson technique has been proposed. In our recent published paper [79], a metaheuristic computational method based on the particle swarm optimization (PSO) technique has been also proposed for the snow-covered PV systems and it has been tested by three different types of commercial PV panels. Comparing the results of the paper shows a close compatibility between the characteristics of the proposed model and the practical test bed [79]. Although these papers modeled the effect of snow on the PV systems, the PV performance has not been examined and modeled under nonuniform snow patterns. Therefore, this motivated us to introduce and propose a comprehensive approach and a universal algorithm to model the PV systems covered with different snow patterns.

1.3.4 Analysis of PV Panels Layout and Prediction of Different PV Technology Performance by Using the Raw Data of Installation Field

As shown in Figure 1, photovoltaic cells use light energy (photons) from the sun to generate electricity using PV technology. Most of the module technologies use wafer-based crystalline silicon cells or thin film cells. A PV module is an assembly of PV cells. To supply the electrical equipment by the direct current electricity generated by the PV systems, a collection of PV modules that is called a PV panel should be arranged to construct PV arrays. The PV panels in the configuration of arrays can be arranged in difference ways such as vertical, horizontal and diagonal, as illustrated in Figure 2. These templates of panel arrangements (i.e. the panel layout) can be selected according to the application of the PV system and the availability of the installation space.

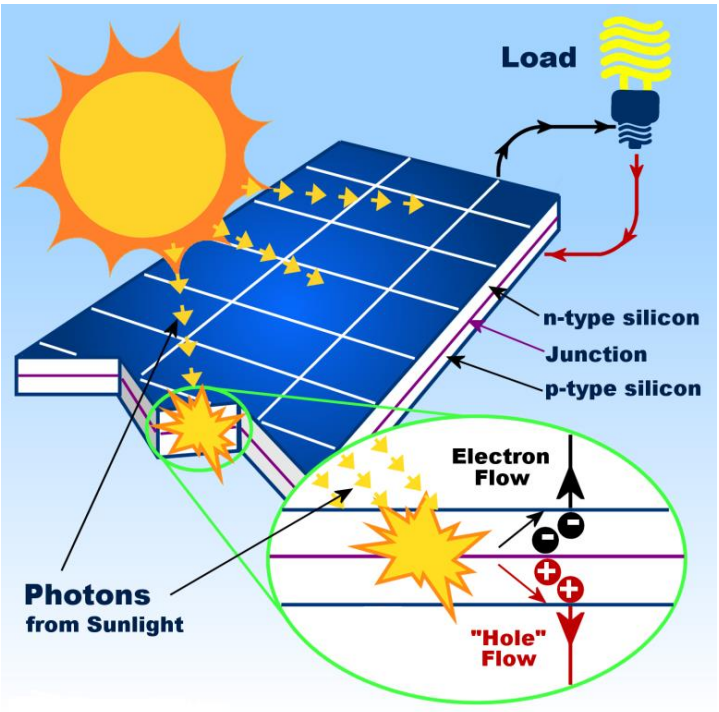

Figure 1. How photovoltaic cells generate electricity form sun light energy [80].

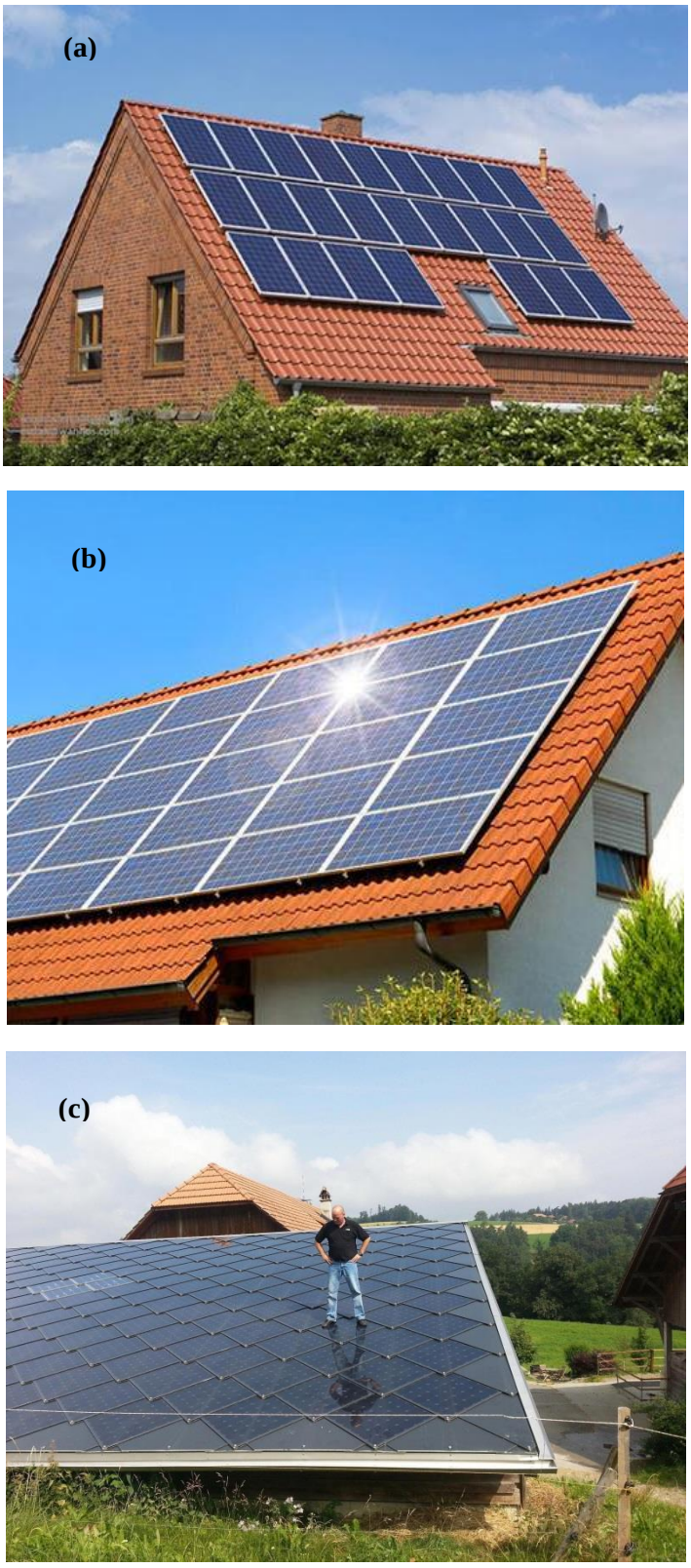

Figure 2. Different ways of PV panels arrangement such as (a) vertical, (b) horizontal and (c) diagonal [81].

Generally, different layouts of PV panels demonstrate the same behavior when they are not shaded. It means that under the uniform sunlight exposure, different arrangements of solar panels perform equally [82]. However, for an economical aspect, the determination of an optimal number of modules required to be installed in a restricted space to respond the energy demand can represent a challenge. For example, for the rooftops arrangement, vertical layout of the panels is the most efficient configuration in terms of production level [83]. Standard rooftop racking systems are optimally designed for the vertical layout. Thus, an installation of the same number of PV panels in the horizontal and diagonal configuration requires more rows, thus increasing the associated cost. To this end, most PV developers select the vertical layout that requires less hardware and simpler wiring, resulting in less complicated and faster implementation in comparison with horizontal and diagonal layouts [84].

The efficiency and maintenance of the PV layout are important factors in designing the solar systems used in a variety of solar applications subjected to snow. In addition, the proper layout of panels plays a key role in generating the electricity in cold regions. In fact, the performance of snow partial shaded PV modules could be affected by the PV panels layout arrangement. In [85], a research based on numerical analysis was conducted on the snow power loss of PV systems for horizontal and vertical panels layouts. However, it was not experimentally validated for different PV layouts as well as snow patterns on their surface. Therefore, the investigation of solar system performance with different PV layouts under the nonuniform snow accretion is significantly important. Hence, an attempt was made in this thesis to carry out a comprehensive research to determine the effect of different PV panels layout and snow patterns on their electrical characteristics.

1.3.5 Prediction Model of Different PV Technology Power Generation by Using the Raw Data of Installation Field

Although the growing market, reliability, and technology advancement of solar systems have been improved over recent years, there are still significant questions regarding the actual performance of PV modules in the field under different environmental conditions that can be realized in day-to-day operations. In addition, the snow and its effect on solar panels are very unpredictable, both from time to time and from site to site.

Normally, with the manufacturer's information and a quality control test, the long-term performance of PV modules, can be estimated in a standard condition, while its interaction with a diverse set of environmental parameters cannot be simply accounted. Therefore, by processing the meteorological data and the historical output power data of the PV system under study, a learning-based algorithm for training a model can be executed to predict the power generation of a real solar installation.

The prediction of power generation through the combination of meteorological and historical generation data of solar energy is gaining considerable attention. In the literature, several forecasting strategies and different scientific investigations have been introduced to estimate the future trends of PV energy production. Firstly, the traditional statistical models were introduced which worked based on the classical time series forecasting of solar energy and weather conditions such as Autoregressive models, Moving Average, and Autoregressive Moving Average [86]. They were often applied to the models with the linear dynamic structures. Next, the Fourier series models [87] based on the physical model were proposed which were less effective for the complex nonlinear systems subjected to the irradiance fluctuation [88]. Finally, the advanced nonlinear models such as Artificial Neural Network (ANN) [89], Support Vector Machines (SVM) [90, 91] and hybrid models [92] promptly attract many attentions in the field of power production forecasting.

In general, the neural networks indicate a universal approximation ability between the variety of artificial intelligence techniques [93]. In neural-based methods, sophisticated circuit modeling and their electrical parameters are avoided and thus, the knowledge about the specification of the PV system is not required. The prediction results of the mentioned system are released by three stages including the train, test, and regression of the read data [74]. For instance, in [94], an ANN approach has been used to predict module output characteristics for any given individual cell temperatures and irradiances using a number of critical points to parameterize the current-voltage curve. Another ANN-based model is proposed which can take into account the variation of the equivalent circuit parameters with respect to operating conditions for characterizing PV arrays with shaded solar cells [95]. A short-term prediction model based on the SVM method has been introduced to estimate the PV energy production for the next day with 15 minutes values using the database of solar irradiance, environmental temperature, and past energy production [96]. In [74], the

Levenberg–Marquardt (L–M) algorithm has been adopted and incorporated into back propagation learning algorithm for training a feed-forward neural network for the modeling of PV power generation.

Employing different techniques of machine learning provides comprehensive prediction models through finding the interrelationships between the parameters of historical data recorded in PV systems. In recent years, investigating the meteorological data using intelligent techniques has shown a great interest in the prediction of PV yield. In [97], the problem of energy prediction for the several PV plants connected to a power grid has been studied and the results were compared for ANNs versus regression trees as learning algorithms. The results obtained from two PV power plant datasets show that the regression trees perform well by improving the prediction by 30 % with respect to the one achieved using artificial neural networks. The authors of [98] propose a prediction model based on Gradient Boost Decision Tree using historical weather data to predict the future PV power output based on the weather forecast. A hybrid prediction model based on the random forest learning algorithm is provided in [99] to estimate the dynamic I–V characteristic curves during the fluctuation of meteorological data that causes random changes in PV performance. Prediction of PV systems power output from seven solar PV sites of the University of Queensland, Australia is investigated in [100]. Meteorological data such as solar irradiance, wind speed, temperature, and humidity are applied as inputs to the multivariate neural network algorithm to forecast the output power of PV systems in smart grids. Other types of machine learning techniques [101-103], as well as different hybrid algorithms [104-106], are widely used to implement various versions of prediction models for the PV output power production in snow free conditions.

Snowfall as an effective parameter that can diminish the production of PV systems has been addressed in some research papers. In [18], historical data for two sets of PV modules are investigated to develop a linear regression model and a non-linear empirical model. In these models, the output power production of PV modules for both cases of snow-covered and manually cleaned modules are compared to take into account the meteorological parameters such as average air temperature, insolation, and average relative humidity in the prediction of the snow loss. The snow-related PV yield based on the meteorological data is obtained in [107] by subtracting the measured output of the PV

system from the values of standard one to build a simple prediction model. Although in the previously mentioned models, the environmental parameters, as well as snow effect, are considered, the results of the model demonstrate a low prediction accuracy. Simulator based-models such as National Renewable Energy Laboratory's System Advisor Model (SAM), DowM simulator, and Iowa energy center solar calculator are also presented in some papers which import the meteorological data to predict the PV output power with and without snow [21, 108]. Through a linear combination of forecasts for the PV power output in normal conditions and snow-covered conditions, an empirical prediction model is introduced which considers the probability of snow [109]. The loss ratio for the PV systems under the exposure of snow, rain and dust is presented in [110] to estimate the monthly PV generation based on the Monte Carlo algorithm. Most recently, a daily snow loss prediction model was proposed using machine learning algorithms based on meteorological data of a PV farm which compared the performance of different computational intelligence techniques [111]. However, the proposed prediction model has not considered the effect of snow shaded areas on the surface of PV modules. Table 4 presents a summary of relevant research works on the prediction models for PV systems available in the literature.

Table 4. Research work on prediction modeling of PV systems.

Research	Input-output training data base	Method	PV technology and site	Application
[95] (E. Karatepe, et al. 2007)	Irradiance, temperature, and parameters of single diode model	ANN	Monocrystalline silicon	Prediction of model parameters to characterize the shaded PV arrays.
[86] (P. Bacher, et al. 2009)	Global irradiance and solar power of entire year 2006	Adaptive linear regression time series	21 rooftop PV systems	Prediction of hourly values of solar power
[93] (E. Karatepe, et al. 2009)	Irradiance and pre-determined shading patterns maximum energy production	Hybrid (ANN) and fuzzy logic	Multicrystalline technology	Prediction of the maximum power generation and the voltage of GMPP under partial shading condition
[18] (T. Townsend, et al. 2011)	Average air temperature, insolation, humidity, and output power production with and without snow	Linear regression	Two different sites	Prediction of snow losses

[90] (. G. da Silva Fonseca, et al. 2011)	Temperature, humidity, cloudiness, horizons, and output power of PV	Support vector regression (SVR)	1 MW PV power plant with multi-crystalline silicon	Prediction of PV power production
[91] (J. G. da Silva Fonseca. 2011)	Temperature, humidity, cloudiness, horizons, and output power of PV	ANN and support vector machines (SVM)	1 MW PV power plant with multi-crystalline silicon	Prediction of PV power production
[94] (J. A. Dolan et al. 2011)	Temperature, irradiance, shading, and number of critical points	ANN	Roof top PV lab with multicrystalline silicon cells	I-V characteristic of PV module estimation and MPPT
[89] (M. Cococcioni, et al. 2012)	Irradiation, temperature, the sampling hour, and daily accumulated energy	ANN	2 Different ground installations of solar systems	Forecasting a one day-ahead of energy production
[107] (R. W. Andrews, et al. 2012)	Irradiance, module temperature, snow depth, and DC power input to each inverter	Simple Comparative	2 large-scale 8MW PV plants	Daily snow loss prediction
[109] (E. Lorenz, et al. 2012)	Numerical weather data, and PV power production with and without snow	Linear combination and simple persistence method	Different PV sites and meteorological stations in the northeast of Germany	Local and regional photovoltaic power prediction
[110] (T. Hong, et al. 2013)	Actual electricity generation of PV facilities	Monte-Carlo algorithm	70 Different PV facilities in Seoul	Calculate loss ratio to estimate the monthly PV generation
[96] (R. De Leone, et al. 2015)	Irradiance, environmental temperature and past energy production	SVR	1 PV plant in Italy	Prediction of PV production
[21] (S. Pisklak. 2016)	15 years data of temperature, irradiance, wind speed, snow depth and	Multi-order polynomial regression	15 different PV sites in USA	Prediction of snow losses
[97] (M. Ceci, et al. 2016)	Rain precipitation, temperature, dew point, ozone, wind speed, humidity, wind bearing and irradiance, geographic coordinates, and historical data on power production	ANNs versus regression trees	Several photovoltaic (PV) plants spread over an extended geographic area in Italy and USA.	Prediction of PV power generation

[108] (A. A. Shishavan, et al. 2016)	Wind speed, irradiance, snow depth, and PV system production	System advisor model (SAM)	Silicon and amorphous silicon in Iowa, USA	Prediction of system losses (considering snow losses) for the analysis of the performance of PV energy yield
[103] (U. K. Das et al. 2017)	Solar irradiance, module temperature, ambient temperature, wind speed, and PV output Power	SVR-based	Monocrystalline, polycrystalline, and thin-film	Forecasting of PV power generation
[98] (J. Wang, et al . 2018)	Weather data (not mentioned in paper)and PV power output	Gradient boosted tree (GBDT)	The 5kW solar power plant in Ashland, USA	Predicting the future PV power output
[100] (M. Q. Raza, et al. 2018)	Irradiance, wind speed, temperature, humidity, and output power of PV systems	Multivariable ANN	seven solar PV sites of the University of Queensland, Australia	Forecasting the output power of PV systems in the smart grids
[101] (H. Zang et al.. 2018)	Solar radiation, temperature, wind speed, and output power of PV arrays	Deep convolutional neural network (CNN)	Two different PV arrays with the capacity of 100 and 200 kW	Forecasting the output power of PV arrays
[99] (I. A. Ibrahim, et al.2019)	Incident irradiance, ambient temperature, module temperature, wind speed, wind direction, relative humidity, month number, day number, and the output current and voltage	Hybrid random forest (RF)	One poly-crystalline PV module	Prediction of PV I–V characteristic curves
[102] (T. Yang, et al . 2019)	Time of record, irradiance, wind direction, temperature, pressure and humidity, and output power of PV system	Long short-term memory (LSTM)	Two PV stations located in one area of China	Prediction of PV power output
[104] (G. Perveen, et al.2019)	Time of record, irradiance, temperature, and output power of PV system	Fuzzy logic, , and adaptive-neural fuzzy-inference system (ANFIS)	250 W multi-crystalline solar PV modules	Forecasting global solar energy
[105] (W. VanDeventer et al. 2019)	Temperature. solar irradiance, and power	A genetic algorithm-based support vector machine (GASVM)	3kW PV system with More than 12 PV modules	Forecasting the output power of residential PV system

[106] (J. Ospina, et al. 2019)	Time of record, irradiance, temperature and statistical features of system output power	Hybrid wavelet-based LSTM with Deep neural nets (DNN)	12.6 MW PV system located in Florida, USA	Forecasting the PV power output for both large-scale and small-scale PV systems
[111] (B. Hashemi, et al. 2020)	Daily snow loss values together with the daily meteorological measurements for snowfall, temperature, humidity, irradiance, and wind speed on the farm site over the duration of four years	ANN, Random forest (RF), GBDT, Decision tree (DT), and SVR	PV farm in Ontario, Canada.	Prediction of snow power losses

Although the state-of-the-art contributions introduce different forecasting approaches to model the energy production of PV systems by considering several parameters and historical datasets, most of the prediction models have not examined and modeled snow shading conditions. To this end, considering the snow shading effect can open up a novel horizon for the PV systems designers and professionals who work in the field of forecasting the trends of power generation of solar installations in the cold areas experiencing different cover of snow patterns.

The final part of thesis aims at developing an improved prediction model for PV modules' energy production estimation based on a combination of meteorological data and historical output power data during the cold months. The physical and optical effects of the snow accumulation as well as the different patterns of the snow shading are also considered as the input parameters for the desired model. In this prediction model, the effective parameters such as humidity, pressure, UV index, and wind speed are involved in the estimation of PV module production.

1.4 Objectives

The universal growth of solar system applications as a safe and trustable renewable energy source encourages both researchers and solar system developers to address the upcoming issues in this field. Besides, it has been statistically proven that plenty of solar investments have been located in the regions that experience snowy winters. Winter months

are actually suitable for solar energy production, as long as PV panels are not covered by snow, but the snow accumulation on PV panels is an issue that needs to be considered for the optimum harvesting of solar energy in cold climate conditions. Therefore, the analysis and modeling of the characteristics of solar systems as well as expected output power and losses in the presence of snow layers are essential. Generally, this thesis aims to enhance the knowledge about the application of PV systems in cold regions. In addition, developing an accurate PV model, and its performance analysis would help the design and selection of PV modules subjected to snow. For this purpose, the specific objectives of this project are presented as follows:

- **Objective 1:** Development of an optimized modeling method for characterizing the performance of PV modules under uniform snow coverage.

- **Objective 2:** Development of a novel modeling technique for PV modules subjected to the nonuniform snow coverage.

- **Objective 3:** Study of the effect of PV panels layout and snow patterns on their electrical characteristics.

- **Objective 4:** Development of a prediction model based on real field data coming from different PV technologies to estimate the maximum power production of snow-covered PV modules.

1.5 Originality and Contributions

Installation of large PV systems is becoming common in cold climate regions, where there is significant snowfall during the winter season. Snow accumulation shades the PV cells in the array and thus limits their ability to generate electricity. While the distribution of snow deposition on a module does not harm the panels, it obstructs sunlight's insolation path to the surface of solar cells. To better understand the effect of degradation in electrical performance of PV cells associated with the presence of snowfall, an accurate modeling and analysis of snow-covered photovoltaic modules is vitally necessary. This thesis brings original contributions to this field as follows:

1.5.1 Modeling of Uniform Snow-covered PV Modules

Related to Objective 1 of the thesis stated in the previous section, one of the main contributions of this thesis in modeling of uniform snow-covered PV modules is the estimation of the irradiation intensity received on the PV surface based on the Giddings-LaChapelle theory [112]. Contrary to the Bouguer-Lambert Law, this theory enables an accurate estimation of the PV module behavior covered with thin and medium snow layers, particularly for critical snow depths less than 2 cm. Furthermore, the particle-swarm optimization (PSO) algorithm, a powerful agent-based algorithm is employed to determine and update instantaneous values of electrical model parameters of PV modules as per variable snow conditions. Moreover, a model that determines normalized PV system losses as a function of snow depth is proposed. The proposed model offers a high accuracy in estimating electrical characteristics of snow-covered PV modules. Such a model can help PV developers to optimally design PV farms in cold environments and take necessary measures for their maintenance, leading to an increase in an efficient lifetime.

1.5.2 Modeling of Partial Snow Shaded PV Modules

Nonuniform snow accretion on PV panels often occurs due to ambient conditions such as wind, temperature variation, partial snow shedding, and ground interference. This leads to power loss that is dependent on the configuration of snow patterns on the PV module. There is still no available electrical model of PV modules that can be used to characterize to their electrical behavior under nonuniform snow patterns. Therefore, it is essential to propose a comprehensive approach and a universal algorithm to model the PV systems covered with different snow patterns. In response to Objective 2, this thesis brings contributions through a novel multi-zone contour-based approach of modeling that separates nonlinear PV characteristics into the multiple linear ones. The proposed solution can operate under any pattern of snow shading and provides an accurate evaluation of solar radiation into the snow cover. A second contribution is the adaptation of a variant of a PSO-based algorithm to instantaneously update and evaluate the output characteristics of PV modules. A final contribution is related to the proposal and validation of a power loss equation using data collected through real field tests and also from a large-scale PV farm.

1.5.3 Analysis of the Physical Layout of Snow-covered PV Panels Impact on Their Performance

The PV modules in an array can be electrically connected together in either series, parallel, or a mixture of the two, to yield the desired voltage and current level. The output power of a PV array not only depends on ambient conditions, but also depends on the interconnection of the individual PV panels. Hence, the physical layout of PV modules arrangements could also affect the PV power production. In this thesis, as a third contribution (related to Objective 3 in section 1.3), the effect of PV panels layout on their performance is investigated through three different positions, namely horizontal, vertical and diagonal layouts. Different snow removal scenarios indicating probable partial snow shading are tested on different technologies of PV modules (with or without bypass diode protection) to analyze their electrical characteristics. This analysis can help to design and select the appropriate panel layout as well as PV module technology in snowy regions.

1.5.4 Development of Prediction Model for Power Generation of Snow Shaded PV Panels

This part of the thesis aims at developing an improved prediction model for PV modules' energy production based on a combination of meteorological data and historical output power data for a PV system during the cold months. The physical and optical parameters of the snow accumulation as well as the depth and area of snow cover for different snow shading patterns are also considered as the input parameters for the model. With the contribution of this comprehensive model, the effective parameters such as irradiance, back surface temperature of modules and the ambient temperatures, humidity, pressure, UV index, and wind speed are employed in the estimation of the PV modules production. In the proposed model, the complexity of circuit-based modeling methods with several electrical parameters is avoided. The solution is a data-driven solution that can predict implicitly the maximum output power of PV modules for a future period of time, under different patterns of snow shading.

1.6 Thesis Outline

The rest of thesis is organized as follows:

Chapter 2 starts with defining the single diode-based model of PV modules and details the way this model can be upgraded by considering the penetration of solar radiation in snow through the Giddings and LaChapelle theory in section 2.2. Section 2.2.2 introduces the main objective of this chapter by proposing a modeling method using a PSO-based algorithm that estimates the characteristics of PV modules under the different depth of uniform snow accretion. The capability of this optimized modeling technique is validated through a series of experimental tests as well as through the use of real data collected by the SCADA system of a 12-MW grid-connected PV farm in section 2.3.2. Finally, a snow-related power loss equation is introduced and validated in section 2.3.2.4 through the use of experimental data.

Chapter 3 introduces an improved version of the PSO-based modeling algorithm for the PV units covered with nonuniform snow patterns. The model is validated through experimental outdoor tests under different scenarios of partial shading in section 3.3.1, and in section 3.3.1.3 the snow losses of the system are formulated in an empirical equation. Section 3.2 describes the novel universal multi-zone modeling approach proposed in this chapter.

Chapter 4 firstly proposes a detailed definition on the effect of bypass diodes on the characteristics of snow shaded PV modules in section 4.1.1. Thereafter, section 4.2.2 presents a power loss analysis of the effect of PV panels layout on their electrical characteristics under partial shading conditions due to nonuniform snow deposits using a series of outdoor experiments. Finally, section 4.3 enables selecting an optimal PV layout in snow conditions.

Chapter 5 starts by describing the stages of a prediction model for the power generated by snow-covered PV panels based on raw data acquired at the installation field in section 5.1.1. Section 5.1.1.1 defines the machine learning algorithms employed in this model that uses a combination of meteorological data and on-site sensor measured parameters of PV modules as input during the snowy months and provides an estimate of the maximum

output power of PV modules. The comparison between the results of different machine learning algorithms of the prediction model over two scenarios for input variables and two cases of model training is depicted in Section 5.2.

Chapter 6 presents the concluding remarks on the work presented in this thesis, the research contributions in section 6.1, and suggests some possible topics for the future work in section 6.2.

Following are the list of publication regarding to this thesis:

Journal Papers:

1. M. Khenar, S. Hosseini, S. Taheri, A.-M. Cretu, E. Pouresmaeil, and H. Taheri, "Particle Swarm Optimisation-based Model and Analysis of Photovoltaic Module Characteristics in Snowy Conditions," *IET Renew. Power Gener.*, vol. 13, no. 11, pp. 1950-1957, Aug 2019. (Nominated as a best paper in 2019 for IET-RPG)

2. M. Khenar, S. Taheri, A.-M. Cretu, S. Hosseini, and E. Pouresmaei, "PSO-Based Modeling and Analysis of Electrical Characteristics of Photovoltaic Module under Nonuniform Snow Patterns," *IEEE Access*, 2020.

2 ANALYSIS OF PHOTOVOLTAIC MODULES CHARACTERISTICS UNDER UNIFORM SNOW COVERAGE

2.1 Overview

The rapid increase of PV systems installed in cold regions during the recent years necessitates addressing the issues that come up with the maturity of PV technologies. For this purpose, the effect of snow as one of the main probable phenomena which hinder the path of solar irradiation to the surface of solar panels needs to be vitally investigated. Therefore, this chapter proposes a modeling method using a PSO-based algorithm that estimates the characteristics of PV modules under the different depth of snow accretion. The developed model utilizes the Giddings and LaChapelle theory which involves both optical and physical properties of snow in the estimation of the attenuated solar irradiance into the layer of snow. The single-diode-five-parameter equivalent circuit model is the base platform for this modeling technique. The optimization algorithm of this model can simultaneously update the parameters of the circuit model through the instantaneous measurements of output voltage and current on the PV module. The capability of the modeling technique is validated through a series of experimental tests on three different commercial PV technologies under different snowy conditions. Besides, the model technique is further validated through the use of real data collected by the SCADA system of a 12-MW grid-connected PV farm. This research can be regarded as a useful reference for designing and selecting the PV modules in the snowy regions.

2.2 PSO-based Model and Analysis of Photovoltaic Module Characteristics under Uniform Snow Coverage

Accurate modeling of I–V and P–V characteristics of a PV cell is required to emulate its behavior under various environmental conditions. The basic circuitry model of the ideal PV cell consists of a linear independent light generated current source connected in parallel

with a single diode. In a real solar system, the electrical characteristics of the PV cell cannot be adequately modeled by an ideal PV cell equivalent circuit. The latter exhibits deficiencies in determining the performance of PV cells when subjected to climatic changes. Consideration of this issue leads to a further extension of the previous model by the inclusion of additional shunt and series resistances. This can lead to an improved PV cell model with respect to the effect of temperature and insolation variation, particularly at low voltage [113]. The addition of extra diodes has been proposed to increase the accuracy of the model. However, this approach increases the model parameters and consequently the computational time. This is not efficient in online modeling of photovoltaic arrays [114]. To this end, the proposed methodology in this thesis employs the single-diode equivalent circuit model as shown Figure 3 [115]. From the theory of semiconductors, the implicit equation, which electrically represents the characteristics of the practical PV module in the output terminal, can be derived as:

$$I = I_{ph} - I_s\left[exp\left(\frac{V + R_s I}{\alpha_0 V_t}\right) - 1\right] - \frac{V + R_s I}{R_{sh}} \quad (1)$$

where R_s and R_{sh} represent the series and shunt resistances respectively, I_{ph} defines the photo-generated current by the incidence of light, I_s is the diode's reverse saturation current, α_0 is the diode ideality factor, and $V_t = N_s k T_c/q$ is the PV module thermal voltage with the cell temperature of T_c (K), $k = 1.3806503 \times 10^{-23}$ J/K is the Boltzmann constant, $q = 1.60217646 \times 10^{-19}$ C is the electron charge, and N_s series connected cells.

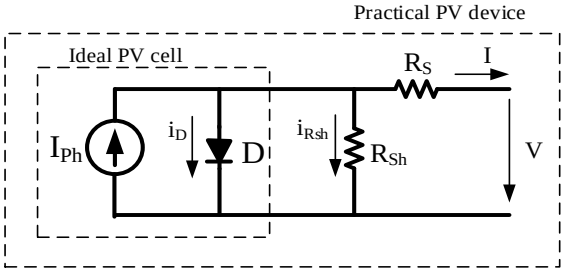

Figure 3. Single-diode model of the ideal PV cell and equivalent circuit of a practical PV device including series and parallel resistances

2.2.1 The Penetration of Solar Radiation in Snow

To build an accurate model for the electrical performance of a snow-covered PV module, one should consider the influence of the penetration of solar radiation in the snow pack. Solar irradiation on the snow coverage is either absorbed by the refraction through some internal layer in the snow or is reflected and lost back into the atmosphere. Thus, the attenuation of incident light in snow is due both the effects of extinction and of reflection. Albedo, which is defined as the ratio of the intensities of reflected radiation to incident radiation, is calculated using radiation intensities averaged over the short-wave radiation spectrum [6, 10]. On the other hand, the extinction of insolation through snow cover can be evaluated by choosing an average value for the extinction coefficient over the solar spectrum.

The albedo and the extinction of solar radiation in snow are coupled and strongly affected by the properties of the adjacent layer of snow on the surface [116, 117]. This coupling phenomenon was investigated through experiments conducted by Giddings and LaChapelle [112]. The penetration phenomenon is analyzed in terms of the physical processes occurred and formulated by the following equations that estimate the shortwave radiation penetration through an isotropic snow at depth x when a horizontal absorbing surface is placed at this depth beneath the laminated snow cover:

$$G_{\downarrow}(x) = \frac{G_{\downarrow}(0)\ \omega\, e^{-k_{ext}\,x}(1+\tanh\ k_{ext}\,x)}{\left\{1+\frac{\omega}{2}\left[1+\frac{e^{-k_{ext}\,x}\left(1-\frac{\omega}{2}\right)}{\frac{\omega}{2}\cosh\ k_{ext}\,x+\sinh\ k_{ext}\,x}\right]\right\}\left(\frac{\omega}{2}+\tanh\ k_{ext}\,x\right)} \tag{2}$$

$$\alpha = \frac{1-\frac{\omega}{2}}{1+\frac{\omega}{2}} \tag{3}$$

where $G_{\downarrow}(0)$ and $G_{\downarrow}(x)$ represent the downward flux of radiation at snow surface and at depth x, respectively, α is the albedo of snowpack, and ω is a dimensionless parameter which is related to reflection feature of snow. Albedo as the important optical property of snow can be empirically calculated as reflective indicator of light from snow accumulation on the surface and the surrounding snow-covered ground of PV panel and k_{ext} is the

extinction coefficient which is represented by the physical properties of snow for evaluating the diminished isolation due to the extinction phenomena through the snow layer.

Although the interpretation and direct measurement of incoming radiation flux within the snow is difficult, the albedo of a snow pack is a simpler, measurable and available parameter. The values of ω can be calculated using equation (3) according to measured values of albedo. Accordingly, for the albedo changes from 0.538 to 0.901, the value of ω varies in the range from 0.60 to 0.10 respectively [112]. In order to determine the extinction coefficient, the following equation that considers ice and snow conditions can be used [118].

$$k_{ext} = \frac{3\rho}{2\rho_i r_{ef}} \tag{4}$$

where ρ is the snow density, ρi is the ice density (= 917 kg m-3), and ref is the effective grain radius. For different types of snow, from the soft new snow to the hard powder one, the value of extinction coefficient may range from around 10 m^{-1} to 55 m^{-1}; for ice accumulation the values of k_{ext} range from 2 m^{-1} for clear ice to 20 m^{-1} for cloudy ice [14].

Table 5. Densities of various types of snow cover.

Snow Type	Density (kg/m^3)
Wild snow	10 to 30
Ordinary new snow immediately after falling in the still air	50 to 65
Settling snow	70 to 90
Very slightly toughened by wind immediately after falling	63 to 80
Average wind-toughened snow	280
Hard wind slab	350
New firm snow	400 to 550
Advanced firm snow	550 to 650
Thawing firm snow	600 to 700

Density appears to be the most common classifying feature and is relied upon to the natural variation. Regarding the comprehensive assessment of the TN Conseil Passive Melting Technology for the PV system affected by the snow and ice accretion in Canada [14], the type of different snow have been classified according to their densities as Table 5.

For a snow depth greater than a critical value of 2-4 cm (Figure 4), the Giddings-LaChapelle model can be merged with the Bouguer-Lambert Law to estimate the level of insolation that reaches the surface of PV cells covered with snow [23], such that:

$$G_{\downarrow}(x) = G_{\downarrow}(0)e^{-k_{ext}\,x} \tag{5}$$

It is important to recall that the Bouguer-Lambert Law exhibits low efficiency for low amounts of snow cover because it only considers the extinction coefficient in its relationship. But by making use of the Giddings-LaChapelle theory, both extinction and reflection effects and their coupling are considered. As such, one can estimate the insolation level reaching to the surface of PV cells for different ranges of snow thickness.

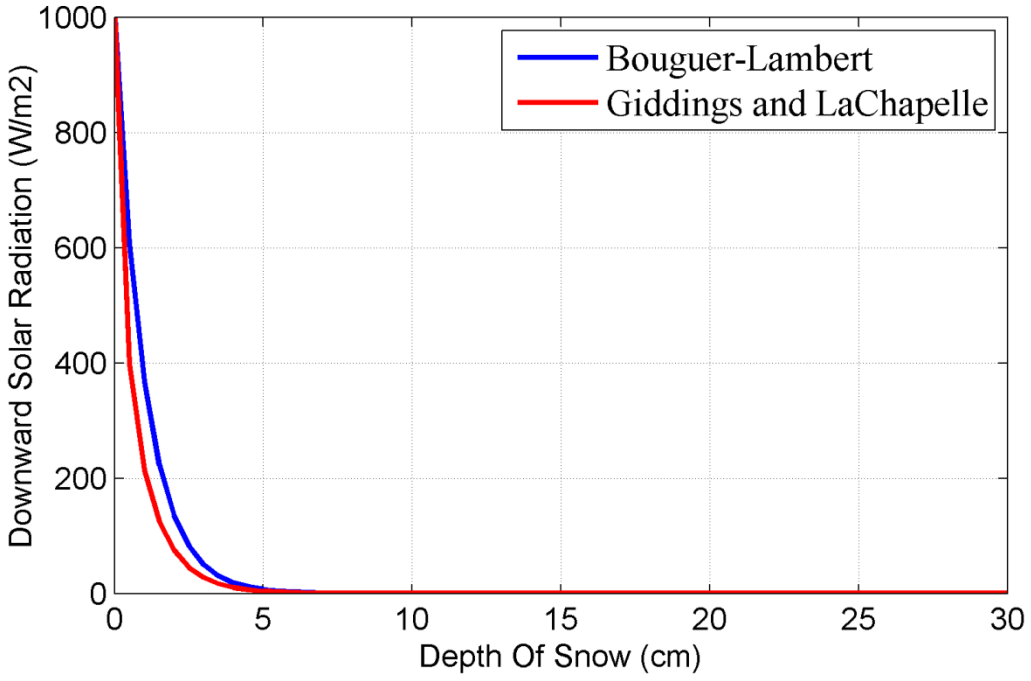

Figure 4. Attenuation of downward solar radiation for an increasing the depth of snow

2.2.2 Determining the PV Module Parameters

In order to determine the current-voltage characteristic of a PV cell, it is required to compute five parameters i.e.,I_{ph}, I_s, a_0, R_s and R_{sh}, from equation (1). In the majority of cases, in order to simplify computations, the model incorporates only the variations of photo-generated current (I_{ph}) and diodes reverse saturation current (I_s), while the remaining parameters are kept constant. However, this simplification can negatively affect the accuracy of the model, particularly in snow conditions. Thus, the proposed approach presented in this thesis computes and updates simultaneously all the above-mentioned five parameters considering environmental conditions using the following steps:

2.2.2.1 Step 1: Photocurrent (I_{ph})

The photocurrent of a PV module covered by snow (I_{ph}) that depends on the intensity of incident insolation on the surface of the PV module and the module temperature can be obtained as [119]:

$$I_{ph} = \frac{G_{\downarrow}(x)}{G_{STC}} . K_{sf} \left[I_{ph,STC} + K_I(\Delta T) \right] \tag{6}$$

where $I_{ph,STC}$ is the photocurrent of the PV module in standard test conditions (STC) where the solar irradiance level has the value $G_{STC} = 1000$ W/m2, $\Delta T = T_c - T_{STC}$ is the temperature variation of the PV cells junction, $T_{STC} = 25$ ℃, and the solar spectral distribution is equal to AM1.5 spectrum, K_{sf} defines the effect of aging and dirt in derating of the PV module, and K_I is the temperature coefficient of short-circuit current reported by manufacturers.

2.2.2.2 Step 2: Diode Reverse Saturation Current (I_s)

In the presence of snow at low irradiance levels, the open-circuit voltage of PV cell relevant to the variation of irradiance and temperature is calculated as follows [119]:

$$V_{oc} = V_{oc,STC} + V_t \, ln\left(G_{\downarrow}(x) . K_{sf} / G_{STC}\right) + K_V(\Delta T) \tag{7}$$

The values of $V_{oc,STC}$, the open-circuit voltage at STC, and K_V, the temperature coefficient of the open-circuit voltage, can be extracted from manufacturer datasheets. As a result, an improved equation which describes the saturation current I_s of the diode by considering both temperature and insolation is given by [120] and [121] as:

$$I_s = \left(I_{ph} - V_{oc}/R_{sh}\right)/(exp(V_{oc}/a_0 V_t) - 1) \tag{8}$$

Equations of voltage and current of the PV module at the MPP can be developed as [120]:

$$V_{mp} = V_{mp,n} + V_t\, ln\left(\frac{G_{\downarrow}(x)}{G_{STC}}.K_{sf}\right) + K_{VP}(\Delta T) \tag{9}$$

$$I_{mp} = \frac{G_{\downarrow}(x)}{G_{STC}}.K_{sf}\left[I_{mp,n} + K_{IP}(\Delta T)\right] \tag{10}$$

where $V_{mp,n}$ and $I_{mp,n}$ are the nominal voltage and current of MPP at STC and their correlate temperature coefficients K_{VP} and K_{IP} respectively, are taken from the manufacturer documents for the verities of PV modules.

Although the aforementioned equations represent the variations of photocurrent (I_{ph}) and diode saturation current (I_s) with respect to the temperature and irradiance in the presence of snow, their optimum values can be obtained by interaction with the remaining parameters (α_0, R_s and R_{sh}) in different climatic conditions.

2.2.2.3 Step 3: Determination of α_0, R_s and R_{sh}

The remaining parameters in (1), i.e. α_0, R_{sh} and R_s are obtained through iteration process. Hence, initial guesses for R_s and R_{sh} are required. By substituting (9) and (10) in (11) which represents the slope of the line segment between the short circuit and the maximum power remarkable points, the minimum values for the resistance can be determined [120].

$$R_s{}' = 0; \quad R_{sh}{}' = \left[V_{mp,n}/(I_{sc,STC} - I_{mp,n})\right] - \left[\left(V_{oc,STC} - V_{mp,n}\right)/I_{mp,n}\right], \tag{11}$$

The ideality factor of diode α_0 typically resides in a known range between $1 \leq \alpha_0 \leq 2$ [120]. In the above equation, $I_{sc,STC}$ which is provided by manufacturer datasheets, represents the short-circuit current under STC.

2.2.2.4 Step 4: Objective Function

The optimization algorithm is applied to tune the values of parameters until the online experimental data are in accord with the I-V relation of (1). Therefore, (1) can be rewritten as below in order to construct a function that specifies the error between measured and calculated pairs of current and voltage values.

$$g(I,V,\psi) = I - I_{ph} + I_D + I_{Rsh} = I - I_{ph} + I_s\left[exp\left(\frac{V+R_sI}{\alpha_0 V_t}\right) - 1\right] + \frac{V+R_sI}{R_{sh}} \qquad (12)$$

where, $\psi = [R_{sh}, R_s, I_{ph}, I_s, \alpha_0]$ is the decision vector that includes the set of unknown parameters to be extracted accurately. In this work, the root mean square of the error function is employed as an objective function as follows:

$$OF = \sqrt{\frac{1}{N}\sum_{k=1}^{N}\left(g(I_k, V_k, \psi)\right)^2} \qquad (13)$$

where I_k and V_k are the values of the kth pair of N data points in the experimentally measured I-V characteristics. Theoretically, the desired value for OF is zero if the exact values of each parameter have been found for any experimental I-V data. However, because of the noise of measurement and computation errors, it is expected to obtain a small value (i.e. $|\varepsilon| < 0.001$) for OF.

2.2.2.5 Step 5: Particle Swarm Optimization (PSO) Algorithm

PSO is a stochastic optimization method, inspired by the behavior of a flock of birds or a school of fish, developed in 1995 [122]. PSO algorithm uses real numbers of particles to guide its search without the need of transformation of binary encoding and special genetic operators which is used in genetic algorithm (GA). Moreover, contrary to other stochastic algorithms, PSO is free from the sophisticate computation of selection, crossover and mutation. In fact, the PSO as a metaheuristic approach is used to optimize a function

that is difficult to express analytically. By considering these great merits of PSO, it has been decided to utilize this efficient agent-based algorithm to solve the optimization problem.

In PSO, the global position is searched by a number of agents (particles) with a continually updated velocity [123]. As shown in Figure 5, the movement of each particle in the search space is controlled by its own best position and the globally best position found by all particles so far.

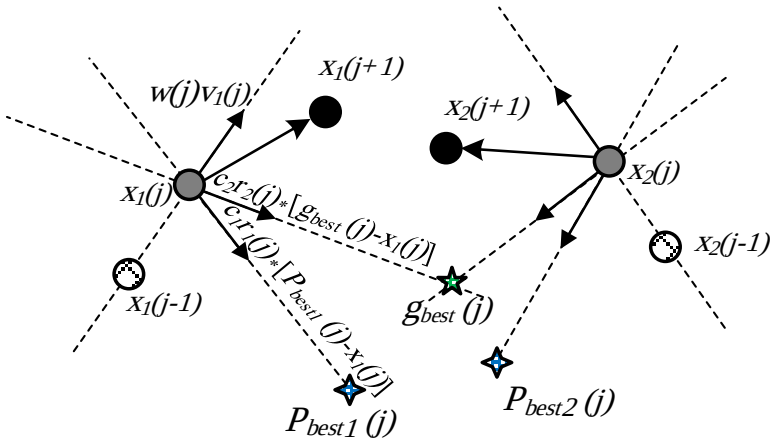

Figure 5. Displacement of particles in PSO search space.

Each particle with the index of i emulates the success of neighboring particles and reaches its own success to find the best position (state) with time in a d-dimensional hyperspace. In each update with iteration index j, the current position $x_i(j+1)$ and velocity $v_i(j+1)$ of particles are dynamically adjusted regarding to their own previous best position experience $pbest_i(j)$ and the previous best solution $gbest(j)$ of the entire swarm as follows [122]:

$$v_i(j+1) = w(j)v_i(j) + c_1\, r_1(j) \times [pbest_i(j) - x_i(j)] + c_2\, r_2(j) \times [gbest(j) - x_i(j)], \quad (14)$$

$$x_i(j+1) = v_i(j+1) + x_i(j), \quad (15)$$

where w is the inertia weight, c_1 and c_2 are the acceleration coefficients, conventionally c_1=c_2=2 and r_1 and r_2 are random (normal distribution) numbers with values between 0 and

1. A possible solution of the optimization problem is represented by the position of each particle that corresponds in the context of this work to the set of solar cell parameter values. The global search and local search of a solution can be ideally balanced by using a value of selected inertia weight as follows:

$$w(j) = w_{max} - (w_{max} - w_{min})\frac{j}{j_{max}}, \tag{16}$$

In this equation, j_{max} indicates the maximum number of iterations (generation size). An improved convergence speed was observed by the variation of inertial weight from $w_{max} = 0.9$ to $w_{min} = 0.4$ over entire search range. It also avoids premature convergence, and reduces the total number of iterations [36].

The changes of velocity vector of each particle in equation (14) can be further updated by the following law:

$$v_i(j+1) = \begin{cases} V_{max}, & if\ v_i(j+1) > V_{max} \\ -V_{max}, & if\ v_i(j+1) < -V_{max} \\ v_i(j+1) & otherwise, \end{cases} \tag{17}$$

In the above relation, V_{max} represents the maximum permitted excursion (is also known as velocity clamping factor) of any particle in that dimension to clamp the unnecessary movement of particles [122].

Personal best position of each particle can be updated by comparing the personal best of each particle to its current fitness through the comparison of objective function (*OF*), and set to the better performance according to the following relation.

$$pbest_i(j) = \begin{cases} pbest_i(j-1), & if\ OF(x_i(j)) \geq OF(pbest_i(j-1)) \\ x_i(j), & if\ OF\big(x_i(j)\big) < OF\big(pbest_i(j-1)\big), \end{cases} \tag{18}$$

The position of the particle with the best fitness within the entire swarm sets the global best as follows:

$$\begin{aligned} gbest(j) \in \{pbest_1(j), pbest_2(j), \dots, pbest_{N_S}(j)\} \big| OF\big(gbest(j)\big) \\ = \min\left\{OF\big(pbest_1(j)\big), OF\big(pbest_2(j)\big), \dots, OF\left(pbest_{N_S}(j)\right)\right\}, \end{aligned} \tag{19}$$

Figure 6 depicts the flow chart of the proposed method in conjunction with the PSO algorithm. After importing the experimental data and environmental information into the algorithm, the coefficients, the population size, and boundary of variables are defined. According to the depth and properties of the snow layer, the received irradiance, as well as the extinction coefficient, are calculated and consequently the initial particle positions and its velocity regarding the model parameters are initialized. Based on stopping constraints (i.e. the maximum iteration number or the tolerance of objective function), the iterations will be stopped and the model parameters will be saved as the best solution. For this purpose, the values of results are compared with the previous iteration to update the personal and global bests and when the stopping constraints are satisfied, the extracted results are the best model parameters with the least deviation from experimental data.

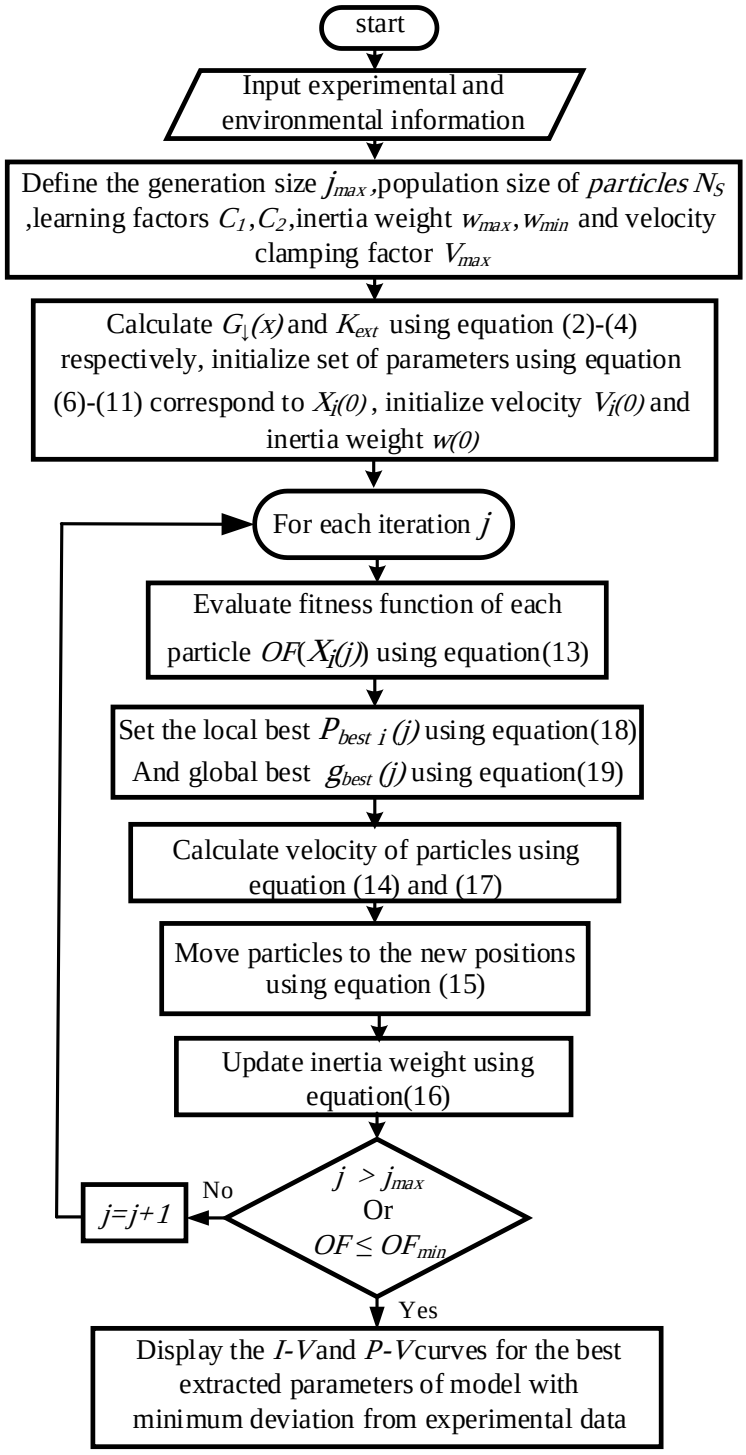

Figure 6. The proposed PSO algorithm for PV modeling

2.3 Results for PSO-based Modeling and Analysis of Photovoltaic Module Characteristics under Uniform Snow Coverage

This section presents experimental results for the model presented in section 2.2. and related to Objective 1 of this thesis. It presents simulated electrical characteristics of PV modules obtained using the proposed model under uniform snow pattern. The validity of the proposed modeling approaches is investigated through real experimental measurements with three commercial PV modules covered with snow as well as through data obtained from a 12-MW grid-connected PV farm.

2.3.1 Simulation Results

The proposed PSO method enables simultaneous computation of unknown values of α_0, R_s and R_{sh} and optimal values of I_{ph} and I_s with respect to the temperature and irradiance in the presence of snow. The values of optimized extracted parameters, their relevant minimum objective functions, the computation time and the bound of search range are shown in Table 6.

If the population size and the number of iterations defined are too small, the algorithm leads to poor results because of the limitation of the space for exploring solutions. As consequence, in the following experiments for operating the modeling algorithm, control variables of PSO have been executed by setting the number of particles as 100 and the maximum number of iterations as 10000. The objective (fitness) function specified as the root mean square error between measured and calculated pair of voltage and current data points vary from 135 to 200 points in different types of panels.

In the optimization problem based on PSO for extracting solar cell parameters, the fitness function and the objective function are identically described as equation (13). The smaller the objective function, the better the fitness of an individual. Furthermore, reaching the maximum iteration number j_{max} or satisfying the minimum fitness function OF_{min} are used as the stopping criteria in this case.

2.3.2 Experimental Validation

The accuracy of the proposed method in determining I-V and P-V characteristics is validated using experimental data of uniformly snow-covered PV modules of different technologies and also using real data acquired using the SCADA system of a grid-connected PV farm.

Table 6. Optimized parameters of the PV modules extracted by the proposed algorithm

Parameters	CS6P-260P			
	Range	1	2	3
I_{ph}(A)	[0,10.14]	5.0763	3.194	0.9823
I_s(A)	[0, 3.5×10^{-8}]	2.617×10^{-11}	1.6464×10^{-11}	5.0589×10^{-12}
α_0	[1,2]	1.0027	1.0052	1.0085
$R_{sh}(\Omega)$	[53,3000]	501.023	782.4833	2348.1286
$R_s(\Omega)$	[0,10]	0.61808	0.98531	3.2224
Time (s)	…..	275	317	243
$OF_{\min}$	…..	4.21×10^{-4}	4.01×10^{-4}	3.97×10^{-4}
	ET-M53695			
I_{ph}(A)	[0,7.34]	3.719	1.3204	0.27923
I_s(A)	[0, 6.6×10^{-9}]	5.1609×10^{-11}	1.8179×10^{-11}	3.5855×10^{-12}
α_0	[1,2]	1.0504	1.0519	1.0532
$R_{sh}(\Omega)$	[41,3000]	112.493	560.0398	1223.696
$R_s(\Omega)$	[0,10]	0.39453	1.1064	5.3276
Time (s)	…..	205	215	328
OF min	…..	4.56×10^{-4}	4.89×10^{-4}	4.78×10^{-4}
	FS 275			
I_{ph}(A)	[0,1.66]	0.84057	0.61658	0.28483
I_s(A)	[0, 1.6×10^{-11}]	1.9551×10^{-14}	1.4434×10^{-14}	6.5289×10^{-15}
α_0	[1,2]	1.0165	1.0069	1.0133
$R_{sh}(\Omega)$	[505,5000]	1411.8196	2230.4348	3128.2938
$R_s(\Omega)$	[0,100]	17.9777	24.0628	53.9588
Time (s)	…..	289	241	314
$OF_{\min}$	…..	4.73×10^{-4}	4.69×10^{-4}	5.03×10^{-4}

2.3.2.1 Test Bed Design and Installation

A series of experiments were carried out using three different types of PV module technologies i.e., an ET-M53695 monocrystalline PV module from ET Solar manufacturer, a CS6P-260P polycrystalline PV module from Canadian Solar manufacturer, and a FS-275 thin film PV module from First Solar manufacturer to measure electric characteristics of PV modules. The parameters of the test-bed panels are provided in Table 7. A comparison between the measured short-circuits current of the PV panels and the ones provided by the

manufacturers datasheet was performed to obtain the value of *Ksf*, used in (6). This coefficient was found to be approximately equal to 1 for the CS6P-260P and FS-275 PV panels as new technologies, while it was determined to equal 0.97 for the ET-M53695 panel.

Table 7. Electrical parameters of the test bed solar panels.

Parameters	CS6P-260P	ET-M53695	FS 275
P_{max}(W)	260	95	75
V_{mp}(V)	30.4	18.52	68.2
I_{mp}(A)	8.56	5.13	1.10
V_{oc}(V)	37.5	22.5	89.6
I_{sc}(A)	9.12	5.57	1.23
N_s	60	36	116
Bypass Diode	3	3	Non

As shown in Figure 6, the PV modules with snow coverage were faced due south with a tilt angle of 30˚ under the test condition. The test bed was racked with the latitude of 45.47°. Data acquisition was conducted using HT Instruments I-V 400 PV Panel Analyzer and irradiance meter test kit to export the PV characteristics. The quick and reliable temperature measurement of the back surface of modules was carried out by a Fluke 62 Mini infrared thermometer. An electronic digital caliper was employed to measure the snow depth. Snow densities were determined using a digital scale. A magnifying glass and a millimeter-scale grid were used to acquire the size of snow grains. For different snow patterns over the experiments, the extinction coefficient ranged between 18 m^{-1} and 54 m^{-1}.

Figure 7. Experimental set-up for the snow-covered PV modules.

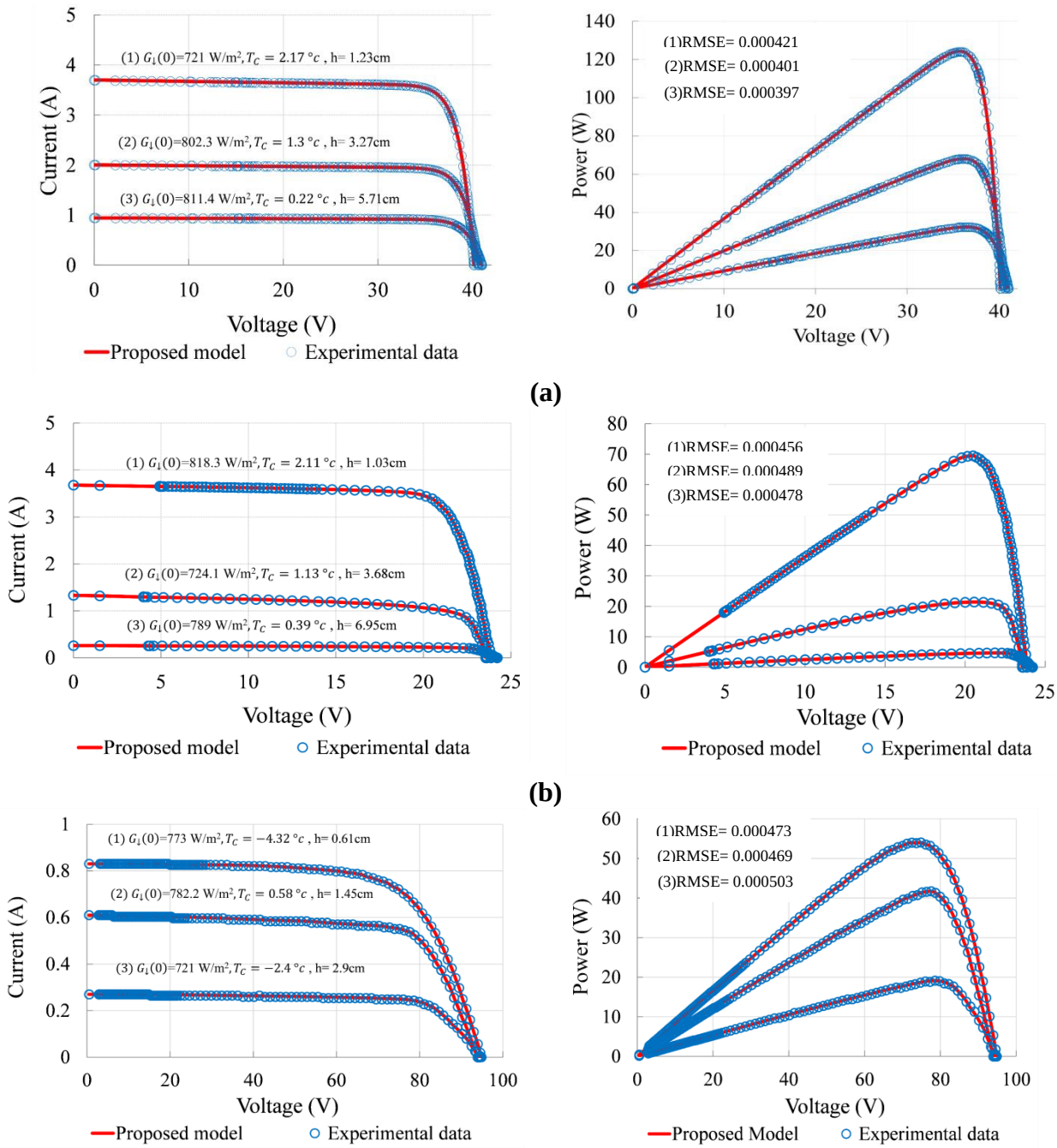

Figure 8. I-V and P-V curves obtained using the proposed model and experimental data under various climate conditions and for different snow depths for: (a) CS6P-260P (polycrystalline), (b) ET-M53695 (monocrystalline), and (c) FS-275 (thin film).

2.3.2.2 Results Validation and Discussion

The I-V and P-V characteristics of the simulated model are compared with those measured from the test field to experimentally validate the effectiveness of the proposed PV model approach as shown in Figure 8. The circle markers in blue represent the experimental measurements, while the modeled results are marked by the red solid lines. A good concordance was identified between the simulated current values obtained by employing the model and the experimental ones. Since the field information, physical characteristics of the snow coverage, including density, depth, and an estimation of grain size as well as manufacturer data are taken into account, the proposed model has the capability to reflect the impact of variable weather conditions on the behavior of PV modules.

A better representation of the degree of agreement between theoretical and measurement results of the proposed model can be more accurately illustrated if the difference in the output quantities is plotted as a function representing the percentage of deviation between the proposed model and the experimental data. Hence, the following equation has been used to calculate and plot the percentage of the output power deviation for the same input quantities of the first graphs in Figure 8 as below:

$$DEV\ \% = \frac{(P_{i-}\ \hat{P}_i)}{P_i} \times 100, \qquad (20)$$

where the P_i is the measured output power and $\hat{P}_i$ is the modeled output power of modules in each point of characteristics indexed by i. The results of power deviation percentage are instantly plotted in Figure 9.

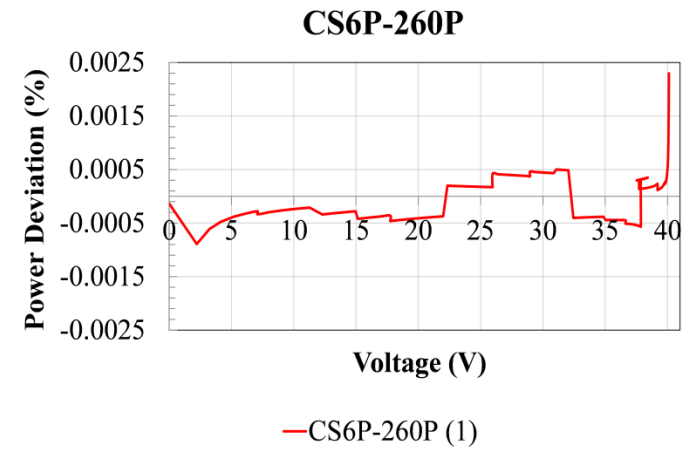

(a)

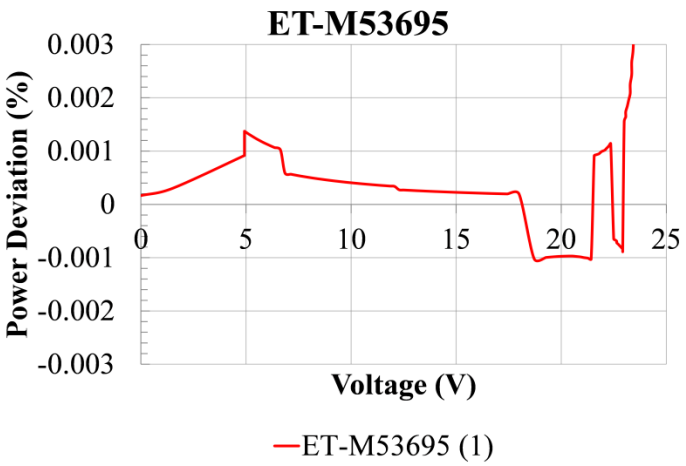

(b)

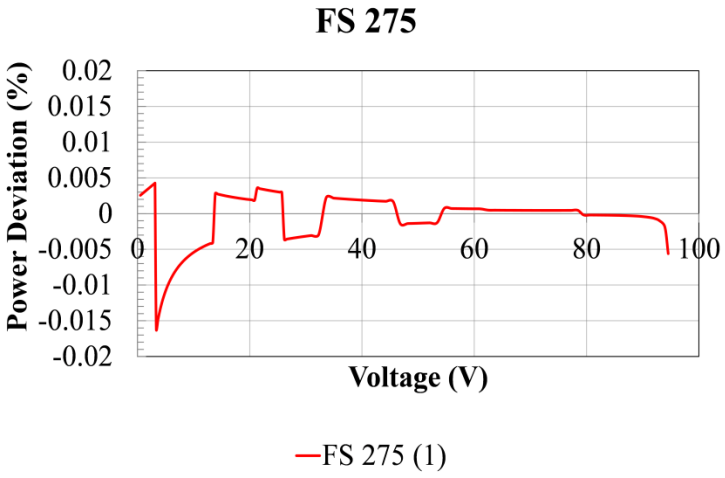

(c)

Figure 9. Percentage of output power deviation between the proposed model and experimental data of the first graphs (1) of figure 8 for: (a) CS6P-260P (polycrystalline), (b) ET-M53695 (monocrystalline), and (c) FS-275 (thin film). These graphs demonstrate the instant variation of power deviation in each point of output voltage.

2.3.2.3 Model Error

Since the plotted graphs of I-V and P-V characteristics for the simulated model and those experimentally measured from the test field in Figure 8 are in close agreement, to further evaluate the accuracy and validate the modeling results, two categories of errors are presented and analyzed for the proposed model, i.e., the errors introduced by the modeling algorithm error and the measurement errors, described as follows:

2.3.2.3.1 Error of Modeling Algorithm

Regarding the concept of this modeling algorithm, the experimental pairs of voltage and current data points are imported into the algorithm to calculate the model parameter and to plot the modeled characteristics. Hence, the average root mean square errors which are calculated based on the difference between the two ranges of data points are the best point-to-point error indicators to discern deviations between measured and modeled data points of characteristics. The values of root mean square error (RMSE) computed between measured and modeled data points of Figure 8 characteristics (which are the same values of minimum objective function ($OF_{\min}$) are provided in Table 6 for a better evaluation of model accuracy. Besides, Figure 10 shows the convergence performance, a fitness index between experimental data and those calculated by the proposed PSO-based PV model for the three different PV technologies as per the objective function of (13). Figure 10 highlights the ability of the model to determine the PV curve characteristics with a RMSE of 0.0004. It exhibits an excellent fitness value OF that offers very high accuracy.

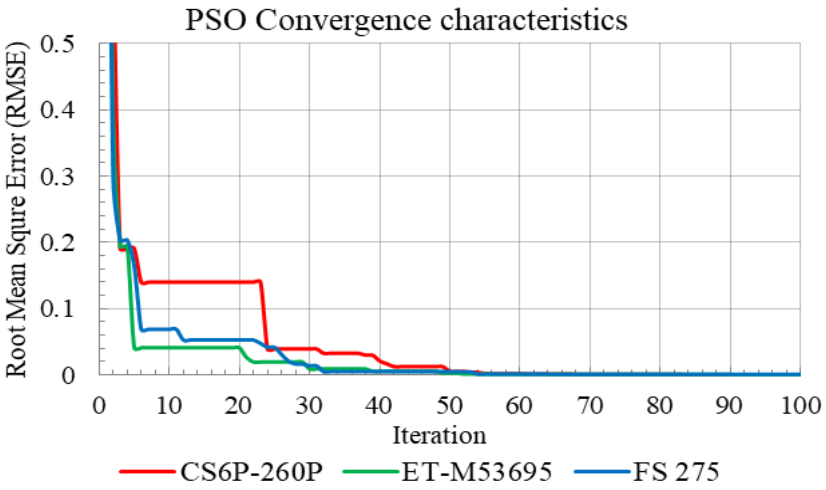

Figure 10. Root mean square error between the proposed model and the experimental data.

2.3.2.3.2 Error of Measurement Equipment

According to the *Guide to the expression of uncertainty in measurement* released by the Bureau International des Poids et Mesures (BIPM) [124], the uncertainty in the result of a measurement generally consists of several components which can be classified into "random" and "systematic" uncertainties. The term of "random" uncertainties can be misleading and should be avoided while the "systematic" term usually can be calculated based on the specification of measurement tools. The HT Instruments I-V 400 PV Panel Analyzer is the data acquisition tool for different measurements of PV systems in this thesis. This section clarifies this uncertainty based on the datasheets of the measurement tools employed during experimentation and the extra information obtained through correspondence with the engineers of HT Instruments company.

The main data acquisition equipment used in this research is the HT Instruments I-V 400 PV Panel Analyzer along with two other sensors: an irradiance meter test kit and a Fluke 62 Mini infrared thermometer. In addition to the pair of voltage and current data points as well as the irradiance on the surface of snow layer and back-surface modules temperature, the information about the maximum power point (MPP) of PV modules can also be acquired using the HT Instruments I-V 400 PV Panel Analyzer. This information can be exported from the equipment using Topview software that accompanies this

measurement tool. Although this equipment is considered as one of the accurate tools in the field of PV systems measurements, there is still a measurement uncertainty referred to as 'accuracy' in the manufacturers' specifications which evaluates the error of measurement for HT Instruments I-V 400. The latter is calculated as $\pm[\%\text{reading} + (\text{number of digits}) \times (\text{resolution})]$ at 23°C$\pm$ 5 °C, at a relative humidity $< 80\%$. This equation indicates that the measurement accuracy (the uncertainties of measurements) for the above instrument is ranged in 1-5%.

2.3.2.4 Snow-Related Power Loss

The performance of PV modules can be negatively affected by snowfall during cold months. In fact, snow accretion can cause obstacles on the PV module surface to receive maximum irradiance, consequently leading to a reduction in energy production. In order to evaluate the impact of snow on the performance of PV modules, a series of measurements of the CS6P-260P polycrystalline PV module under different snow depths were carried out and the MPP values of P-V curves were recorded. A comparison between the expected MPPs of the snow-free PV module and those obtained from snow-covered one, as shown in Figure 8, highlights a significant reduction in the output power with an increase in the snow depth. In order normalize power losses due to snow, the percentage of loss, obtained by comparing the MPPs of the snow-covered PV modules with those obtained for clean modules, is also shown in Figure 11. It can be observed from this figure that a PV module can experience power losses more than 50% when the snow depth reaches the critical depth of 2 cm.

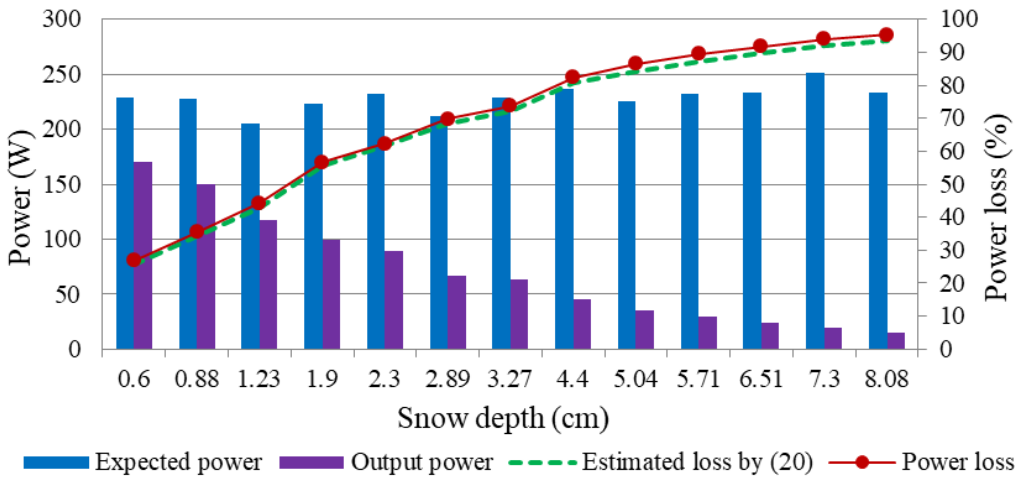

Figure 11. Effect of different snow depths on power production and loss of CS6P-260P.

The percentage of loss in the power generation of PV modules as a function of snow depth, average amount of extinction coefficient k_{ext} and ω can be expressed by (21). The dashed line in green in Figure 11 illustrates the amount of the estimated power loss by considering average values of 35.5 m^{-1} and 0.315 for the extinction coefficient and ω respectively. The proposed power loss equation can offer a good tool to select PV modules for locations exposed to freezing conditions. Contrary to the power loss model proposed in [22], the proposed Giddings and LaChapelle-based power loss model shows a higher accuracy in predicting the energy efficiency. This is due the fact that Giddings and LaChapelle approach shows better performance under light and medium snow accretion in comparison with the Bouger-Lambert Law.

$$P_{loss}(\%) = \left[1 - \omega\, e^{-k_{ext}\,x}(1+\tanh\, k_{ext}\,x) \Big/ \left\{1+\frac{\omega}{2}\left[1+\frac{e^{-k_{ext}\,x}\left(1-\frac{\omega}{2}\right)}{\frac{\omega}{2}\cosh\, k_{ext}\,x+\sinh\, k_{ext}\,x}\right]\right\}\left(\frac{\omega}{2}+\tanh\, k_{ext}\,x\right)\right]\times 100 \quad (21)$$

2.3.2.5 Industrial Case

The great merit of the proposed PV modeling method can be accentuated by calculating power losses of a 12-MW grid-connected PV farm. The data we used comes from a farm that is located in Ontario, Canada. This location consists of the south-facing

thin film PV panels with a fixed tilt angle. Hourly-average data acquisition of the PV farm such as the back-surface temperature and the tilted irradiance of PV panels, along with the module DC voltage, DC current and the AC power of the inverters is recorded by the SCADA system of the PV farm. The maximum power of the PV arrays is extracted by assigning an MPPT control for the grid-connected inverters in PV farms. Data of the SCADA system such as the snow properties and its depth as well as the irradiance and temperature were acquired when PV modules were covered with snow for two typical days of December 2015 and January 2016 after the precipitation are traced in Figure 12.

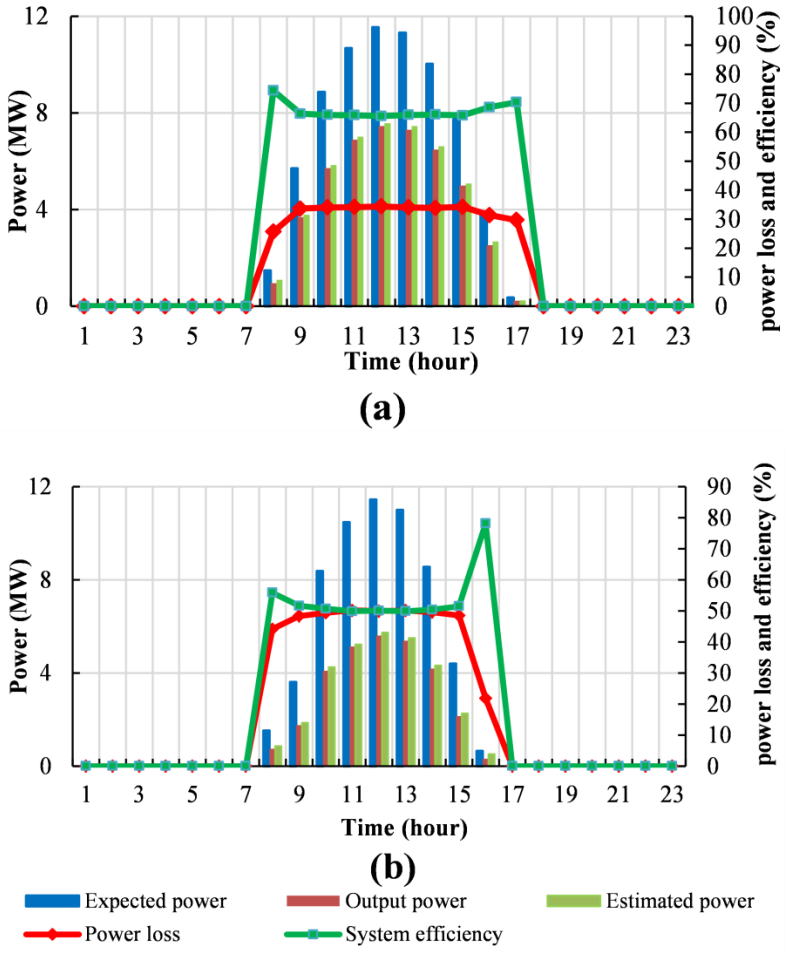

Figure 12. Output and expected DC power of a 12-MW grid-connected PV farm from SCADA database along with the estimation of output power, loss and efficiency of system using the proposed model for two different days with snow depths of (a) h=1.6 cm (day 1), and (b) h=2.55 cm (day 2).

Table 8 indicates the energy generation of the12-MW PV farm for these two mentioned days based on the novel approach proposed in this thesis and the previous model presented in [22] for the same case study. It can be seen that a higher level of accuracy is achieved in comparison with the previous model since the proposed approach uses the Giddings and LaChapelle law that shows high efficiency in determining receiving solar radiation on the PV module surface.

Table 8. Energy generation of a 12-MW PV Farm for Two Typical Days.

	Day 1 (h=1.6 cm)	Day 2 (h=2.55 cm)
SCADA database	46.234 MWh	29.418 MWh
Proposed modeling algorithm	47.58 MWh	30.48 MWh
Error of proposed modeling algorithm	2.92 %	3.6 %
Error of reference [22]	6.3 %	6.8 %

The published paper of [22] is the results of Ph.D. thesis of its author [125] which firstly presented an accurate algorithm to characterize the output of the snow covered PV modules. It achieves interesting results in the field of PV systems modeling under snowy conditions. The case studies that have been considered in [125], such as the PV farm data and PV technologies, are mostly the same as in the current thesis. Hence, [22] is the best case of comparison for the evaluation of the modeling methodology presented in this thesis.

2.4 Summary for the Analysis and Modeling of Uniform Snow-covered PV Modules

This chapter proposed an accurate PSO-based modeling method of snow-covered PV modules. The realistic behaviour of PV systems, when subjected to the variation of climatic parameters in the presence of snowfall, is considered and the Giddings and LaChapelle theory was employed to accurately determine the receiving solar radiation on the PV module surface. The model parameters were simultaneously updated using the PSO algorithm to derive the electrical characteristics of the PV modules under different snow conditions. The experimental validation of the modeling technique was performed using real field data obtained using three different technologies of commercial PV modules. It was observed that the results of the testbed are in close agreement with the model prediction. The power loss of a snow-covered PV module was also formulated by an empirical equation that allows to estimate the power production of PV system under different depths of snow. Furthermore, the accuracy of the proposed model was also evaluated by an additional study that was conducted to correlate the SCADA information of a 12-MW PV farm (as a prominent PV market) with the results of the modeling method. It can be concluded that for a large range of environmental conditions, the step by step methodology in this work can be considered as a valuable modeling tool for deriving the electrical characteristics of the uniformly snow-covered PV modules.

3 MODELING OF PV UNITS COVERED WITH NONUNIFORM SNOW PATTERNS

3.1 Overview

The accretion of snow on the surface of PV systems which strongly diminishes the energy production of PV modules is known as the snow shading. The shading phenomena may happen in uniform (as presented in the previous chapter) and nonuniform patterns. This chapter aims to investigate the effect of nonuniform snow accretion as the second possible form of shading which happens when a part of accumulated snow on surface melts or slides down. This nonuniform shading causes an uneven reception of solar irradiance to the surface of PV modules (known as a mismatch condition) and leads to multi-zone characteristics of shaded modules. To address this issue, a novel universal approach of PV modeling is proposed in this chapter to determine the electrical characteristics of PV modules under snow partial shading conditions. The proposed modeling algorithm utilizes the contour-based discretization methodology to separate the PV characteristics into multiple sub-zones. The PSO-based technique is again employed to simultaneously extract the optimum values of model parameters for each sub-zone. The modeling method is validated through experimental outdoor tests under different scenarios of partial shading, and the snow losses of the system are formulated in an empirical equation. The following sections outline the proposed methodology and the results obtained from the proposed model respectively.

3.2 A Novel Universal Multi-Zone Approach for Modeling of PV Units Covered With Nonuniform Snow Patterns

According to the level of granularity, each unit of the PV system is composed of several cells connected in series and parallel, as shown in Figure 13. The electrical behavior of a solar system corresponds directly to the incident solar irradiance and the surface temperature of PV panels. Hence, the electrical parameters of their circuitry model are not constant and change under the variation of meteorological conditions. Before analyzing the

performance of a PV array, it is necessary to assess the performance of a PV cell in the presence of nonuniform snow. In the theory of semiconductors, an ideal PV cell can be modeled by a current source in parallel with a diode. However, to emulate an accurate behavior of a PV cell, additional series and parallel resistances should be added [126]. In addition to the fundamental equivalent circuit, the modeling of PV systems requires mathematical equations, a set of parameters, and an applicable methodology to calculate the unknown values and characterize the electrical response of the system. From simple piecewise linear (PL) equivalent model [127] to more sophisticated circuit model with a couple of diodes [128] and multi-quadrant performance [129], the single-diode electrical equivalent which is also known as one-diode or five parameters model is the most widely used model [130]. This is due to the best compromise between the accuracy and computational time burden [114].

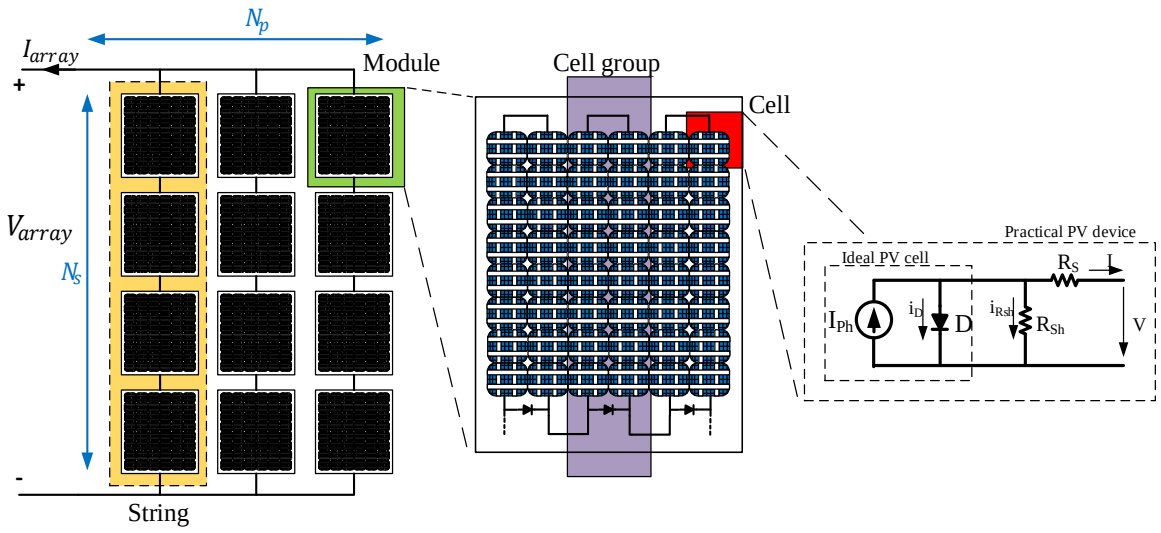

Figure 13. Level of granularity in a PV unit.

3.2.1 Model Development of Partial Shaded PV Systems from Cell to Array

As illustrated in Figure 13 the PV cell is the fundamental component of the solar system whose electrical behavior varies depending on the environmental conditions. The basic models of PV module and their different operation modes under mismatched conditions especially when shadowing occurs are defined in [131]. Based on the Shockley law for the diodes [132] and its interaction with the rest of the elements in the circuit

topology, the nonlinear characteristic of a real PV cell was represented in (1). The model of solar system requires a systematic approach to derive and updated a set of five parameters, i.e., R_s, R_{sh}, I_{ph}, I_s, and α_0 to thoroughly represent the behaviour of solar system under any atmospheric conditions.

3.2.1.1 PV Unit Model

Taking into account that fact that the cells in the units are considered similar, the mathematical voltage-current relation of these units can be derived by defining the basis of the output current and voltage of the constitutive cells as follows:

$$\begin{cases} I_{unit} = N_p I \\ V_{unit} = N_s V \end{cases} \tag{22}$$

where N_s and N_p are the number of the cells in series and parallel, respectively. By substituting equation (21) in equation (1), the voltage-current relation of the unit will be as follows:

$$I_{unit} = N_p . \left\{ I_{ph} - I_s \left[exp\left(\frac{V_{unit} + \frac{N_s}{N_p} R_s I_{unit}}{\alpha_0 N_s V_t} \right) - 1 \right] \right\} - \frac{V_{unit} + \frac{N_s}{N_p} R_s I_{unit}}{\frac{N_s}{N_p} R_{sh}} \tag{22}$$

By comparing equations (1) and (23), the values of each element in the PV unit can be summarized as follows:

$$I_{ph,unit} = N_p . I_{ph} \text{ ,} \quad I_{s,unit} = N_p . I_s \text{ ,} \quad R_{s,unit} = \frac{N_s}{N_p} R_s \text{ ,} \quad R_{sh,unit} = \frac{N_s}{N_p} R_{sh}$$

$$\text{,and} \quad \alpha_{0,unit} = N_s . \alpha_0 \tag{23}$$

3.2.1.2 Distribution of Solar Radiation on the Surface of Snow-covered, Partially Shaded PV Modules

The incident light to the surface of a partially snow-covered PV unit is composed of two different components of irradiance based on the level of radiation, depth, and the area of snow coverage: G_{ir} is the component of irradiance which affects the non-shaded surface

of a PV unit (direct irradiance) and D_{ir} is the diffuse component of the reduced irradiance through the snow shaded areas. For this purpose, the factor of the area should be involved in the calculation of the total solar radiation in the presence of partial coverage of snow. Hence, in the ith shaded contour with the uniform coverage of snow, x_i is the depth of snow layer where the shading factor $\propto_{\mathrm{i}}$ is defined as the ratio of shaded area $A_{sh,i}$ to the total area of contour $A_{T,i}$.

$$\propto_i = {A_{sh,i}}/{A_{T,i}} \tag{25}$$

Therefore, the total solar radiation received on the surface of the PV unit is represented by equation (26) as follows:

$$G_{tot} = G_{ir} \cdot \left(1 - \sum_{i=1}^{k} \propto_i\right) + \sum_{i=1}^{k} D_{ir}(x_i) \cdot \propto_i \tag{26}$$

The precise characterization of the snow-covered PV model requires an accurate evaluation of the total radiation received. Although the direct irradiance is an available property and can be measured easily in the ambient of PV installation, the diffusion of irradiance beneath the snow layer is not accessible and needs to be investigated for a better estimation of electrical model performance. The diffuse radiation on the snow coverage is either attenuated by the refraction of the light beam through penetrating into the snow layer or can be lost by reflecting back to the atmosphere. Thus, the diffusion phenomena in the irradiance collision with the snow pack consist of both the effect of extinction and reflection. The factor of light extinction can be involved in the evaluation by selecting an average value for the extinction coefficient over the spectrum of solar radiation. By considering the reflection indicator (Albedo) as the ratio of intensities of reflected irradiation to the average of incident irradiation [10] and direct coupling between the albedo and extinction of solar radiation were investigated experimentally by Giddings and LaChapelle [112]. $D_{ir}(x)$ is the diffuse downward flux of radiation into the snow pack at depth of x can be calculated by equation (2) where the direct incident solar radiation in the surface of snow is G_{ir} .

3.2.1.3 Extraction of the Partially Shaded PV System's Parameters

In order to characterize the current-voltage curve of a PV cell, its relevant electrical of the single-diode model (Figure 3) consisting of five unknown parameters i.e., I_{ph}, I_s, a_0, R_s, and R_{sh} should be extracted. Although most manufacturers provide some information related to the technology of PV cells in the standard test condition (STC), these parameters are usually unavailable in the PV module datasheets. Hence, they need to be extracted by an accurate computational method as per particular environmental conditions. Moreover, in the mathematical relation in (1), the model parameters are conjugated by an implicit nonlinear current-voltage characteristic in which complex analytical methods are required [133]. In addition, the well-known Newton-based method shows a deficiency in computation since some parameters, for the sake of simplicity, are considered constant [134]. Therefore, the accuracy of the modeling method necessitates the simultaneous computation of the unknown parameters that are significantly affected by irradiance and temperature variations.

Under non-uniform snow coverage, the PV unit experiences different layers of snowpack or snow-free areas. This leads to a complex PV characteristic, characterized by multiple peaks due to the bypass diodes. In this situation, a PV panel covered with a non-uniform snow pattern cannot be characterized by one set of parameters for the whole range of its current-voltage curve. Hence, to deal with this situation, this thesis proposes to divide the PV curve with multiple peaks into several zones containing single peaks.

For instance, Figure 14 shows an electrical characteristic of a partially shaded PV module that experiences three different irradiance levels. Then, this non-uniform curve is divided into three zones (sub-curves) with a uniform reception of irradiance in the relevant range of current and voltage. Then, each sub-curve can be characterized as a PV panel under a uniform snow coverage.

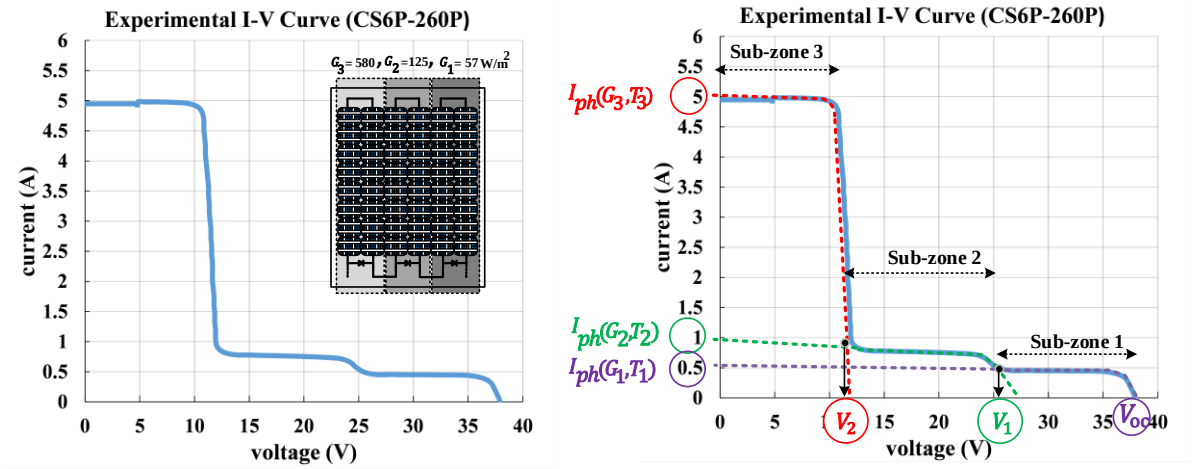

(a) (b)

Figure 14. I-V curve a) non-uniform characteristic of a snowy PV module under three different level of irradiance b) discretization of curve to the three uniform sub-zones.

Since the PV characteristic is divided into several subsections, the relevant photocurrent according to the irradiance level and temperature of each zone can be calculated by equation (6) and arranged in the vector of I_{ph} by ascending order as follows:

$$I_{ph} = [I_{ph}(G_1, T_1), I_{ph}(G_2, T_2), I_{ph}(G_3, T_3), \dots, I_{ph}(G_m, T_m)] \; ; \; G_1 < G_2 < G_3 < \cdots < G_m \quad (27)$$

This vector can be used for defining the range of current for each sub-zone in the next steps of the modeling approach. For the PV technology, which is not protected by the bypass diodes, one value of I_{ph} from equation (27) is needed.

The primary equations of the parameter extraction methodology for each sub-zone of the discretized characteristic can follow the same equations (equation (6) to (11)) of the previously mentioned steps until the new description of step 4, for defining the multi-objective function with multi-constraints as follows:

3.2.1.3.1 Step 4: Defining the Multi-Objective Function of PV System

In this step, the modeling of system is defined as an optimization problem with multi-objective function counterpart to the number of sub-zones. The optimization algorithm aims

to adjust the values of the parameters in a way that the online experimental data become in close accordance with those calculated by equation (1). Due to the generation of new sub-zones under non-uniform snow accretion, the error function for the m sub-zone is generalized by the following equation, which indicates the error between measured and calculated values of current and voltage.

$$g_m(I,V,\psi_m,\ G_m,T_m) = I - I_{ph} + I_D + I_{Rsh} = \quad (28)$$
$$I - I_{ph}(G_m,T_m) + I_{s_m}\left[exp\left(\frac{V+R_{s_m}I}{\alpha_{0_m}V_t}\right)-1\right] + \frac{V+R_{s_m}I}{R_{sh_m}}$$

where the set of unknown parameters in each sub-zone is represented by the decision vector $\psi_m = \left[R_{sh_m}, R_{s_m}, I_{ph_m}, I_{s_m}, \alpha_{0_m}\right]$. The optimization algorithm should be applied to the main error function (equation (29)). According to the range of the current in each sub-zone which is divided by different $I_{ph}(G_m)$, their counterpart voltage points $(V_1, V_2, \dots, V_{m-1})$ separate the voltage range of each sub-zone as shown in Figure 14.

$$F_m(I,V,\psi_m,\ G_m,T_m) \quad (29)$$
$$= \begin{cases} I - I_{ph}(G_1,T_1) + I_{s_1}\left[exp\left(\frac{V+R_{s_1}I}{\alpha_{0_1}V_t}\right)-1\right] + \frac{V+R_{s_1}I}{R_{sh_1}} & 0 \le I \le I_{ph}(G_1)\ , V_1 \le I \le V_{oc} \\ I - I_{ph}(G_2,,T_2) + I_{s_1}\left[exp\left(\frac{V+R_{s_2}I}{\alpha_{0_2}V_t}\right)-1\right] + \frac{V+R_{s_2}I}{R_{sh_2}} & I_{ph}(G_1) \le I \le I_{ph}(G_2)\ , V_2 \le I \le V_1 \\ \vdots & \vdots \\ I - I_{ph}(G_m,T_m) + I_{s_m}\left[exp\left(\frac{V+R_{s_m}I}{\alpha_{0_m}V_t}\right)-1\right] + \frac{V+R_{s_m}I}{R_{sh_m}} & I_{ph}(G_{m-1}) \le I \le I_{ph}(G_m)\ , 0 \le V \le V_{m-1} \end{cases}$$

The best coincidence between the experimental and calculated data can be achieved when the parameters of the decision vector are calculated as close as possible to the real values when each sub-zone contains N_m number of points. Hence, in this work the root mean square of the error function is employed as the objective function for each sub-zone as follows:

$$OF_m = RMSE_m = \sqrt{\frac{1}{N_m}\sum_{k=1}^{N_m}\left(F_m(I_k,V_k,\psi_m,\ G_m,T_m)\right)^2}\ , \quad (30)$$

A global optimization can be achieved when the relative average error as equation (31) for all the points related to the sub-zones is minimal.

$$EF_M = \frac{1}{N}\sum_{m=1}^{M} N_m . RMSE_m \ , \tag{31}$$

Theoretically, in ideal conditions, the value of $RMSE_m$ should be equal to zero. However, due to the noise in measurements and computational errors, a predefined tolerance (i.e. $|\varepsilon| < 0.001$) is accepted.

3.2.1.3.2 Step 5: Particle Swarm Optimization (PSO) Algorithm

In this work, a variant of the PSO algorithm with an optimization ability over a multi-dimensional search space is employed as the search engine of a multi-objective optimization problem. The stochastic exploration ability of PSO works by spreading a population of candidate solutions called particles in a bounded search space. As we described in section 2.2.2.5, each particle with the index i explores around the search space where its position $x_i(j+1)$ is dynamically updated with time in the iteration j by its own previous best position experience $pbest_i(j)$ and the previous globally best position $gbest(j)$ discovered by the entire swarm so far as represented in equation (14) and (15).

By the systematically variation of inertia weight in the predefined range by equation (16) and clamping the velocity of particles based on the maximum permitted displacement of any particle in that dimension as equation (17), each particle visits different personal best positions during its life (up to the jth iteration and serves as memory for keeping the knowledge about each particle when it is updated by comparing it to its current fitness. The value of personal best is saved as a better experience according to the equation (18).

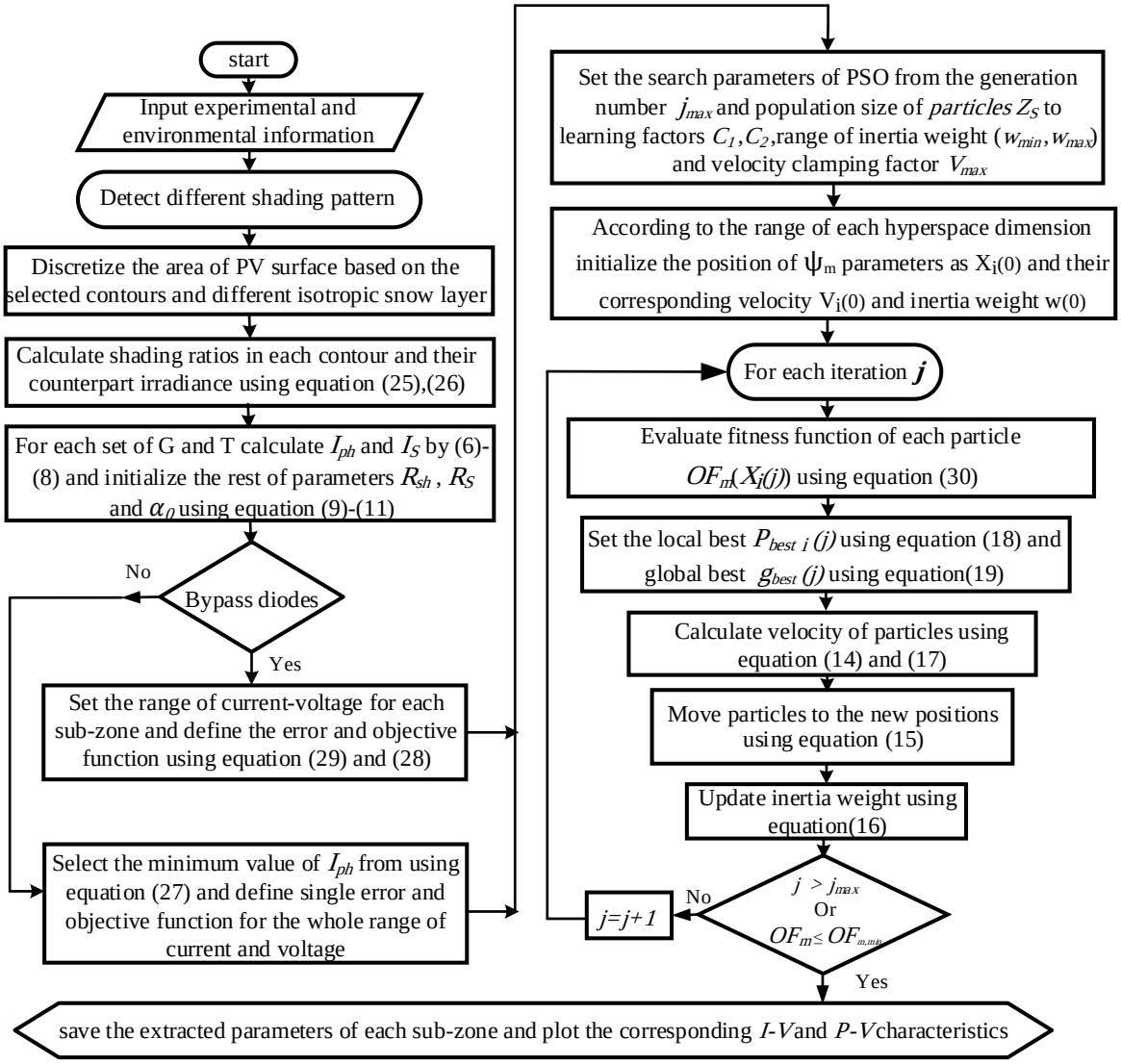

Figure 15. The proposed PSO algorithm for the modeling of partially shaded PV modules covered by snow.

By conducting the previous steps (from step 1 to step 5) so far, it is expected that the swarm is attracted toward the best solution. Eventually, the position of the particle with the best fitness over the whole swarm becomes the global best as (19).

According to the sequence of stages in the flowchart of the proposed algorithm shown in Figure 15, the partially shaded surface of the panel is separated into multiple zones (sub-sections). The shading pattern in each contour defines different shading ratios along with the surface of the shaded area to calculate their counterpart irradiances. Consequently, each set of irradiance and temperature initializes a set of model parameters which indicates the

parameters of each sub-zone in the characteristic of PV. Since the PV characteristic is separated into the different subsections, the photo generated currents for each set of irradiance and temperature are calculated and arranged by ascending order as in equation (27). These values play a key role in defining the range of current and voltage in each sub-zone. If the technologies of PV modules are protected by the bypass diodes, the algorithm is continued to solve a multi-objective function problem, represented by equation (30). Otherwise, the minimum value of the photo generated current from equation (27) is selected as the initial value of I_{ph} and the optimization problem is considered as a single objective function like the objective of first problem. The optimization problem in each sub-zone is simultaneously solved by a PSO algorithm, similar to the approach employed in section *2.2.2.5*. The proposed PSO method simultaneously finds the optimized values for the unknown parameters with respect to the temperatures and irradiances for a PV module covered partially with snow, in each dimension of the search space. Finally, the tolerance of fitness function defines the constrain for selecting the best solution between the results of algorithm.

3.3 Results for the Proposed Multi-Zone Approach for Modeling of PV Units Covered with Nonuniform Snow Patterns

In this section, the simulation results from the proposed model in section 3.2 are compared with those obtained experimentally using different technologies of PV modules under different non-uniform snow patterns.

3.3.1 Experimental Validation

3.3.1.1 Installation of the Outdoor Test Bed

Several experiments of different non-uniform snow patterns using three different types of PV module technologies, i.e., an ET-M53695 monocrystalline PV module from ET Solar manufacturer, a CS6P-260P polycrystalline PV module from Canadian Solar manufacturer, and a FS-275 thin film PV module from First Solar manufacturer were conducted.

Figure 16 shows the installation of the test bed with the field latitude of 45.47° where the PV modules were mounted on the rack facing south with a tilt angle of 30°, in an open area under the exposure of snow precipitation. Similar to section 2.3.2.1, the data acquisition unit was equipped with the HT Instruments I-V 400 PV Panel Analyzer along with an irradiance meter test kit to measure I–V and P–V graphs. The back-surface temperature of each module was quickly measured in each period of data saving by a Fluke 62 Mini infrared thermometer. An electronic caliper was used to digitally measure the depth of the snow layer. The snow densities were obtained using a digital scale. A millimeter-scale grid and a magnifying glass were used to estimate the grain size. Moreover, artificial non-uniform patterns (Figure 16 a and b) were created by partly removing the snow coverage that helps eliminate the problems related to randomness in the position of snow free areas.

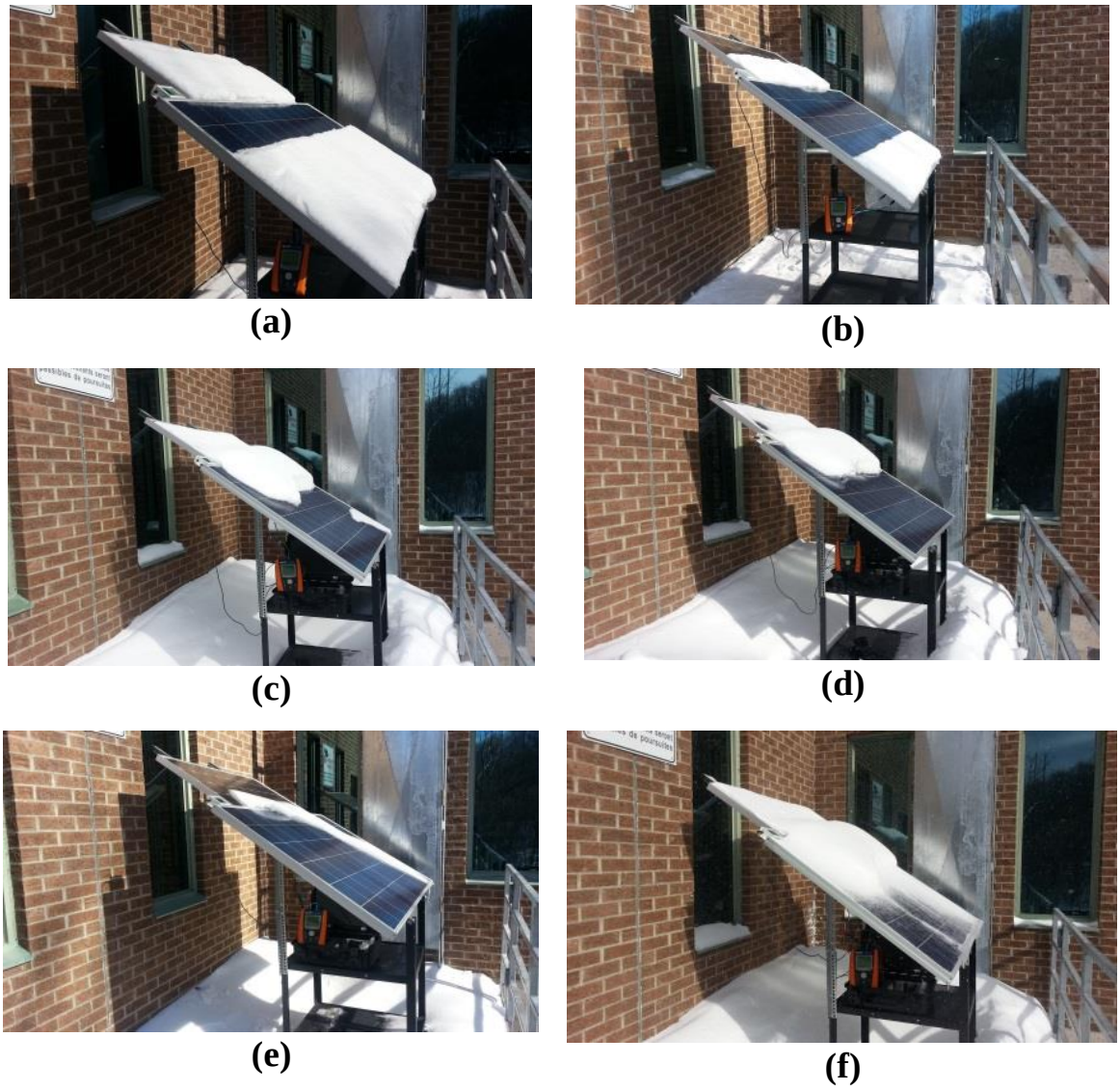

Figure 16. Different scenarios of partial shading for the PV panels under snow coverage.

3.3.1.2 Evaluation of PV Characteristics and Discussion

To confirm the accuracy of the proposed model in determining PV characteristics, the simulated I-V and P-V curves are compared to those obtained from PV modules covered with snow, as shown in Figure 14. As can be observed in Figure 17 to Figure 23, a good degree of agreement exists between the PV characteristics calculated from the model and the experimental ones. This accuracy is due to the fact that the proposed model can calculate and update the PV parameters simultaneously as per irradiance, temperature, PV technology, and snow pattern.

The performance of a PV module can be affected by temperature, irradiance, shading, and module configuration. The power produced by a PV module is directly proportional to the amount of light that a PV module receives. However, when a number of series-connected PV cells in a PV module receive less irradiance due to the snow coverage, they behave as a resistor instead of a generator that may cause a hot-spot problem. To mitigate this situation, bypass diodes are normally used in parallel with the solar module. Moreover, they can guarantee power generation from the rest of the module. From the experimental results for the PV technologies of CS6P-260P and ET-M53695, protected by three bypass diodes, it can be seen that the PV curve is characterized by multiple peaks under the nonuniform snow deposit. This is due to the fact that bypass diodes conduct current. Thus, the number of power peaks under partial shading conditions mainly depends on the number of bypass diodes. On the contrary, for those PV technologies (e.g. FS-275) without bypass diodes, a single peak can be seen in the PV characteristics even under partial shading conditions (Figure 23). The good alignment between the modeled and the measured data in the obtained results (Figure 17 to 23) demonstrates the ability of the proposed modeling method to successfully deal with different variations of the shading pattern, for any technology of PV modules, with or without bypass diodes.

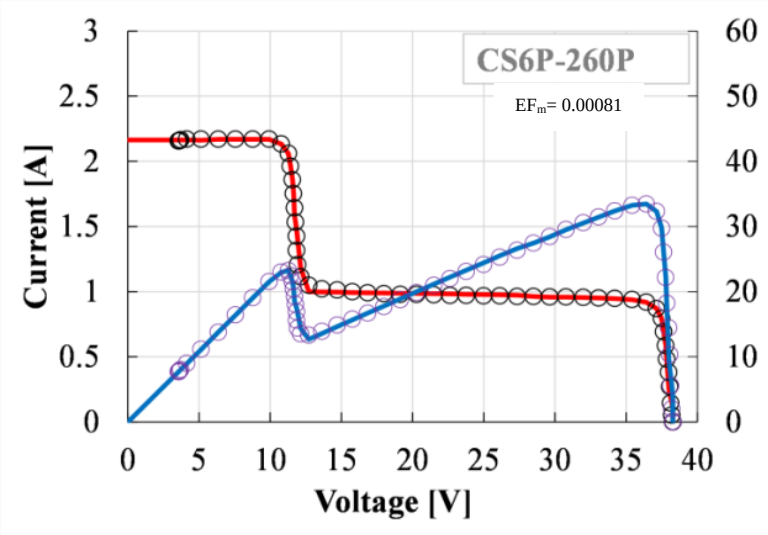

(a)

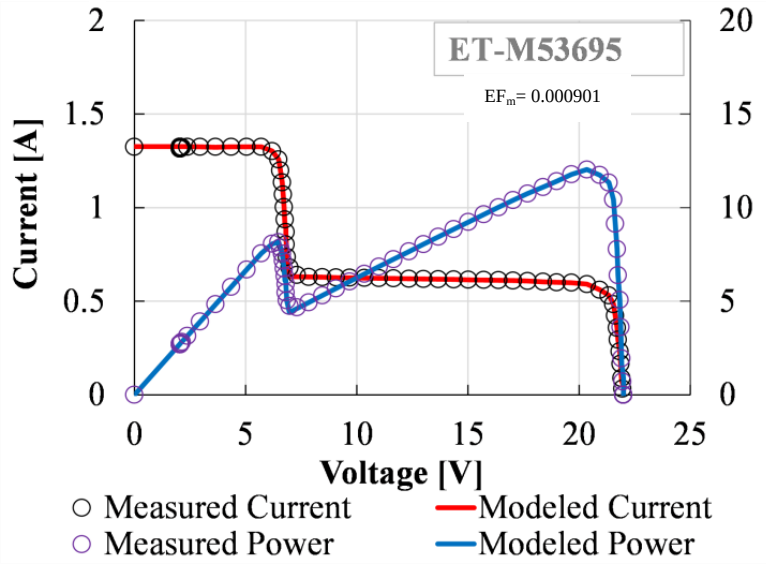

(b)

Figure 17. I-V and P-V curves obtained using the proposed model and experimental data for the scenario a with irradiance level of 677W/m2 and back-surface module temperature of -14.36 °C: (a) CS6P-260P (polycrystalline), (b) ET-M53695 (monocrystalline).

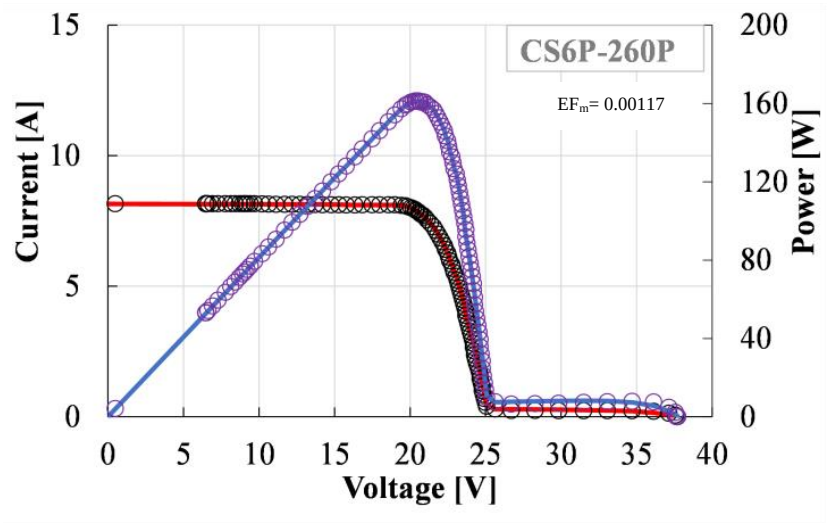

(a)

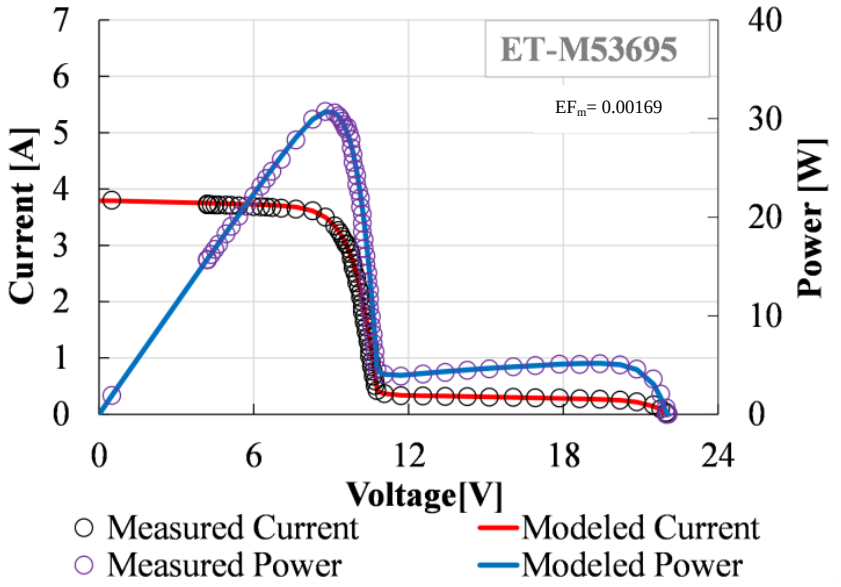

(b)

Figure 18. I-V and P-V curves obtained using the proposed model and experimental data for the scenario b with irradiance level of 328W/m2 and back-surface module temperature of -3.41 °C: (a) CS6P-260P (polycrystalline), (b) ET-M53695 (monocrystalline).

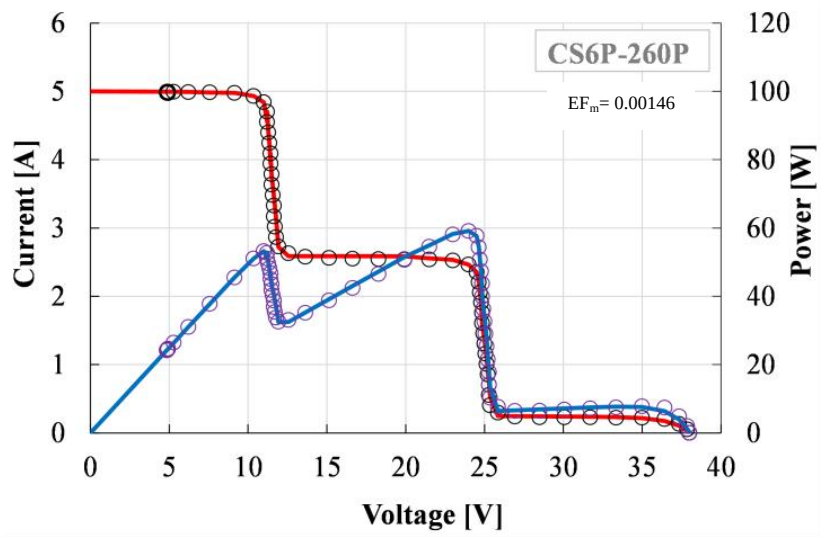

(a)

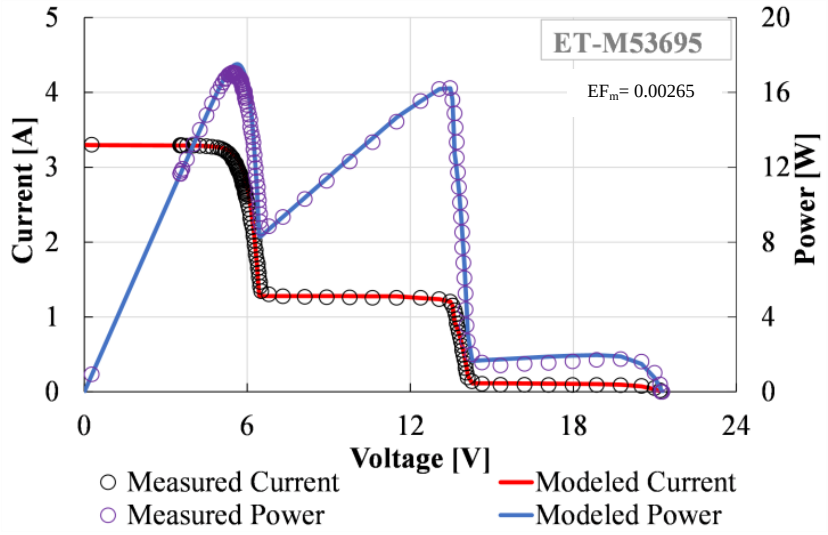

(b)

Figure 19. I-V and P-V curves obtained using the proposed model and experimental data for the scenario c with irradiance level of 825W/m2 and back-surface module temperature of -8.41 °C: (a) CS6P-260P (polycrystalline), (b) ET-M53695 (monocrystalline).

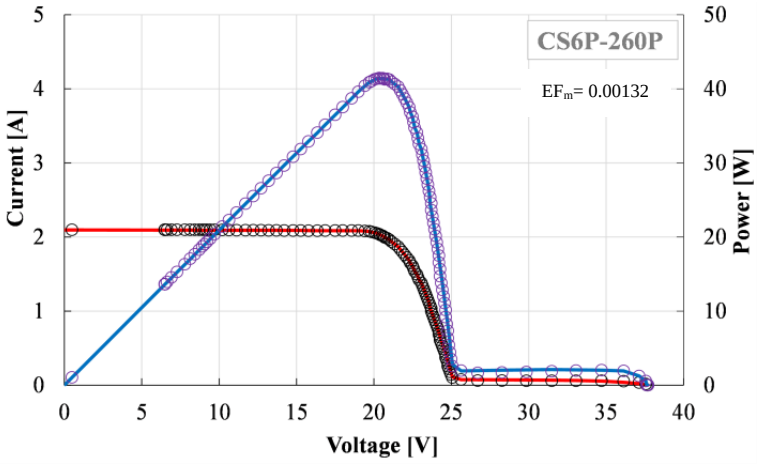

(a)

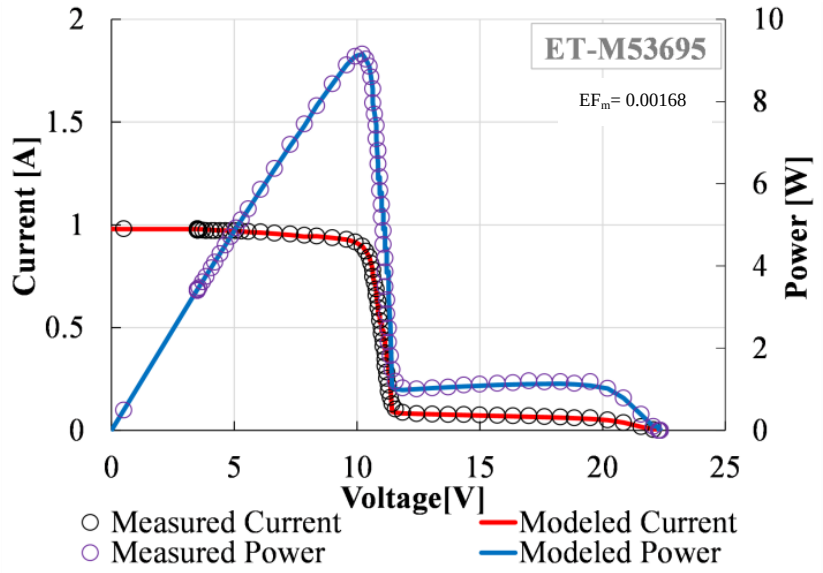

(b)

Figure 20. I-V and P-V curves obtained using the proposed model and experimental data for the scenario d with irradiance level of 210W/m2 and back-surface module temperature of -11.13°C: (a) CS6P-260P (polycrystalline), (b) ET-M53695 (monocrystalline).

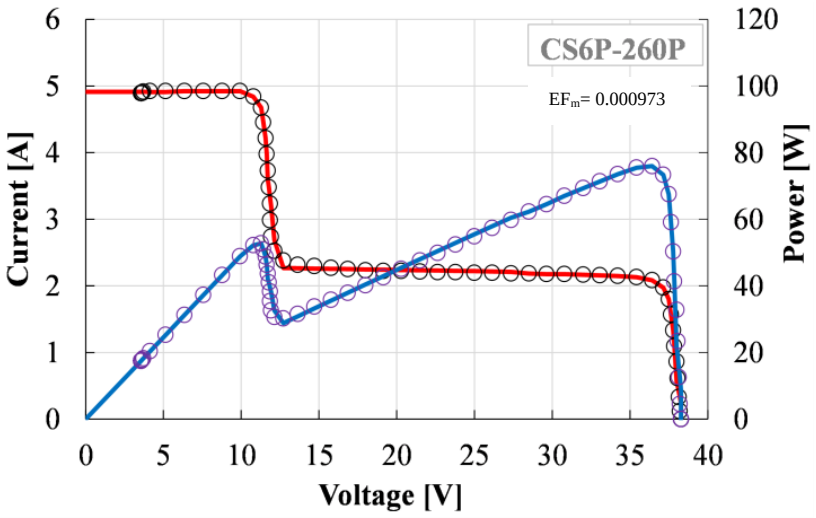

(a)

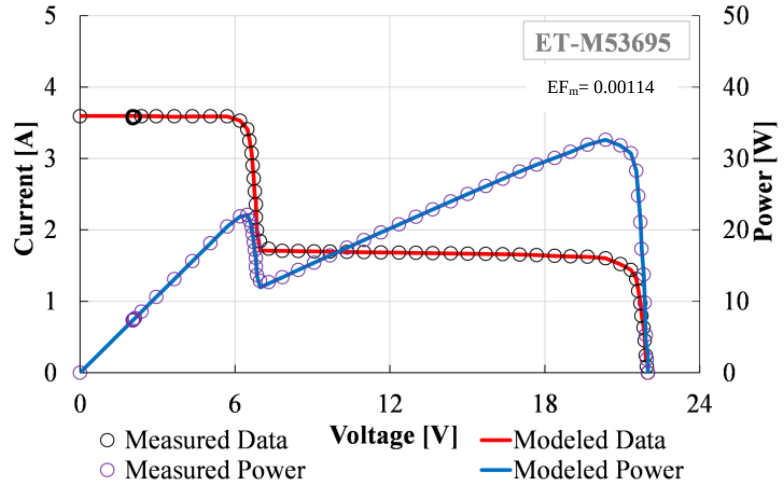

(b)

Figure 21. I-V and P-V curves obtained using the proposed model and experimental data for the scenario e with irradiance level of 525W/m2 and back-surface module temperature of -4.36°C: (a) CS6P-260P (polycrystalline), (b) ET-M53695 (monocrystalline).

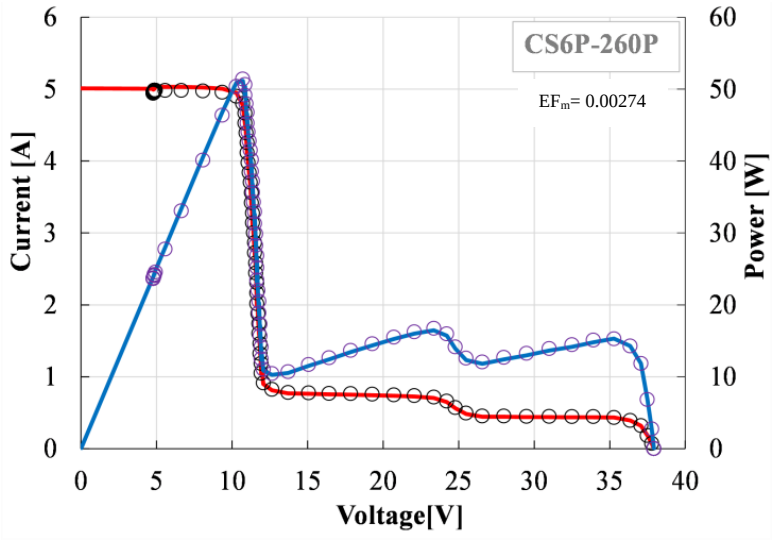

(a)

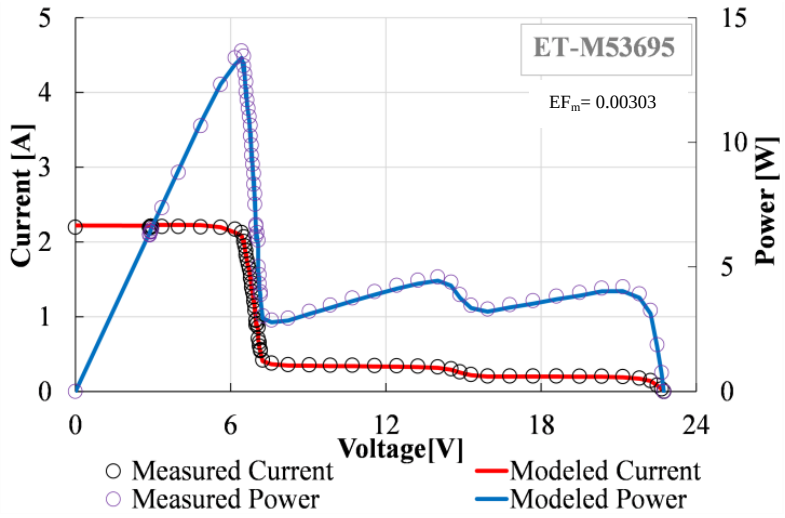

(b)

Figure 22. I-V and P-V curves obtained using the proposed model and experimental data for the scenario f with irradiance level of 710W/m2 and back-surface module temperature of -9.43 °C: (a) CS6P-260P (polycrystalline), (b) ET-M53695 (monocrystalline).

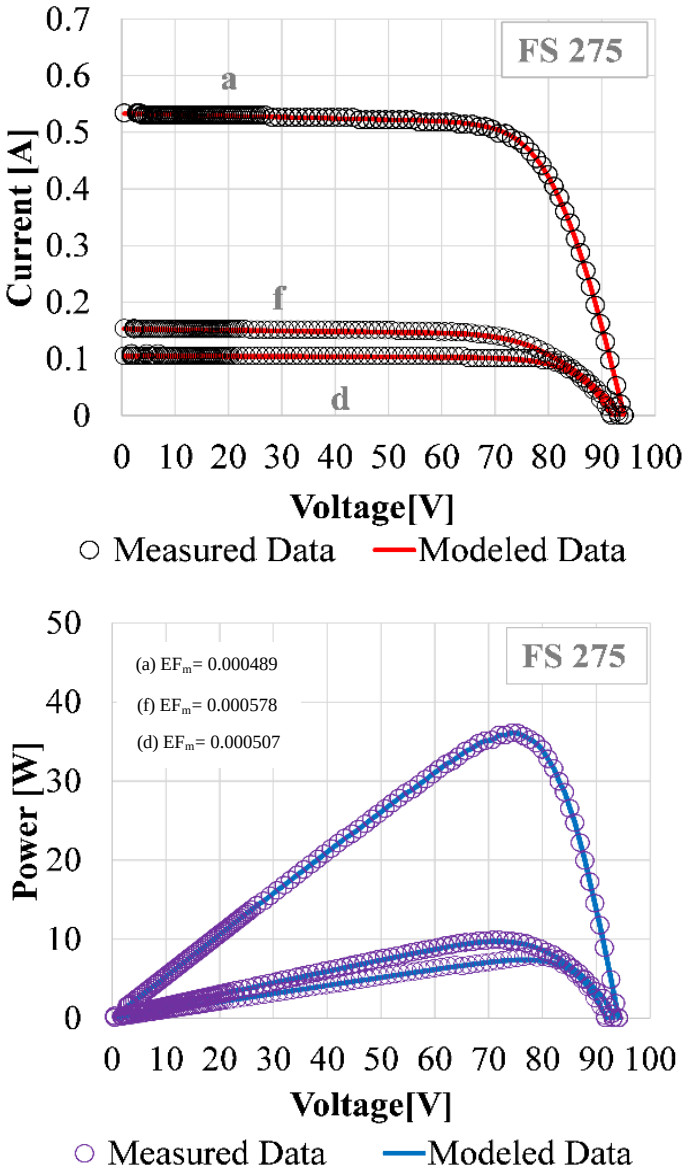

Figure 23. I-V and P-V curves obtained using the proposed model and experimental data under different partial shading conditions for the technology of FS-275 without bypass diodes where irradiance levels and back-surface module temperatures for the respective scenarios are a: G_{ir}= 482.4 W/m2; T_c= -21.11°C, d: G_{ir}= 517.8 W/m2; T_c= -15.24°C , f: G_{ir}= 479.8 W/m2; T_c= -18.99°C.

According to the function of equation (20), the percentage of output power deviation is also plotted for the most complicated characteristics of different PV modules technologies to illustrate the degree of agreement between the theoretical and measurement results as follows:

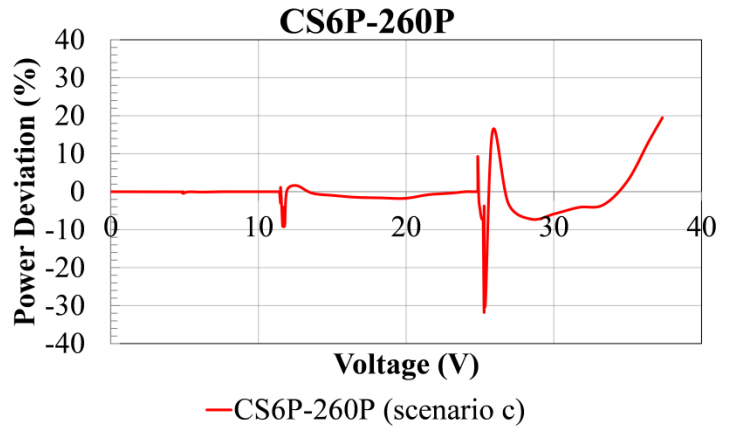

(a)

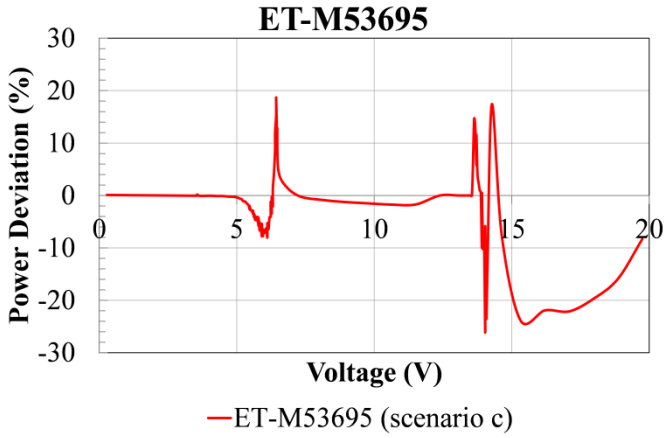

(b)

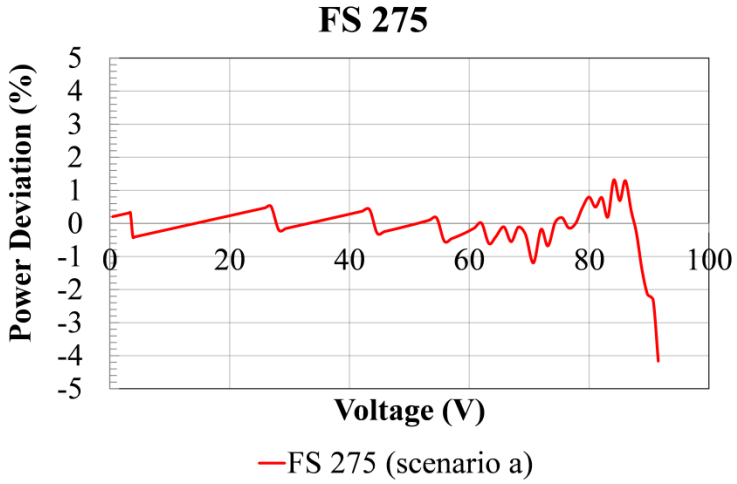

(c)

Figure 24. Percentage of output power deviation between the proposed model and experimental data for: (a) CS6P-260P (polycrystalline), (b) ET-M53695 (monocrystalline), and (c) FS-275 (thin film). These graphs demonstrate the instant variation of power deviation in each point of output voltage which shows sharp spikes in peak point of characteristics.

3.3.1.2.1 Errors of Modeling Algorithm

According to the inherent feature of the proposed modeling method, the pairs of voltage and current data points of experimental characteristics should be imported to the modeling algorithm for extracting the model parameters and then the modeled characteristics will be plotted based on the extracted parameters. Hence, the total accuracy of the proposed modeling method can be evaluated based on the mismatch between the pairs of data points that form the measured and modeled characteristics. Therefore, the root mean square error which is calculated based on the difference between the two different sorts of data points is the best error function to confirm the agreement between the measured and modeled data. Hence, for each curve of I-V and P-V characteristics in Figures 17 to 23, the value of the average root mean square error (EF_m) is calculated as an indicator on the relative point-to-point deviation between the simulated model and data experimentally measured from the test field. These values are provided in Table 9 (related to Figs. 17 to 23), for a better evaluation of the model accuracy. Although, the values of errors for the modeling method demonstrate the accuracy of the proposed algorithm, the measurement error relevant to the measurement uncertainty of data acquisition equipment (HT Instruments I-V 400 PV Panel Analyzer) should be considered too. As mentioned in section 2.3.2.3.2, as per the manufacturers' specifications, this error is ranged in 1-5%. The latter error can be useful to give a perspective about the quality of measured data used for the theoretical part of algorithm.

Table 9 Average root mean square error of modeling method

Scenarios	CS6P-260P	ET-M53695	FS 275
a	0.00081	0.000901	0.000489
b	0.00117	0.00169	–
c	0.00146	0.00265	–
d	0.00132	0.00168	0.00507
e	0.000973	0.00114	–
f	0.00274	0.00303	0.000578

The relative point-to-point average root mean square error (EF_m) as a fitness index between the measured and the simulated curves is shown in Figure 25. This figure demonstrates the good accuracy achieved by the proposed modeling approach.

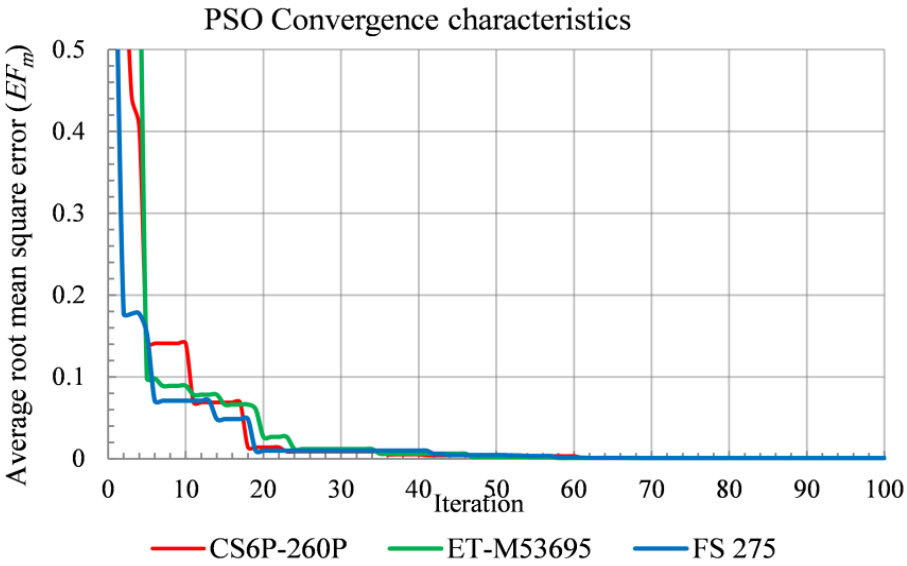

Figure 25. Average root mean square error between the proposed model and the experimental data.

The first part of experimental results was extracted from the PV technologies of CS6P-260P and ET-M53695 were both protected by three bypass diodes. Thus, the P-V curves of these modules have at most three peak points in the case of snow partial shading. For better understanding the effect of bypass diodes on the characteristics of PV systems, the technology of FS-275 PV panel which manufactured with no bypass diode was also experimentally tested. As depicted in the Figure 23, under different conditions of snow partial shading the P-V curve has only single peak point of power with corresponding single knee in the I-V curve.

3.3.1.3 Snow-related Power Loss and Efficiency of Snow Shaded Modules

Solar systems show a good performance in harsh cold weather because the low temperature can increase positively the output power. However, the accumulation of snow on the surface of PV modules can decrease or even stop electricity generation leading to considerable power losses. Therefore, a series of tests were carried out on a CS6P-260P polycrystalline PV technology to determine the impact of snow accretion on PV power

losses. In fact, the measured values of MPPs under different snow thickness were compared with a snow-free condition to determine the power losses in percentage. Figure 26 and Figure 27 show the performance of the PV module under different snow patterns. As can be seen from Figure 26, the snow depth is a determining parameter for the energy losses in which the performance of the PV module decreases to a critical value of 50%. Figure 27 shows that the variation of snow losses increases with an increase in the shaded area by snow.

The percentage of power losses can be evaluated as a function of the shading factor $\propto_i$, the snow depth in each contour x_i, the average amount of extinction coefficient k_{ext}, and ω using equation (32). By considering the average value of the extinction coefficient 35.5 m^{-1} and 0.315 for ω in the test, the estimated power loss is calculated and shown by the dashed green line in Figure 26 and Figure 27. The accordance between the estimated power loss calculated using equation (32) and the real snow loss of the system demonstrates that the proposed power loss equation can be regarded as a tool for the selection and proper installation of PV modules subjected to snow accretion.

$$P_{loss}(\%) = \left[\sum_{i=1}^{k} \propto_i \cdot \left(1 - \frac{\omega\, e^{-k_{ext}\, x_i}(1+\tanh\, k_{ext}\, x_i)}{\left\{1+\frac{\omega}{2}\left[1+\frac{e^{-k_{ext}\, x_i\left(1-\frac{\omega}{2}\right)}}{\frac{\omega}{2}\cosh\, k_{ext}\, x_i+\sinh\, k_{ext}\, x_i}\right]\right\}\left(\frac{\omega}{2}+\tanh\, k_{ext}\, x_i\right)}\right)\right] \times 100 \qquad (32)$$

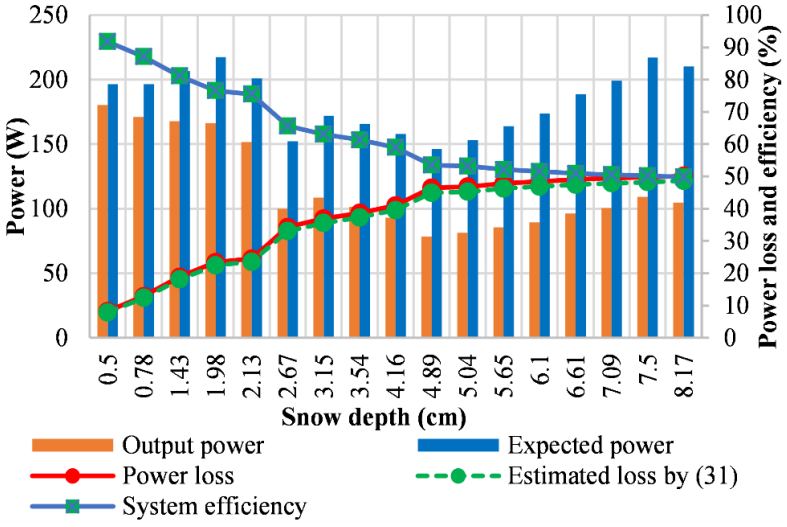

Figure 26. Effect of different snow depths on power production, losses and efficiency of CS6P-260P with the shading factor of 0.5.

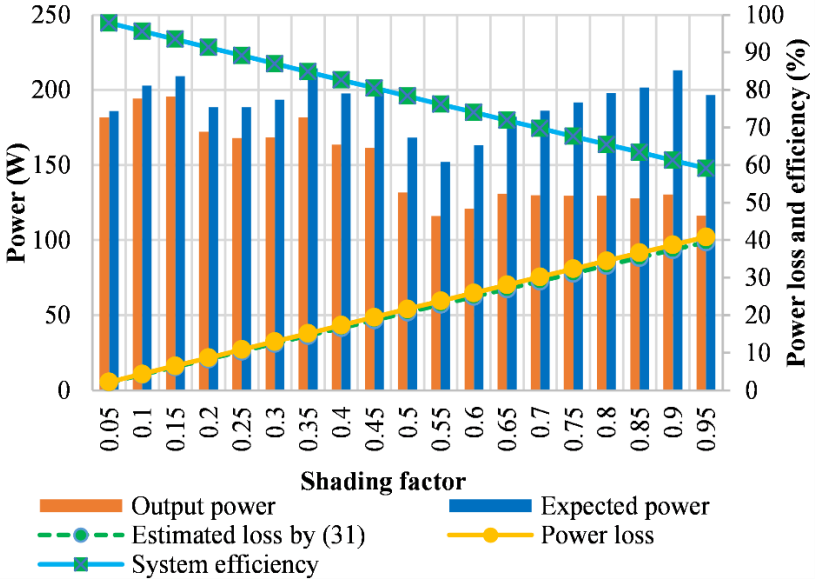

Figure 27. Effect of different shading factor on power production, losses and efficiency of CS6P-260P with the snow depth of h= 1.4 cm.

3.4 Summary for the Modeling of PV Modules Covered with Nonuniform Snow

This chapter focused on the modeling of the effect of nonuniform snow on electrical behavior of PV systems. Hence, the idea of multi-zone analysis of PV characteristics was developed to model the behaviour of PV modules covered with nonuniform snow patterns under partial shading conditions. The platform of the proposed modeling approach was designed based on the single-diode-five-parameter equivalent circuit, incorporating the Giddings and LaChapelle theory to accurately estimate the received irradiance to the underneath surface of PV modules in the presence of snow. Through a contour-based discretization methodology, any nonlinear PV characteristics were divided into the separate linear ones, each one including a single peak. A swarm-based optimization methodology was adapted to instantaneously update and evaluate the modeling parameters of each sub-zone to accurately characterize the output of the PV system. Moreover, a power loss equation of non-uniformly-covered snowy PV panels was introduced and validated using real data from experimental tests. Finally, the proposed model was successfully validated using three different commercial types of PV technologies commonly used in North

America. This research work can be regarded as a basis for the development of PV models and a practical tool for the design and selection of PV modules subjected to snow.

4 ANALYSIS OF PV PANELS LAYOUT UNDER SNOW CONDITION

4.1 Overview

One of the main strengths of PV systems is their robustness in severe environments, as they do not involve moving parts or components that can be easily broken physically. However, during cold months, the snow accumulation diminishes the received irradiance at the surface of PV panels. The snow coverage blocks the sunlight's path to the solar cells and significantly reduces the electricity production of PV modules. In the previous chapters, the performance of PV panels under different forms of snow shading were introduced and modeled in terms of output characteristics, power generation, and snow losses. Contrary to uniform snow deposit, the panel layout influences the efficiency of the PV under snow partial shading conditions. This chapter proposes an analysis of the effect of PV panels layout on their electrical characteristics under partial shading conditions due to nonuniform snow deposits. A series of outdoor experiments are conducted taking into account different snow removal scenarios on different technologies of PV modules (i.e. with and without bypass diodes protection) to determine snow losses. Moreover, the performance of the bypass diodes' protection and their effect on the output characteristics of the partially shaded PV modules are studied. The results of this section can be helpful for PV system developers for selecting the appropriate PV panels layout in the cold regions.

4.1.1 Effect of Bypass Diodes on the Characteristics of Snow Shaded PV Modules

In a partially shaded module, solar cells that belong to the same string experience different polarization. It means that a reverse biasing which occurs for the shaded cells makes them as electrical loads for the power generated by the other cells. Therefore, a current limitation will happen for the normal cells in the whole string. This leads to power dissipation, which dramatically reduces the output power of the PV module, and results in hotspot phenomena and irreversible damage in the shaded cells [135]. To avoid the detrimental effects of hotspot destruction, a bypass diode is connected in anti-parallel with

cell strings to route a replacement current pass and cut off the output power of the mismatched cells. For the efficient utilization of the solar system in both commercial and research applications, it is essential to deal with the nonlinear characteristics of its output. This nonlinear behavior gets more complicated if the PV module is affected by the non-ideal operating in partial shading conditions. Under this mismatch condition, with respect to the electrical properties and structure of PV modules, as well as the shading pattern and intensity, PV system characteristics deviate from their standard form. For the PV modules with more than one bypass diode, partial shading leads to the multi-peaks P-V curve and multi-knees I-V curve. Hence, in order to predict, analyze, and design the PV system for all conditions of operation, the effect of bypass diode that causes multiple local maxima under partial shading conditions should be considered in the modeling of PV modules production [136].

Although the PV manufacturers normally use bypass diodes to prevent the hot-spot problem and to stop unproductive cells from disrupting the production of active cells, the PV characteristics of the shaded PV array become more complicated showing multiple peaks in the P-V graph. This phenomenon can be seen in Figures 15 to 21 in which the P-V characteristics bear multiple peaks under the condition where the bypass diodes operate to protect cells. In fact, the number of peaks over a partially shaded module depends on the number of bypass diodes and the irradiance level.

As shown in Figure 28(a) the shape of the I-V curves of PV modules in a normal operating condition has only a single-knee curve. On the other hand, Figure 28(b) illustrates the behavior of PV module characteristics when subjected to the partial shading conditions due to nonuniform snow (Figure 16(a) where its characteristic contains a double-knee I-V curve (analysis of the Figure 17). The counterpart P-V curve of this shading scenario has two peak points; the left-most peak point in the curve indicates the transition point where the two bypass diodes are protecting the cell strings switches from non-conducting state to the conducting state or vice versa. Based on the trend of voltage and current from the origin, within the left region of the left peak point, the value of current is large while the voltage value is small. Thus, the bypass diodes protecting the shaded cell strings are in a conducting state and the other one is in a non-conducting state. Within the right region of the left peak point the current value is decreasing while the value of voltage is increasing.

Therefore, the state of all three bypass diodes switches to the non-conducting state and the second peak point is generated for the rest part of the characteristic.

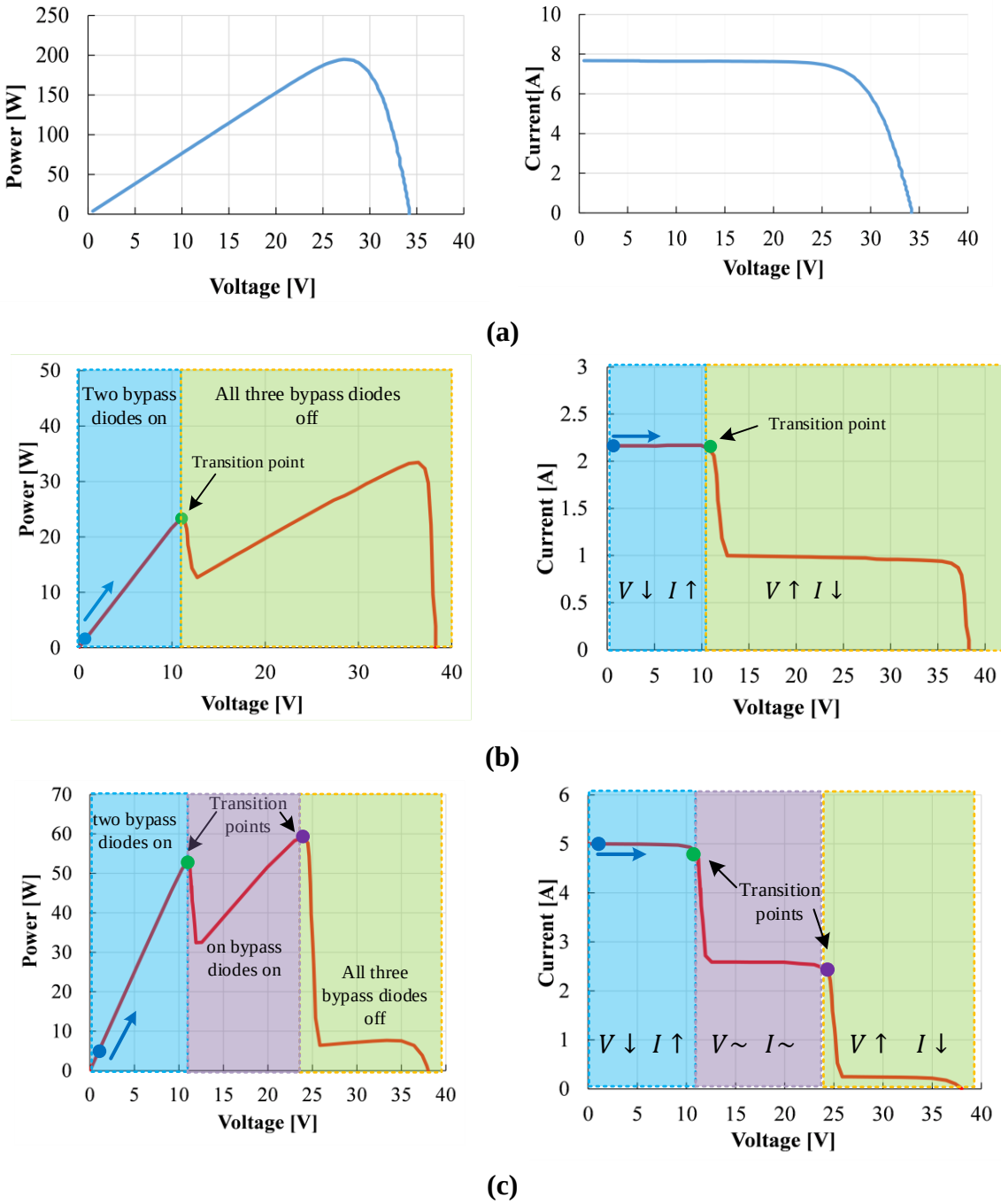

Figure 28. Analysis of PV modules characteristics under different condition: (a) normal operation with uniform irradiance (b) nonuniform irradiance with double steps (c) nonuniform irradiance with triple steps.

For the second scenario of shading (Figure 18), the snow coverage area only affects one cell string and consequently one bypass diode that corresponds to this shaded area

switches in different regions of the curve in Figure 17 similar to the analysis of shading for the first scenario in Figure 28(b). The I-V and P-V curves can include triple steps of current when the all three bypass diodes are affected by the shaded areas on the entire cell strings of PV module. The characteristic in Figure 19, divided into the three regions, as shown in Figure 28(c), where at the left-most power peak point, the two bypass diodes with the more shaded area will be in conducting state. Within the region between the left-most peak point and the middle peak point, the bypass diode with the most shaded area will remain in conducting state and the other two will be in the non-conducting state; finally, for the right side area of the middle peak point, all bypass diodes will switch to the non-conducting state.

4.1.2 Effect of PV Panels Layout

For the sake of optimal use of PV systems, a detailed plan for designing the layout of the solar panels with respect to their applications is required. The output power production of a PV system is determined according to the number of solar modules installed within the available space. It is possible to install photovoltaic modules in a landscape, portrait, or diagonal layouts depending on the configuration of a specific area. For instance, for some applications, i.e. for the rooftops installation, it is recommended to use portrait panels layout [83].

Concerning the solar energy efficiency, the layout of panels is not an issue for the non-shaded PV panels. In other words, under the uniform irradiation, solar panels mounted horizontally perform as well as those mounted vertically and diagonally. With regard to cost, a vertical mounting layout is recommended for standard rooftop racking systems. Thus, installing the PV modules with a horizontal or diagonal layout requires more rows and consequently, additional hardware and increased cost [82]. With less hardware, wiring can be less complicated for the vertical installation rather than horizontal and diagonal-mounted solar panels that leads to an easier and quicker installation task [84].

Although the abovementioned instructions recommended for selecting the appropriate PV panels layout under snow free condition is useful, they could be improper for solar systems under variable cold weather conditions. For the PV systems subjected to the snow

accretion, particularly under nonuniform snow accumulation, the PV panel layout could represent a unique challenging issue. To the best of our knowledge, there is a lack of research to investigate the effect of snow partial shading on the energy production of PV modules. Recently, a research was carried out to characterize the electrical behaviour of snow-covered PV cells under two different PV layouts. However, due to lack of systematic experimental results, this numerical based-investigation could not represent the real effect of PV layouts under different common snow patters [85]. To this end, this chapter deals with the effect of different PV panels layouts on energy losses under partial shading condition, in a comprehensive, experimental way.

4.2 Results on the Analysis of PV Panels Layout

4.2.1 Effect of PV Panels Layout on Their Electrical Behavior under Partial Shading Conditions

In this part of the thesis, three scenarios for snow shading patterns were considered to evaluate the behavior of PV modules as illustrated in Figure 29. To eliminate the problems related to the randomness in the position and size of shaded zones, artificial nonuniform patterns were manually created by partially removing the snow coverage. According to the layout of the PV modules in the configuration of PV arrays, these scenarios are the probable partial shading patterns when some parts of snow on the surface melt or slide down. Several measurements of the environmental conditions, as well as electrical, optical, and thermal variables were recorded under different variations of irradiance, temperature, and snow depth.

The experiments were performed on monocrystalline technology with three bypass diodes as well as thin film technology without bypass diodes. Shading profiles are categorized into three scenarios as follows:

- Vertical shading profile (scenario 1): a snow removal vertically from 100% (fully shaded) to 0% (snow free) coverage as illustrated in Figure 29(a).
- Horizontal shading profile (scenario 2): a snow removal horizontally from 100% (fully shaded) to 0% (snow free) coverage as illustrated in Figure 29(b).

- Diagonal shading profile (scenario 3): a snow removal diagonally from step 1 to step 10 (snow free) coverage as illustrated in Figure 29(c).

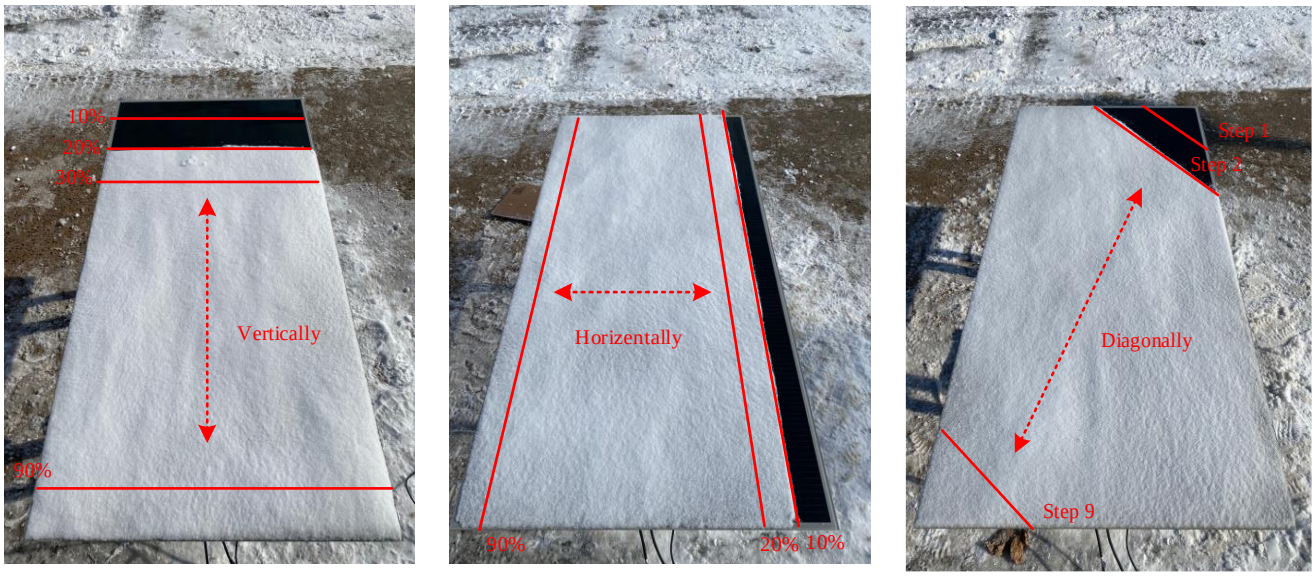

(a) **(b)** **(c)**

Figure 29. Shading scenarios of PV modules: (a) vertical shading profile (b) horizontal shading profile (c) Diagonal shading profile.

The results of the current-voltage and power-voltage characteristics obtained from the experiments on two PV modules technology under different shading scenarios are depicted in Figures 31 – 36 for two PV technologies. According to the trajectory of characteristics variation, some linear and nonlinear changes are recorded, which have not been investigated before in the modeling of snow shaded modules. In the following section, the electrical characteristics of monocrystalline (with bypass diodes) and thin film (without bypass diodes) are analyzed.

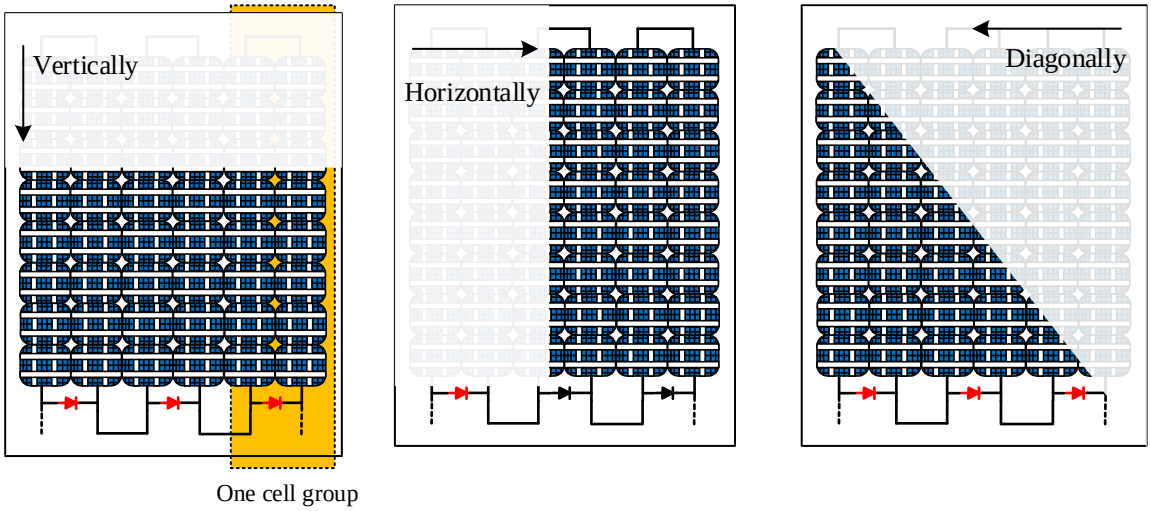

Figure 30. The state of bypass diodes for monocrystalline technology under different snow shading scenarios (a) vertical (b) horizontal (c) diagonal

4.2.1.1 Monocrystalline Technology

In the monocrystalline technology, the cell groups are horizontally arranged and for each group of cells, a bypass diode is considered to protect all cells in the group. Hence, in each scenario, if a group of cells is covered, its relevant protection bypass diodes get turned on. In addition, the effect of diode protection is that it causes a rapid reduction in the output peak power and leads to a step change in the electrical characteristic for each irradiance level. The behavior of electrical characteristics PV modules is analyzed according to relevant scenarios, represented in Figure 31 with bypass diodes, as follows:

- Scenario 1**:** as illustrated in Figure 30(a) all three cell groups are simultaneously affected by the snow layer. Hence, all three bypass diodes are in conducting state. Therefore, as shown in Figure 31, the PV characteristics do not show multi-steps current-voltage characteristic in this condition and the peak power decreases considerably with an increase in snow coverage.

- Scenario 2**:** as long as each group of cells gets free of snow gradually, their relevant bypass diodes get turned off as shown in Figure 30(b). Thus, the PV characteristics demonstrate step changes with respect to the level of the incident irradiance (Figure 32). Therefore, in this scenario, the bypass diodes show nonlinear behaviors that cause multi-steps current-voltage characteristics.

- Scenario 3: Regarding the snow coverage in Figure 30(c), the cell groups are mostly under coverage at the same time. Thus, the bypass diodes are conducting altogether and the characteristics demonstrate generally linear variations. However, in the case in which some of the cell groups get completely free of snow, their relevant bypass diodes get turned off, leading to multi-steps in the PV characteristics, i.e., in the two last steps of removing in Figure 33 (steps 11 and 12).

4.2.1.2 Thin film Technology

A thin film solar cell is a second-generation solar cell that is made by depositing one or more thin layers or thin film (TF) of photovoltaic material on a substrate, such as glass, plastic or metal. Thin film technology has always been cheaper but less efficient than conventional first-generation crystalline silicon solar cell (c-Si) technology. However, its performance has significantly improved over the years. There is no bypass diode in this technology that results in a linear behavior of electrical characteristics with respect to the snow thickness and a sole single peak even under partial snow shading condition (without multi-steps curvature).

As shown in Figures 34 to 36 from vertical to diagonal layouts, the output characteristics of thin film technology exhibit a single peak due to the lack of bypass diodes. In addition, in comparison with horizontal and diagonal layouts, in the vertical layout, the power production of modules dramatically decreases with an increase in a shaded area and the PV module characteristics still demonstrate linear variation. Hence, although the thin film technology demonstrates simpler characteristics but its efficiency is lower than monocrystalline technology because the MPP is dropped dramatically by increasing the shading area. A visual comparison between the characteristics of Figure 31 to 33 and their counterpart characteristics in Figure 34 to 36 which demonstrate the same snow removal scenarios in two different technologies indicates that the thin film technology has always a single peak characteristic of power-voltage which can utilize simpler MPPT controllers, while its efficiency is lower than monocrystalline technology.

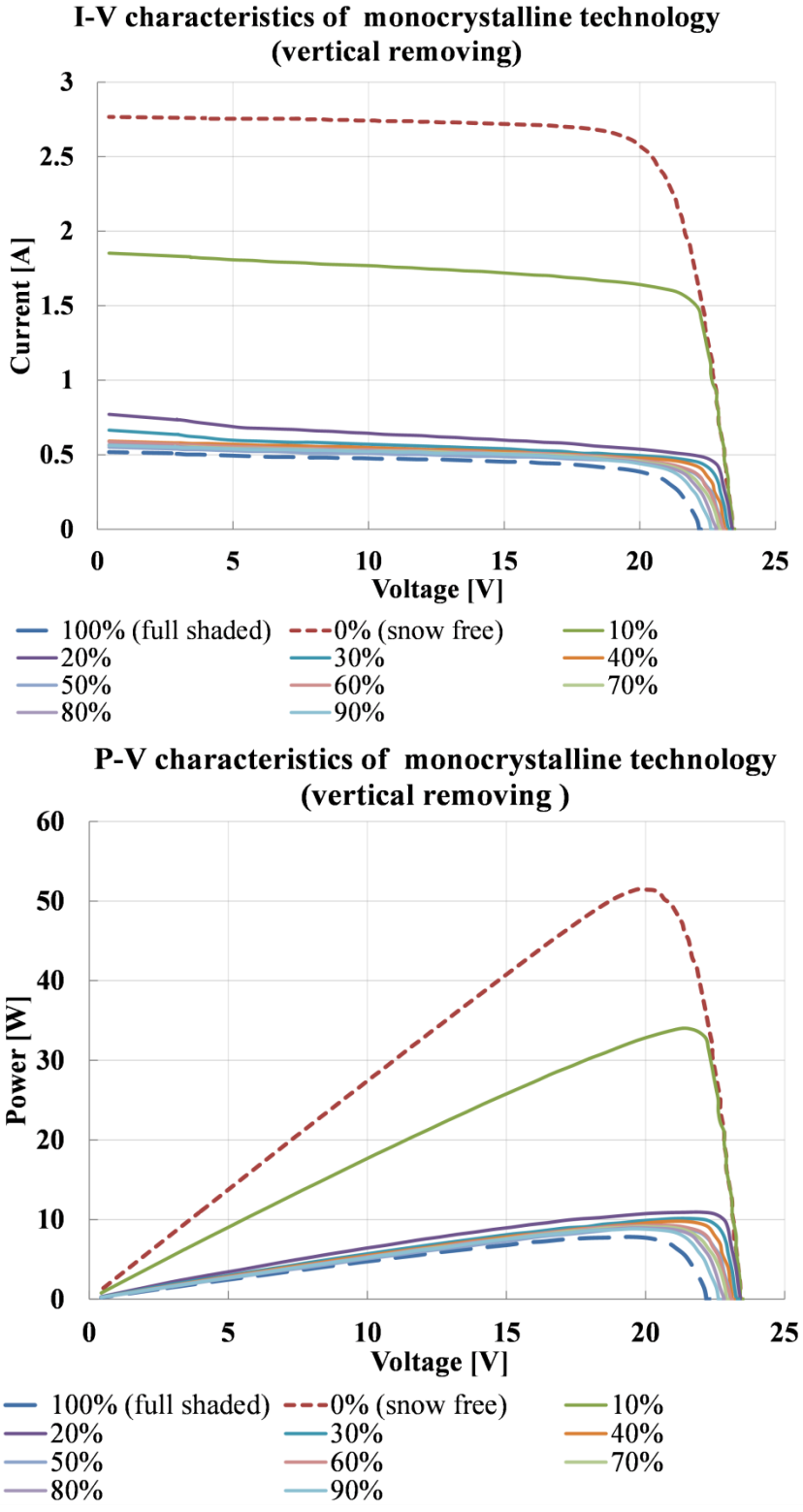

Figure 31. Characteristics of PV module with monocrystalline technology under the vertical snow removing scenario for the snow depth of 3.9 mm when the module temperature and surface irradiance vary from -0.3 °C to -4°C and 420 to 426 W/m2, respectively.

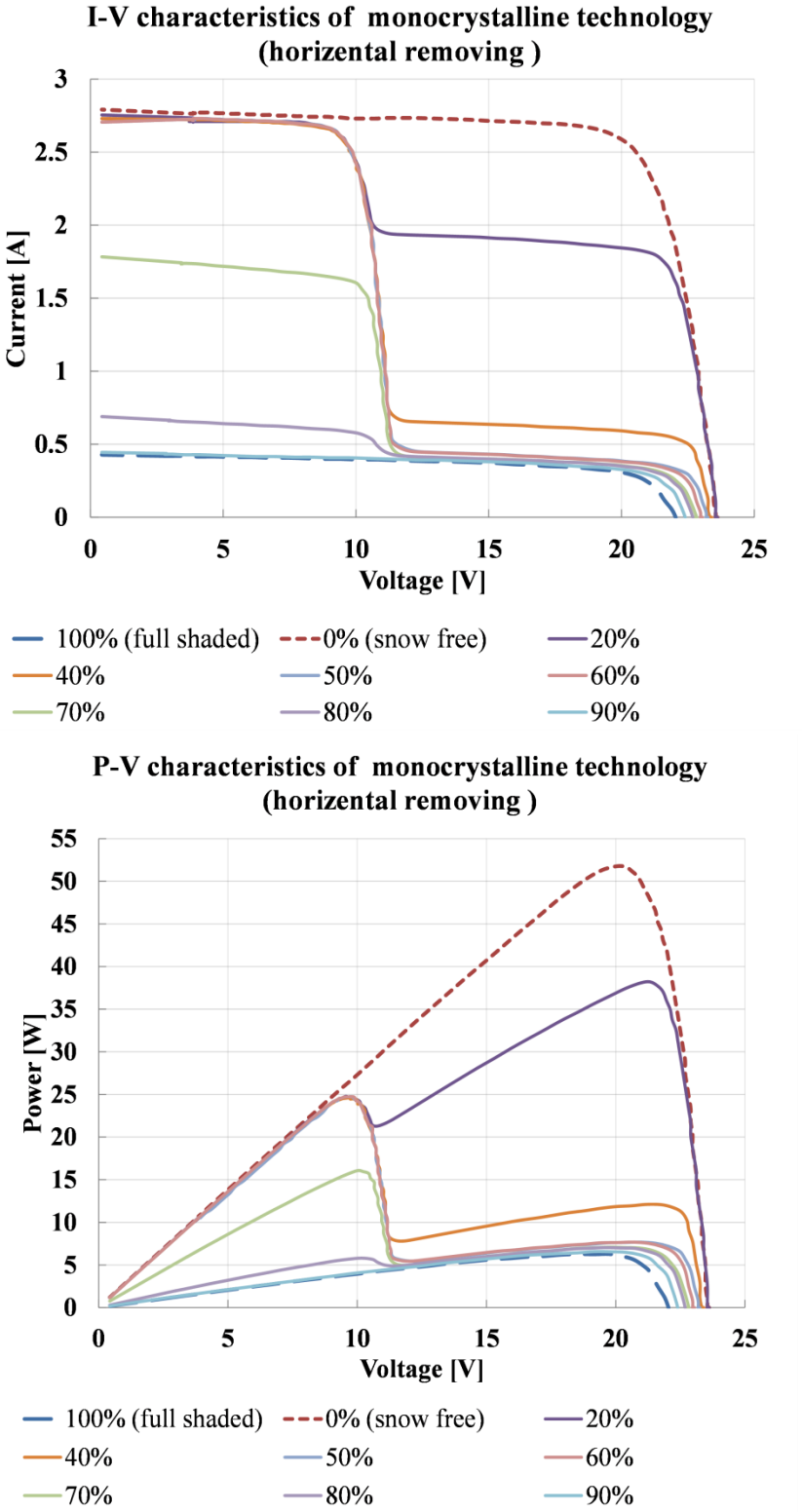

Figure 32. Characteristics of PV module with monocrystalline technology under the horizontal snow removing scenario for the snow depth of 10 mm when the module temperature and surface irradiance vary from -1.3 °C to -4.4°C and 397 to 455 W/m2, respectively.

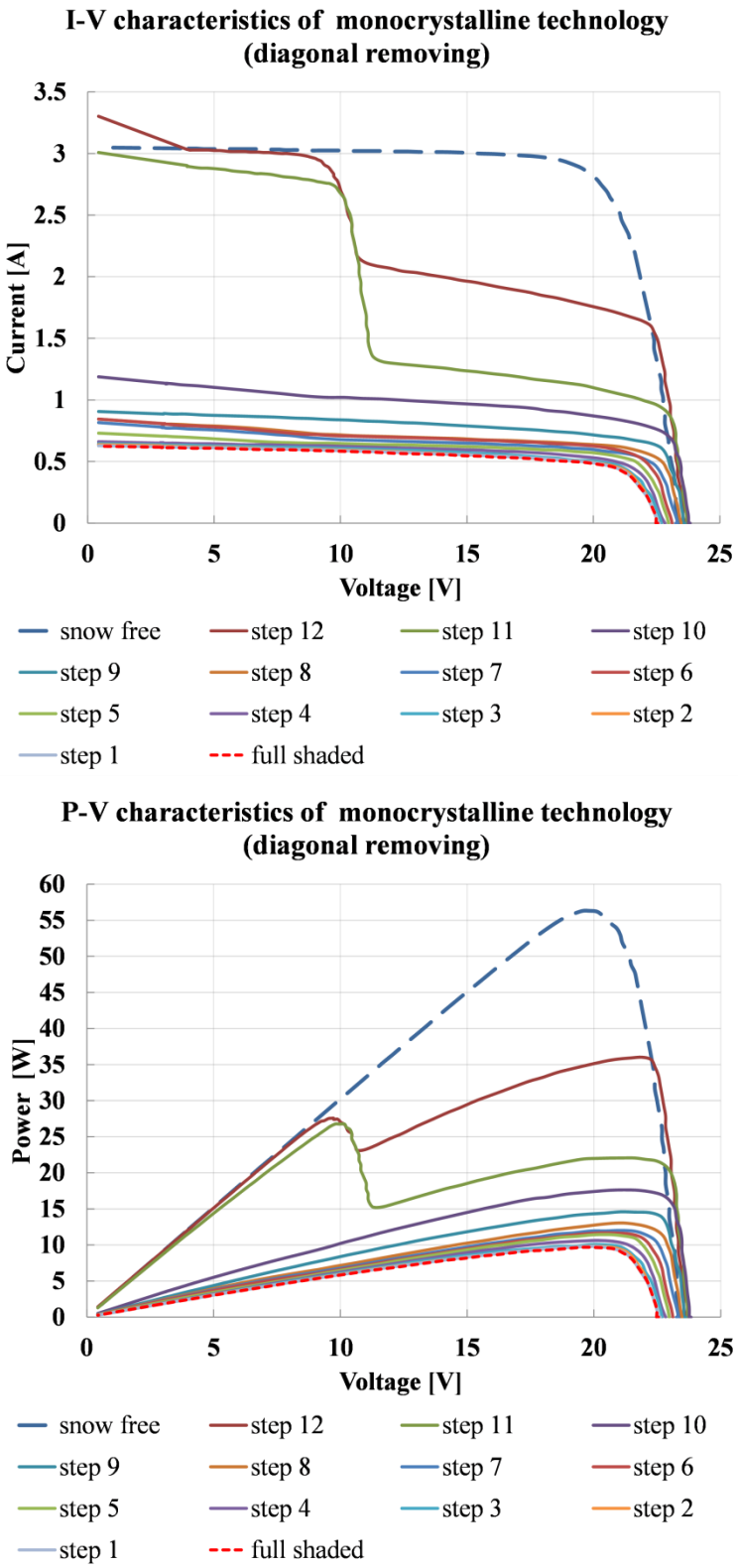

Figure 33. Characteristics of PV module with monocrystalline technology under the diagonal snow removing scenario for the snow depth of 4.9 mm when the module temperature and surface irradiance vary from -6.8 °C to -9.5°C and 479 to 486 W/m2, respectively.

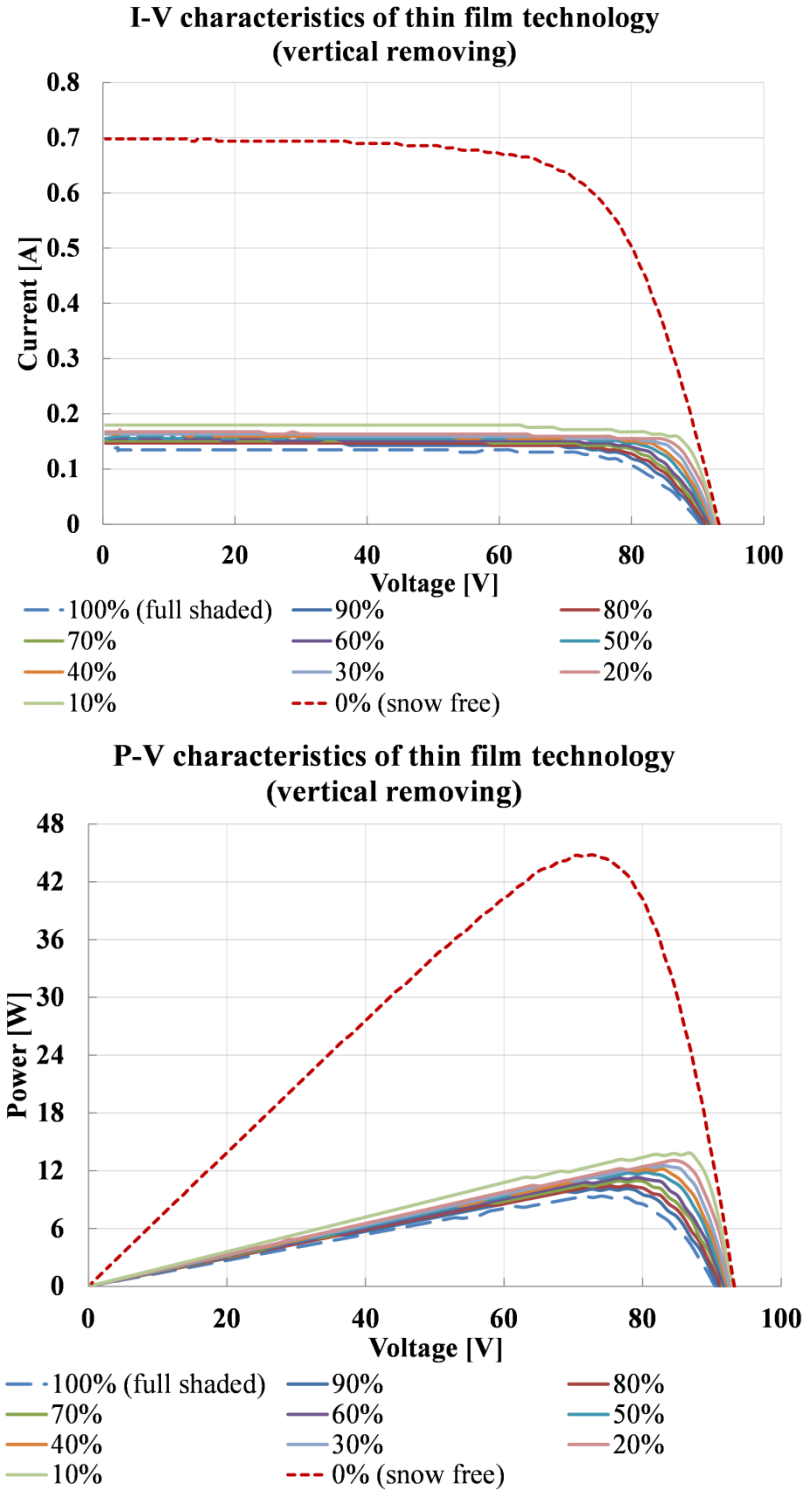

Figure 34. Characteristics of PV module with thin film technology under the vertical snow removing scenario for the snow depth of 4.7 mm when the module temperature and surface irradiance vary from -0.7 °C to +4.3°C and 420 to 426 W/m2, respectively.

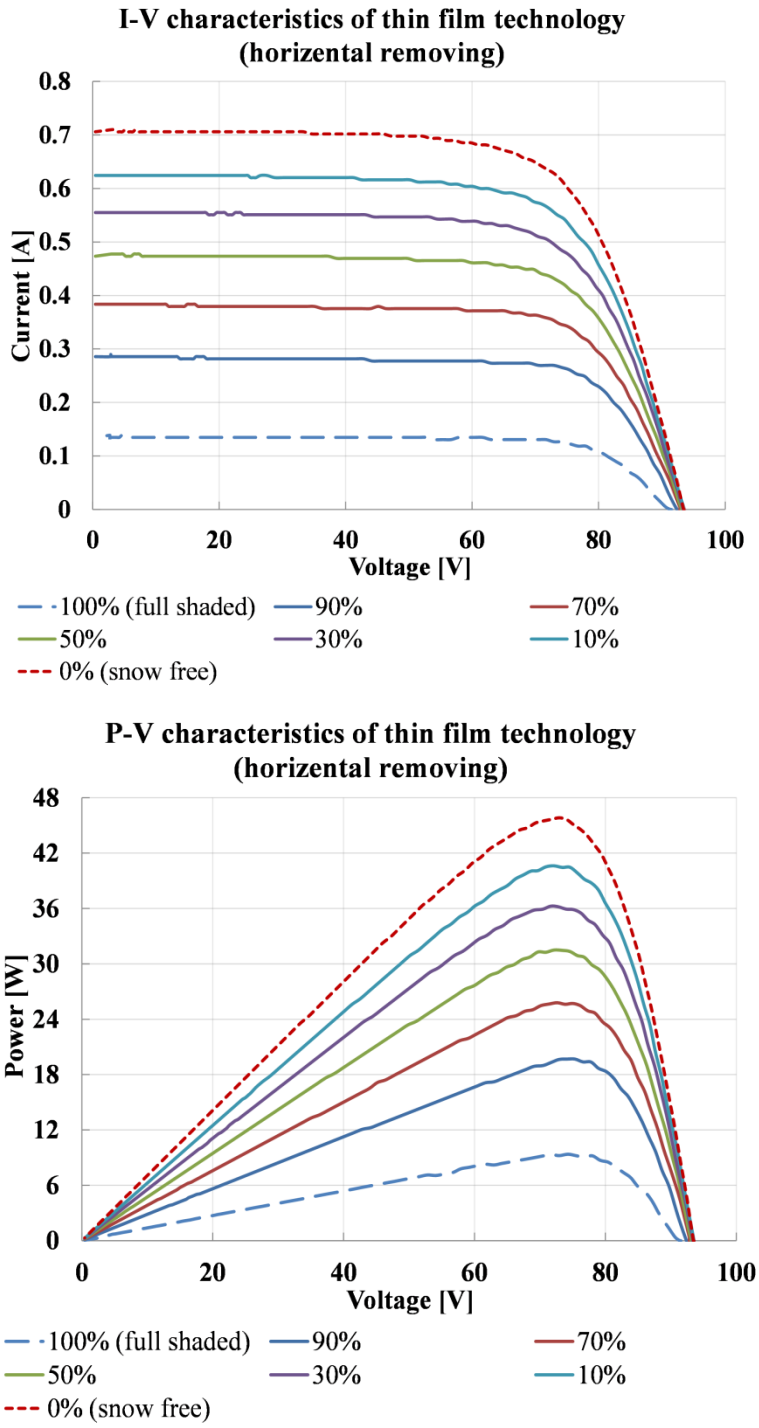

Figure 35. Characteristics of PV module with thin film technology under the horizontal snow removing scenario for the snow depth of 4.5 mm when the module temperature and surface irradiance vary from -0.7 °C to +2.9°C and 454 to 484 W/m2, respectively.

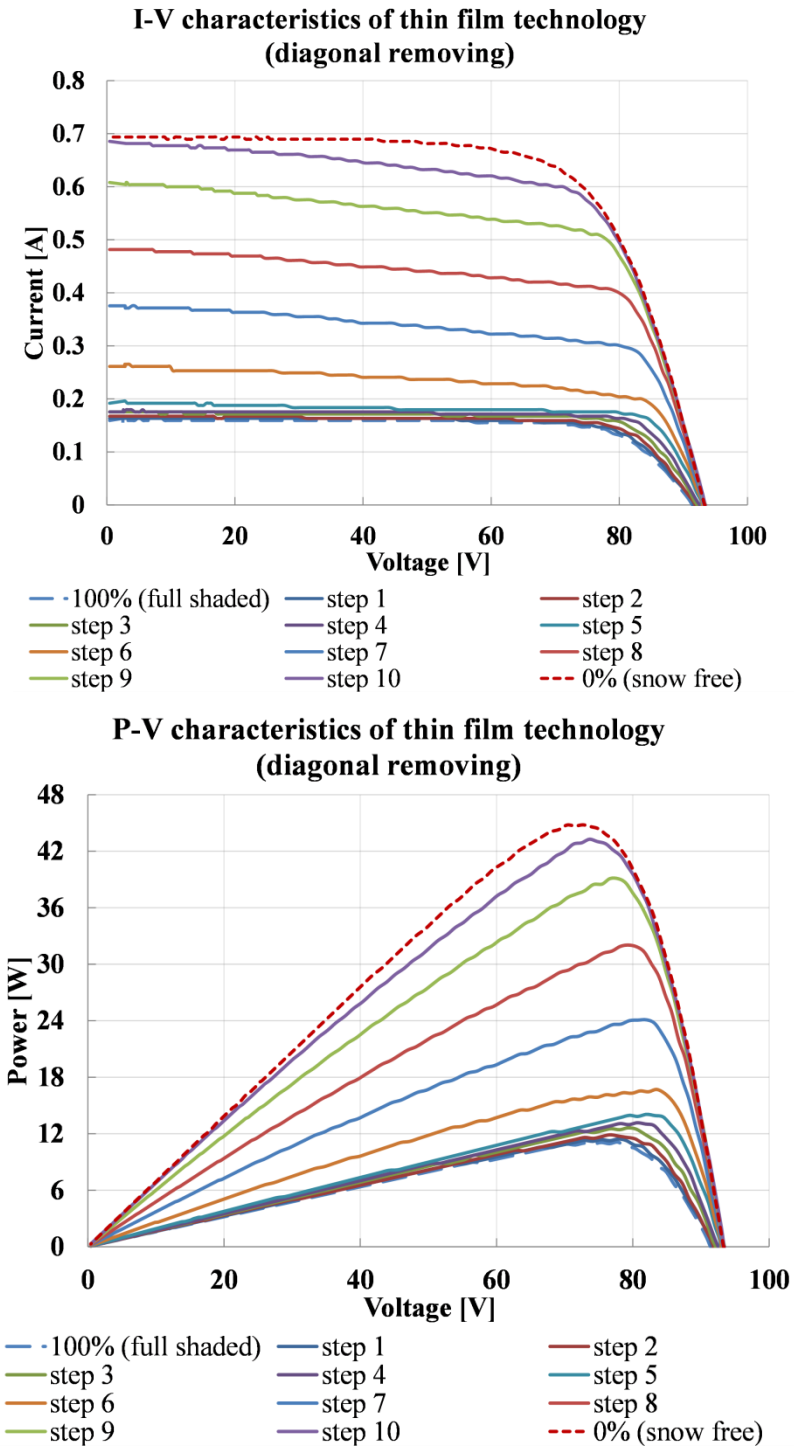

Figure 36. Characteristics of PV module with thin film technology under the diagonal snow removing scenario for the snow depth of 5.1 mm when the module temperature and surface irradiance vary from -0.5°C to +2.8°C and 473 to 498 W/m2, respectively.

4.2.2 Analysis of Snow Power Losses for Different PV Panels Layout

As PV systems are expected to make a significant contribution to supply electricity in a more secure and economic way, it is essential to carry on verifying the effect of their configuration and layout on snow power losses. The percentage of snow power losses for different layouts is determined through a comparison between the power values of global MPP of the snow-covered PV modules against their expected MPP without the snow shading for the same irradiance and temperature. The calculated values of snow losses for the different technologies of PV modules are plotted versus shaded area in Figure 37 (monocrystalline technology) and 38 (thin film technology). For a better comparison, the shaded areas for three different layouts are normalized to have the same condition in term of snow-covered areas.

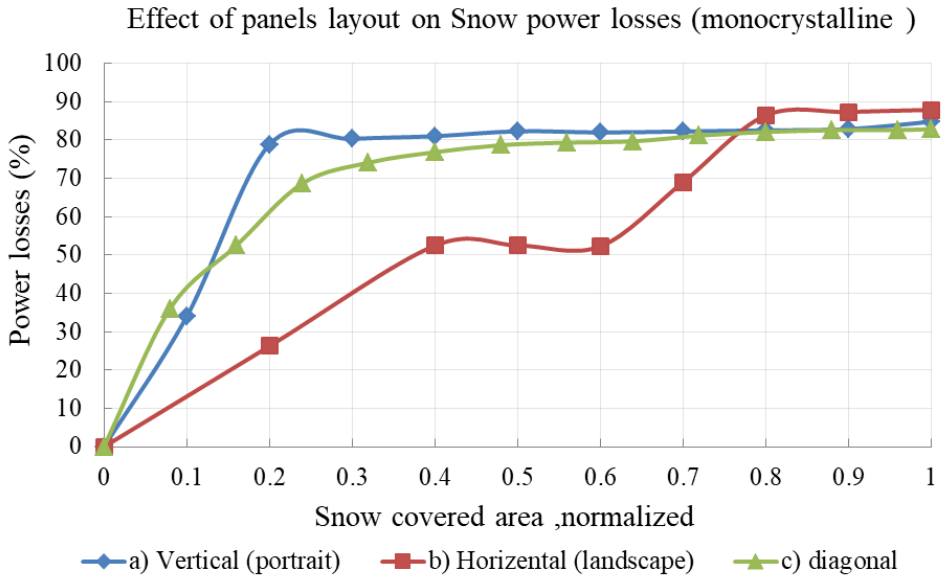

Figure 37. Snow power losses for the monocrystalline technology of PV module under different panels layout: a) portrait layout with the snow depth of 3.9mm, b) landscape layout with the snow depth of 10 mm, and c) diagonal layout with the snow depth of 4.9 mm.

As shown in Figure 35, for the monocrystalline technology, the trajectory of curves depicts that by increasing the shading area, the values of power losses increase with a steeper slope for the vertical and diagonal layouts when compared to the horizontal one. Furthermore, the trajectory of the curve for the horizontal layout evolves into two steps. The creation of these two steps can be due to the bypass diodes in the cell strings arranged

horizontally. It can be observed that, although the depth of snow on the horizontal layout is greater than other layouts, it achieves a lower power loss under snow partial shading.

Table 10. Average snow power losses for different layouts of monocrystalline technology

Layout	Vertical (Portrait)	Horizontal (Landscape)	Diagonal
Depth of snow (mm)	3.9	10	4.9
Average power losses (%)	70.06884	57.11557	68.36463

Table 10 presents the average snow power loss of the abovementioned layouts based on different depths of nonuniform snow patterns. It can be highlighted that, in contrast to the higher depth of snow in diagonal and horizontal layouts in comparison with the vertical layout, the horizontal layout has the lowest average power loss. Thus, the horizontal layout can be considered an optimal configuration for the monocrystalline technology under snow partial shading condition. Although the vertical panel layout is the most popular layout for the arrangement of PV systems, it bears the greatest losses when subjected to snow partial shading conditions.

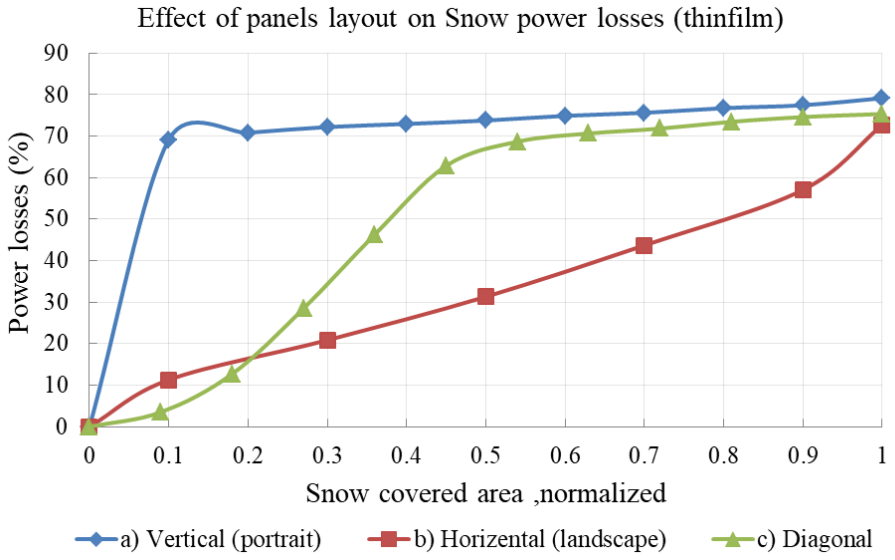

Figure 38. Snow power losses for the thin film technology of PV module under different panels layout: a) portrait layout with the snow depth of 4.7mm, b) landscape layout with the snow depth of 4.5 mm, and c) diagonal layout with the snow depth of 5.1 mm.

For the thin film technology, the power loss due to snow is also experimentally verified when the snow-covered area on PV panels change horizontally, diagonally and vertically, as shown in Figure 38. As snow coverage reduces vertically and diagonally, the reduction in snow loss is small until it reaches the critical shading factors of 0.1 and 0.5, respectively. On the other hand, for the horizontal snow coverage variation, the linear reduction in snow loss when the snow-covered area reduces is significant.

Table 11 presents the average power losses for three layouts for a similar snow depth. Similar to the monocrystalline technology, it can be observed that the horizontal layout is the configuration of PV panels with the lowest power losses. This analysis along with knowledge of snow-melting patterns is helpful for a proper installation of PV panels in cold climates in order to minimize their power loss due to snow.

Table 11. Average snow power losses for different layouts of thin film technology

Layout	Vertical (Portrait)	Horizontal (Landscape)	Diagonal
Depth of snow (mm)	4.7	4.5	5.1
Average power losses (%)	67.53218	33.84083	49.04161

4.3 Summary on PV Layout Analysis

The focus of this chapter was primarily to provide an analysis of different installation layouts of PV modules under snow accretion based on a series of systematic tests. Different scenarios of snow removal were created in vertical, horizontal, and diagonal configurations to emulate their corresponding installation layouts (i.e. vertical, horizontal, and diagonal positions). The output characteristics of the PV modules in different layouts were investigated to determine an appropriate layout according to the application of solar systems. The experiments were conducted on two different technologies of PV modules with or without bypass diode protection. The effect of bypass diodes protection on the performance of PV panels was also investigated and discussed. The results of average power losses in different PV layouts and technologies were also presented under various shading patterns. The horizontal layout of PV panels showed the lowest power losses.

5 PREDICTION MODEL OF SNOW SHADED PV SOLAR SYSTEMS

5.1 Overview

The maximum output power of the PV system can be regarded as an important factor for the actual performance of PV modules in the field, under different environmental conditions. The snow and its effect on solar panels are very unpredictable, both from time to time and from site to site. Hence, through recorded meteorological data together with the output power data of the snow-covered PV system during the cold months, a learning-based algorithm can be implemented to predict the power generation of a real solar installation. In this thesis, several prediction models for the estimation of maximum output power of snow shaded solar PV systems based on different algorithms have been studied, implemented and tested. These algorithms include decision (regression) trees, gradient boosted trees, random forest, and artificial neural networks (ANN) which all lead to interesting results. The ability of the prediction model has been validated over two cases of data set: firstly using 75%-25% holdout, and secondly, in order to use the entire data in our limited dataset, using 4-fold nested cross-validation technique. Through the grid optimization method, different combinations of hyperparameters of each algorithm were tested to identify an optimized set of these parameters to be used in the prediction model. The results of the model obtained for two different technologies of solar cells are presented and the performance of models is evaluated by reporting the root mean square error (RMSE) between the real and modeled data as well as the optimized hyperparameters of each algorithm.

5.1.1 Prediction Model

In a few research papers, the thermodynamics of PV modules have been considered when the linkage between the convection and radiation is defined as a dynamic factor [137]. However, these models do not incorporate the electro-optical and electro-thermodynamic coupling for the standard PV modules [138]. These fully coupled electrical, thermal, and optical dynamics are not generally considered simultaneously in a model. To

this end, a combined effort to include these factors into a unified model has been considered to efficiently utilize an experimentally measured dataset to train a machine learning-based model. The flowchart diagram of this prediction model is depicted in Figure 39. This modeling method aims to predict the maximum output power of the PV module through the following procedure:

1. In the data acquisition stage, different physical, optical, environmental, and the meteorological parameters such as snow depth, snow-covered area, back surface modules temperature, irradiance, wind speed, pressure, humidity, ambient temperature and UV index need to be acquired as well as the maximum output power of PV modules as the output variable of system (that defines the solar energy production).

2. The experimental dataset is generated by acquiring measurements of the PV module for several days of the cold months. The measured data set is then divided into two sets: one for the training the model (i.e. the training data set) and the other one for the evaluation of the prediction accuracy of the model (i.e. the test data set).

3. Once the model is trained for each technology of PV module, according to the climatology of the location such as wind speed, pressure, humidity, and UV index, the prediction model can be used for providing an estimate of the output of the solar energy production at any ambient temperature, solar irradiance, and shading pattern of snow. The trained model thus provides a prediction of the PV system output power for a future time period.

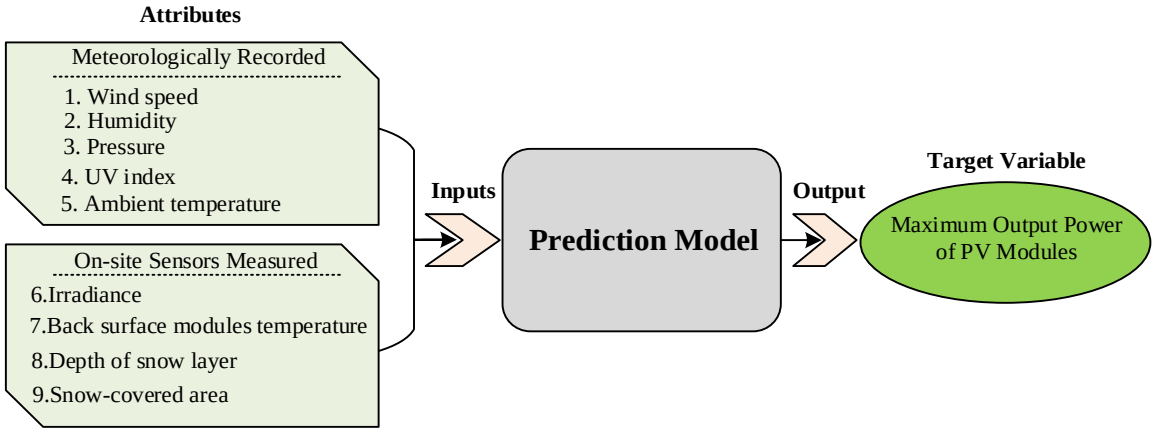

Figure 39. Prediction model for calculation of snow-covered PV modules production.

In the data acquisition stage, data records of the technical parameters of the solar panels including the maximum output power of PV modules (W) as well as module temperatures (°C) together with the meteorological on-site measurements including irradiance (W/m^2), and ambient temperature (°C) are collected over the winter 2020 by the sensors of two different technologies of PV panels located at the Université du Québec en Outaouais (UQO), Gatineau, Québec, Canada. In addition, the database of Canadian government is used for retrieving other climatological data such as humidity (%), wind speed (Mph), UV index, and pressure, measured in inch of mercury (inHg) because the corresponding sensors were not available on the test site [139]. Moreover, the snow depth (mm) and the percentage of snow-covered area (the area of snow-covered part divided by the area of panel) of PV modules are measured directly on the snow-covered panels. The acquired dataset consists of 228 data points directly measured in the test field, from which 96 belong to the monocrystalline, and 132 to thin film technology.

For the proposed prediction models, data are imported to the algorithms and using the grid optimization method, different combinations of hyperparameters are tested for each model. The optimal hyperparameters are selected in order to achieve the best results of the prediction model, i.e., the minimum root mean square error (RMSE). To achieve a suitable range of variation and diversity of parameters, the whole dataset is shuffled and two cases are considered for creating the training and test datasets. First, 75% of the dataset has been considered as a training set and the rest of 25% kept as a testing set. In the other case, in order to take advantage of the entire available data and compute a more realistic evaluation of the models' performance that is independent of the composition of training and testing datasets, the cross validation technique has been considered as well. This approach involves randomly dividing the set of observations into k groups, or folds, of approximately equal size. Based on the number of folds, in each variation of this technique, one fold is considered as a test set, and the model is trained on the remaining $k - 1$ folds and final results are reported as the average for each different k variation. The choice of 4 folds cross validation in this thesis is justified by the fact that it uses the same amount of data for training and testing in each fold as in the case of 75%-25% holdout. As such, the shuffled

data was equally divided into four parts, from which three were used to train the model and the other one to test the model. Because we are interested at the same time to identify the best hyperparameters, we are using nested cross-validation. As such, we used an outer 4-fold cross-validation loop to split the data into training and test datasets, and an inner loop to select the model via 4-fold cross-validation on the training dataset. The test dataset is then used to evaluate the model performance. Although the nested cross validation is computationally slower than normal cross validation, it is possibly one of the best approaches to estimate a truer error, that is almost unbiased and with low variance [140].

5.1.1.1 Machine Learning Algorithms Employed for Prediction

The production of PV modules is a complex phenomenon that depends on different physical, optical, environmental, and meteorological parameters. These parameters in conjugation with more sophisticated parameters regarding features of snow layers on both surfaces and the surrounding area of PV modules such as extinction and reflection features of snow as well as type, depth, and snow-covered area on the panel's surface are also correlated in the yield of snow shaded PV modules. Hence, the best way to consider all these parameters in the calculation of PV system production is using the real data field information of PV system installation to develop a model that is trained to predict the output power of the system. This goal can be achieved by the inherent strength of machine learning techniques which can explore available data to identify an intelligent prediction model of the PV system output. For this purpose, in this thesis, a supervised learning approach is implemented using machine learning algorithms for a multiple univariate regression problem with 9 attributes including meteorologically recorded parameters such as humidity, wind speed, pressure, UV index, and ambient temperature, as well as on-site sensors to measure solar irradiance, back surface modules temperature, depth and snow-covered area for different shading patterns and a numeric target variable which is the maximum output power. In order to develop prediction models, different algorithms are used, as described in the following sections.

A. Decision trees

Among the predictive modeling algorithms used in machine learning, decision trees are popular ones that give intelligibility and simplicity. This decision support tool that works based on the conditional control statements is presented as a tree-like graph that consists of a root node, non-leaf nodes, leaf nodes, and branches. In the flowchart-like structure of this learning algorithm, the root node is the starting point of the algorithm that contains all data records of the training dataset and it is split into two or more sub-nodes. In each non-leaf node, a test is conducted on an attribute to split at a certain value of the particular attribute, each branch represents the outcome of the test, and each leaf node represents a decision taken about a target value after computing all attributes. According to the problem objective, the cost function (RMSE in this thesis) is minimized when the best choice of attribute and split criterion is obtained. Decision trees are called as regression trees in the cases where the target variable take continuous values (typically real numbers) [141]. The path from the root to the decision about each attribute in branches and to the conclusions about the attribute's target values in the leaves represents regression rules.

The decision tree is built by implementing the Recursive Binary Splitting method which divides the records of every attribute j into two regions R_1 and R_2 :

$$R_1\,(j,s) = \{x \,|\, x_j \le s\} and\; R_2\,(j,s) = \{x \,|\, x_j > s\} \tag{33}$$

where x represents an attribute i.e. humidity, wind speed, pressure, UV index, ambient and back-surface module temperature, irradiance, depth and snow-covered area as the input parameters for the case of this prediction model. When the values of j (the feature number) and s (the value of the feature at the splitting point) are specified, the Residual Sum of Squares (RSS) of the tree is minimized as follows [142]:

$$RSS = \sum_{x_i \in R_1} (y_i - \overline{y}_{R_1})^2 + \sum_{x_i \in R_2} (y_i - \overline{y}_{R_2})^2 \tag{34}$$

where y_i and $\overline{y}_{R_1}$ represent the target value of data point i and the average target value of region R, respectively. The best division criterion can be determined when RSS is

calculated for different values of j and s. Then, regarding the specified division criterion the whole dataset is split into two separate sets in two sub-nodes. For the other sub-nodes the same procedure is followed to reach the desired tree depth. In the context of this prediction model, the maximum depth of the tree is considered as one of the hyperparameters of learning algorithm which is optimized over a validation set (i.e. 25% of training dataset).

B. Gradient Boosted Tree

Gradient boosted trees are based on the concept of regression trees and build a model in a stage-wise fashion like other boosting methods [143]. In the first stage, a regression tree is built based on the training data. Then, the training data is fed into the developed model and the predicted values of the target variable are obtained. The measured target value and the predicted target value are then compared to calculate the first stage error corresponding to each data record i of the training data as follows:

$$\mathrm{Err}^1 = \mathrm{M}_i - P_i^1, \qquad \forall\, i \in N \tag{35}$$

where $\mathrm{M_i}$, $\mathrm{P_i^1}$, Err^1, and N are the measured target value, the predicted target value in first stage, the error of prediction in the first stage, and the number of data records in the training data, respectively. The second stage is implemented by feeding the training data to the new tree to obtain the prediction of first stage error values which are used to find the new prediction for target value in the second stage as follows:

$$P_i^2 = P_i^1 + (LR \times P_i^{\mathrm{Err1}}), \qquad \forall\, i \in N \tag{36}$$

where P_i^2, P_i^{Err1}, and LR are the predicted target value in second stage, the predicted error value in second stage, and the learning rate (usually selected from the range between zero and one), respectively. The two stages defined by equations (35) and (36) are repeated iteratively to calculate a new prediction for the target value until the stopping criterion is satisfied. In this work, the number of iterations is considered as the stopping criterion to end up the iteration of this algorithm.

C. Random Forest

Random forests were introduced to correct the overfitting that can occur with the use decision trees and therefore the main concept of these both algorithms is the same [143]. Random forests algorithm is an ensemble learning algorithm built on a series of regression decision trees. In order to build regression trees for the samples, all attributes or a subset of attributes with more than one member can be used. The model is trained using several sample datasets randomly extracted from the training data. After training the individual regression trees of the forest, the test dataset is fed into the trained model to obtain the predicted target values using each tree. The final prediction result is computed as the mean prediction of target values over the individual trees through averaging the outputs of all trees for each data point in the test data.

D. Artificial Neural Network

Artificial neural networks (ANNs) consist of neuron nodes, called processing units, interconnected like a network designed to simulate the way the human brain analyzes and processes information [144]. The self-learning capability of ANNs enables forming probability-weighted associations between the input and output layers, as well as (in most cases) one or more hidden layers to find a pattern in data set. The behavior of the processing unit can be characterized as the following function [141]:

$$o = f(net_j) = f(\sum_{i=0}^{p} w_{j,i} x_i) \tag{36}$$

where f denotes the activation function which determines the output o , x_i is the ith input between P different inputs of the unit and $w_{j,i}$ is the connection weight of input i in unit j. The ANN model should be constructed by first defining the number of inputs, outputs, and hidden layers as well as the activation function and type of the model including feed-forward ANN or recurrent ANN. Second, the connection weight should be determined. The back-propagation learning method is used for this purpose. This method searches for a set of connection weights (including biases) that minimizes the output error. The search, which

is called the gradient descent search, changes the weights in the direction of reducing the output error after passing the inputs through the model in iterations.

Two different scenarios for implementing the prediction model have been designed to evaluate the effect of different input variables for this prediction model.

Scenario 1) In the first scenario of the prediction model, the main input variables such as irradiance, module temperatures, snow-covered area, and snow depth have been considered (lower left corner of Figure 39). The best results of this scenario for different algorithms are numerically and visually reported in this section. The identified optimal values of the hyperparameters through grid search and the RMSE of the models are tabulated in Table 11 for two different generations of PV cells, namely the crystalline based (ET-M53695) and the thin film based (FS275) technologies. The comparative results between the real and predicted values of system output are plotted in Figures 40 and 41 for the first scenario, for the two technologies, respectively.

Table 12. Parameters and numerical results for the selected models for scenario 1.

		Case 1 (75%-25% holdout)		Case 2 (4-fold cross-validation)	
Technology	Model	RMSE	parameters	RMSE	parameters
Monocrystalline (ET-M53695)	Decision trees	0.043	maximal_depth = 4 minimal_leaf_size = 3 apply_prepruning prepruning_alternatives = 0	0.073	maximal_depth = 38 minimal_leaf_size = 2 apply_prepruning prepruning_alternatives = 60
	Random forest	0.053	Num_of_trees = 340 maximal_depth = 15 apply_prepruning	0.045	number_of_trees = 422 maximal_depth = 12 apply_prepruning
	Gradient boosted trees	0.071	Num_of_trees = 7 maximal_depth =3 learning_rate = 0.7	0.048	Num_of_trees = 47 maximal_depth = 7 learning_rate = 0.33
	ANN	0.048	training_cycles = 477 learning_rate = 0.0185 Num hidden layer = 2	0.087	training_cycles = 481 learning_rate = 0.0169 Num hidden layer = 2
Thin film (FS275)	Decision trees	0.081	maximal_depth = 5 minimal_leaf_size = 4 apply_prepruning prepruning_alternatives = 0	0.0133	maximal_depth = 10 minimal_leaf_size = 4 apply_prepruning prepruning_alternatives = 10
	Random forest	0.116	Num_of_trees = 2 maximal_depth = 45 apply_prepruning	0.080	Num_of_trees = 247 maximal_depth = 15 apply_prepruning
	Gradient boosted trees	0.110	Num_of_trees = 41 maximal_depth = 5 learning_rate = 1.0	0.046	Num_of_trees = 110 maximal_depth = 6 learning_rate = 0.37
	ANN	0.077	training_cycles = 55 learning_rate = 0.0143 Num hidden layer = 2	0.161	training_cycles = 89 learning_rate = 0.0147 Num hidden layer = 2

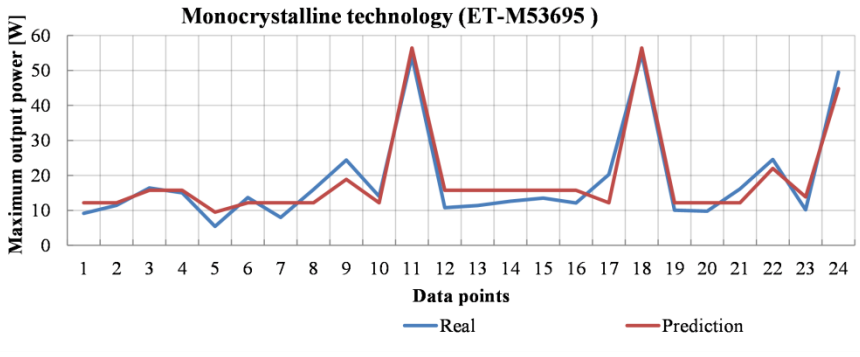

(a)

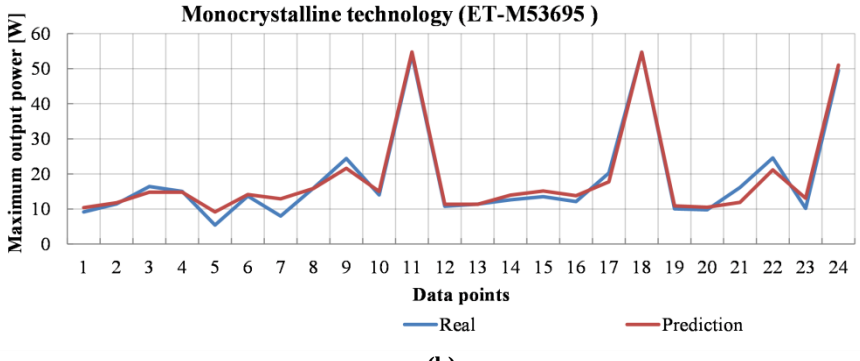

(b)

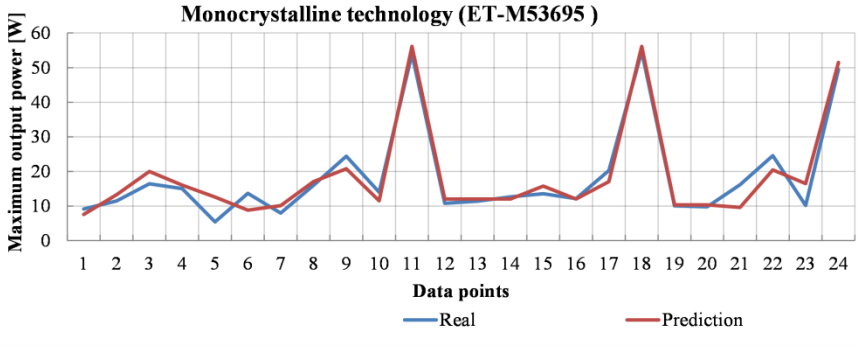

(c)

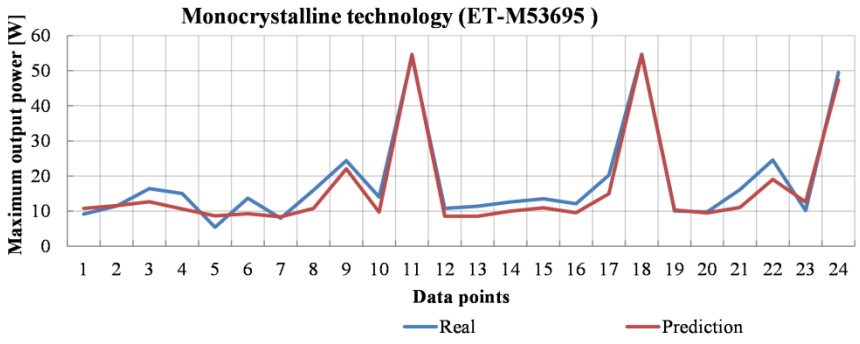

(d)

Figure 40. Comparative results of 75%-25% holdout in scenario 1 between the real and prediction of maximum output power of snow covered modules of Monocrystalline technology for the different models: a) decision trees, b) random forest, c) gradient boosted trees, and d) ANN.

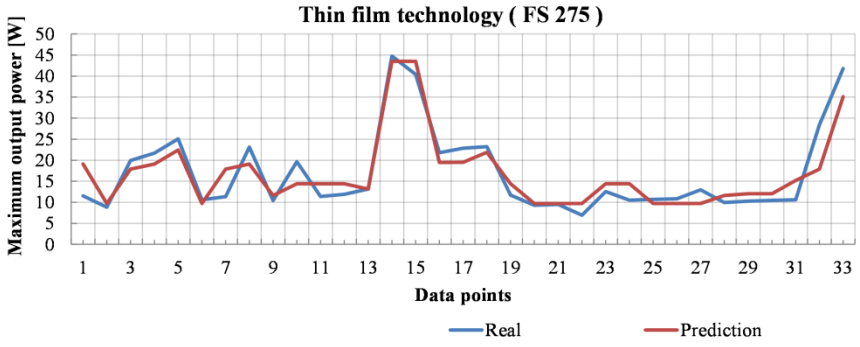

(a)

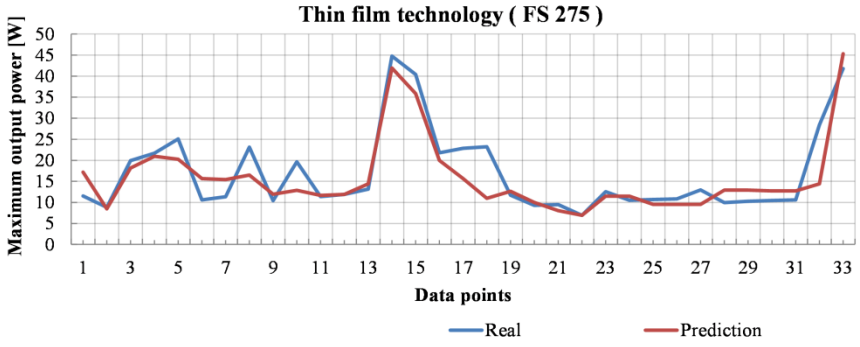

(b)

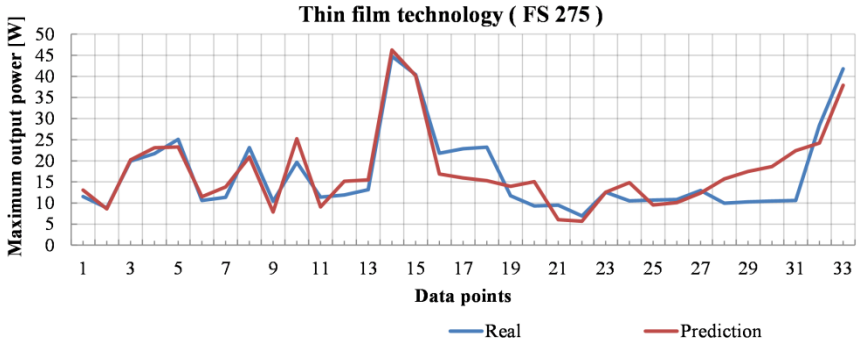

(c)

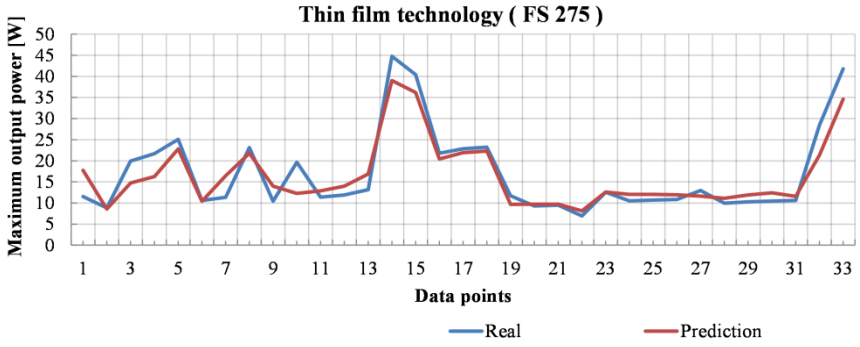

(d)

Figure 41. Comparative results of 75%-25% holdout in scenario 1 between the real and prediction of maximum output power of snow covered modules of thin film technology for the different models: a) decision trees, b) random forest, c) gradient boosted trees, and d) ANN.

By comparing the results of different models in this first scenario, it can be observed that the decision tree model reaches the best results with a root mean square error of 0.043 in the case of 75%-25% holdout. In the case of nested cross validation, the values of RMSE are higher for decision tree and ANN while these values are lower for gradient boosted tree and random forest in comparison with the case of 75%-25% holdout. These results are expected because nested cross validation offers a more accurate estimation of the real performance of the model (i.e. it is not biased by the specific data contained in the training/test dataset as the 75%-25% holdout can be).

Scenario 2) In the second scenario, the other climatological recorded parameters such as humidity, ambient temperature, wind speed, UV index, and pressure have also been considered for implementing the prediction models (top and bottom left corners of Figure 39). The values of chosen hyperparameters and the RMSE achieved by the four considered machine learning models are tabulated in Table 12 for the same two different PV technologies. The comparative results between the real and predicted values of system output are plotted respectively for the two technologies in Figures 42 and 43.

Table 13. Numerical results of selected models for the scenario 2.

		Case 1 (75%-25% holdout)		Case 2 (4-fold cross-validation)	
Technology	Model	RMSE	parameters	RMSE	parameters
Monocrystalline (ET-M53695)	Decision trees	0.034	maximal_depth = 3 minimal_leaf_size = 2 apply_prepruning prepruning_alternatives =0	0.041	maximal_depth = 15 minimal_leaf_size = 85 apply_prepruning prepruning_alternatives = 0
	Random forest	0.044	Num_of_trees = 8 maximal_depth = 4 apply_prepruning	0.049	number_of_trees = 79 maximal_depth = 12 apply_prepruning
	Gradient boosted trees	0.063	Num_of_trees = 3 maximal_depth = 2 learning_rate = 0.5	0.052	Num_of_trees = 49 maximal_depth = 8 learning_rate = 0.23
	ANN	0.041	training_cycles =313 learning_rate = 0.02 Num hidden layer = 2	0.038	training_cycles = 485 learning_rate = 0.0175 Num hidden layer = 2
Thin film (FS275)	Decision trees	0.036	maximal_depth = 4 minimal_leaf_size = 1 apply_prepruning prepruning_alternatives = 0	0.101	maximal_depth = 15 minimal_leaf_size = 7 apply_prepruning prepruning_alternatives = 7
	Random forest	0.100	Num_of_trees = 2 maximal_depth = 10 apply_prepruning	0.069	Num_of_trees = 63 maximal_depth = 12 apply_prepruning
	Gradient boosted trees	0.084	Num_of_trees = 6 maximal_depth = 1 learning_rate = 1.0	0.051	Num_of_trees = 35 maximal_depth = 4 learning_rate = 0.45
	ANN	0.051	training_cycles = 99 learning_rate = 0.0197 Num hidden layer = 2	0.063	training_cycles = 96 learning_rate = 0.0144 Num hidden layer = 2

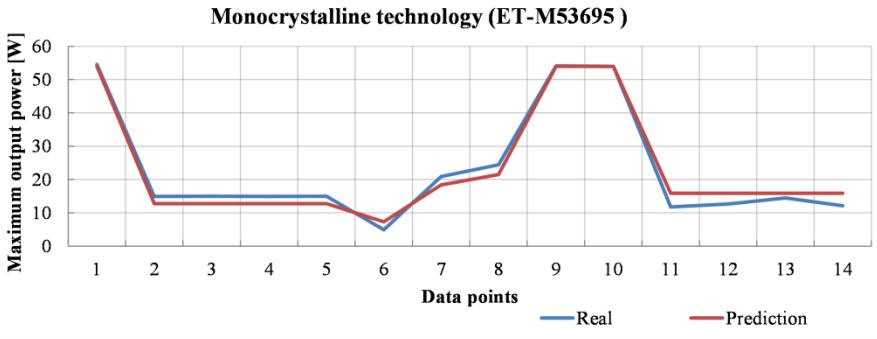

(a)

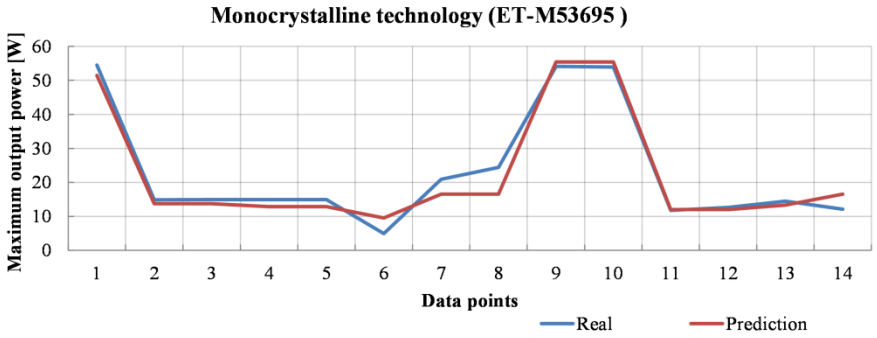

(b)

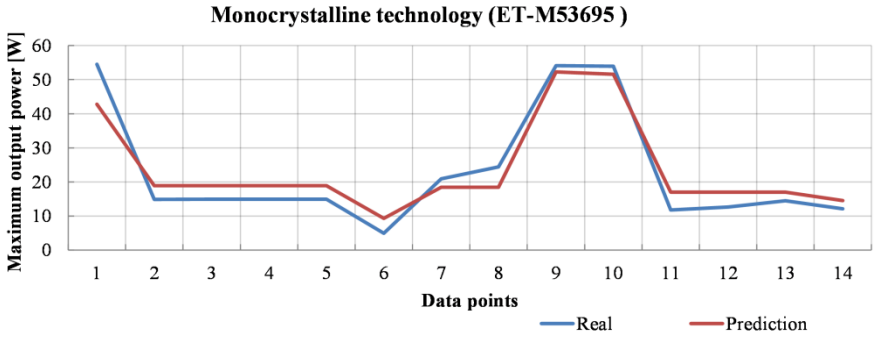

(c)

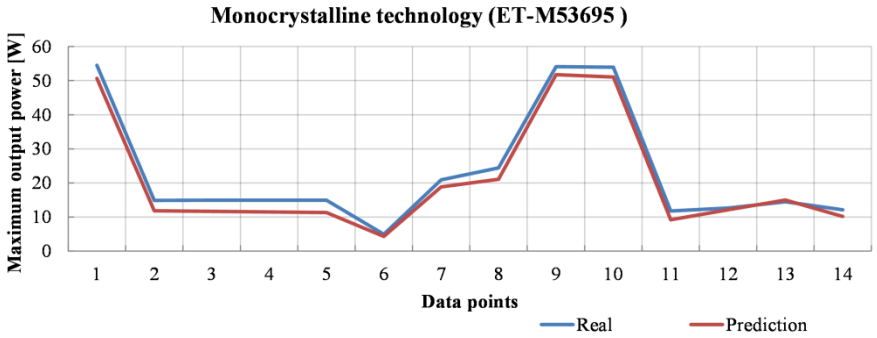

(d)

Figure 42. Comparative results of 75%-25% holdout in scenario 2 between the real and prediction of maximum output power of snow covered modules of Monocrystalline technology for the different models: a) decision trees, b) random forest, c) gradient boosted trees, and d) ANN.

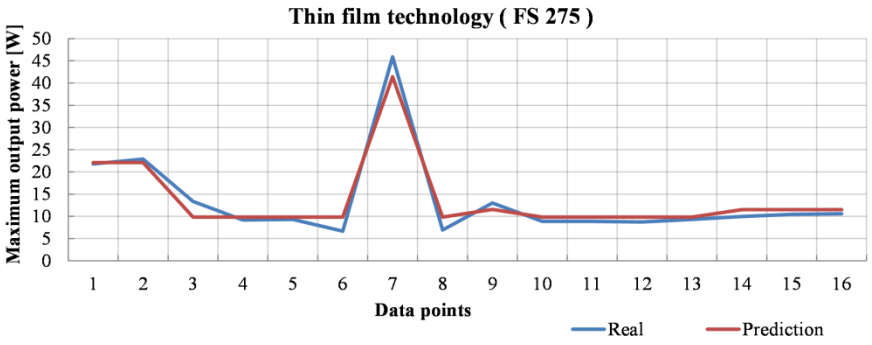

(a)

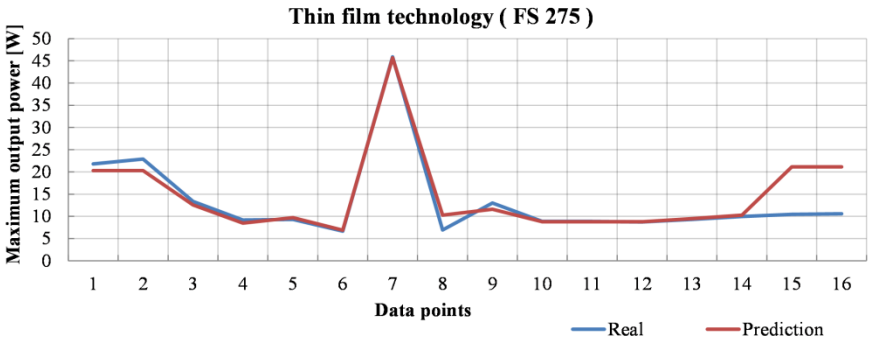

(b)

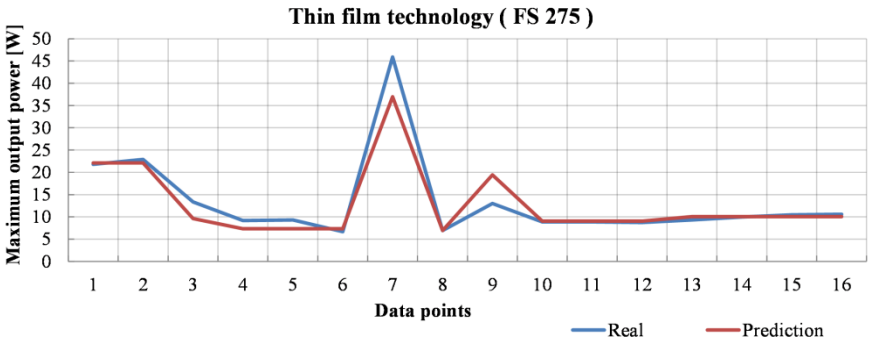

(c)

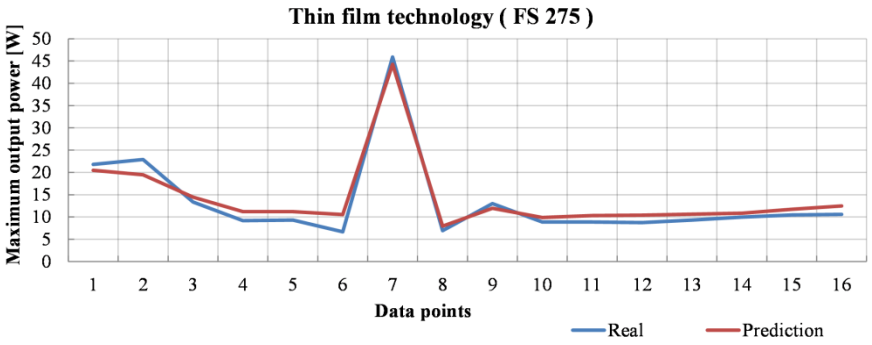

(d)

Figure 43. Comparative results of 75%-25% holdout in scenario 2 between the real and prediction of maximum output power of snow covered modules of thin film technology for the different models: a) decision trees, b) random forest, c) gradient boosted trees, and d) ANN.

According to the results of modeling in this second scenario, in the case of 75%-25% holdout, the prediction of maximum output power is more accurate, reaching RMSEs of 0.034 and 0.036 for the model based on the decision trees for the monocrystalline and the thin film technology, respectively. These errors are respectively 0.009 and 0.045 lower for the two technologies than the best RMSEs achieved in the first scenario for the same algorithm. Moreover, the values of RMSE for the model based on the algorithm of gradient boosted trees and random forests are decreased by 0.008 and 0.009, respectively which demonstrate a good accordance between the real and predicted values in the second scenario. As such, the use of meteorological parameters such as humidity, ambient temperature, wind speed, UV index, and pressure along with on-site sensor data on the irradiance, back-surface module temperature, snow-covered area, and snow depth led to an improvement in the accuracy of prediction model. The same facts are confirmed for the cross validation. The best results achieved in the second scenario with RMSE values of 0.041 and 0.038, respectively for the algorithms of decision trees and ANN are decreased by 0.032 and 0.049 respectively with respect to the best RMSEs achieved in the first scenario for the same two algorithms. The results achieved using 4-fold nested cross validation demonstrate a more realistic estimation of system performance because the dataset in not highly dependent on the composition of specific data in the training and testing set as in the case of 75%-25% holdout.

5.2 Summary on Machine Learning Algorithms Employed for Prediction

In this section of the thesis, a prediction model was proposed to estimate the power production of a snow shaded PV solar system for two different commercial types of PV technologies commonly used in North America. Different physical, optical, environmental, and meteorological parameters of academic PV panels located in the Université du Québec en Outaouais (UQO), Gatineau, Québec, Canada were recorded to predict the maximum power production of these solar systems for the cold months of winter 2020. The prediction model was implemented through the use of four machine learning algorithms including decision trees, gradient boosted trees, random forest, and artificial neural networks. For the

training and test data set, the recorded dataset was divided into two ways, including 75%–25% holdout and cross-validation to compare the performance of prediction model. Moreover, two different scenarios corresponding to different combinations of input parameters were tested. In the first scenario, the main input parameters such as irradiance, module temperatures, snow-covered area, and snow depth have been just considered, while in the second scenario other meteorological parameters such as humidity, ambient temperature, wind speed, UV index, and pressure have been also involved for implementing the prediction models. The best results were achieved in the second scenario with more comprehensive meteorological inputs by adding other input parameters such as humidity, ambient temperature, wind speed, UV index, and pressure to the attributes. According to the numerical results, the model built using decision trees achieved the best performance in the case of 75%-25% holdout with the RMSE values of 0.034 and 0.036 with the algorithm of decision trees for the monocrystalline and thin film technologies respectively. In the case of cross validation for the second scenario, the model based on ANN with RMSE of 0.038 for the monocrystalline technology and the model based on Gradient boosted trees with a RMSE of 0.051 for the thin film technology represent the best performance achieved. These results of the proposed prediction model demonstrate that it can be useful for the estimation of solar energy production in locations with a considerable amount of snowfall.

6 CONCLUSIONS

6.1 Concluding Remarks

The increasing world's energy demands and environmental pollution are motivating the trend of energy production using the sun as one of the main renewable energy sources available in nature. The harvest of this inexhaustible energy source is possible by the direct production of electricity through PV systems. Accordingly, the research and technology investments are allocated to improve PV systems integration. Although the low maintenance, high-reliability, and noiseless operation of PV systems make them a strategic power supply option among the diversity of power generation sources, their electricity production can be greatly challenged by snowfall during cold months. Hence, the impact of snow on the performance of PV modules needs to be studied in depth. In addition, the effective use of PV panels requires reliable modeling methods, targeting to predict the behavior of a PV system at conditions different from those characterized by the manufacturer datasheet. The PV model can be used for simulating the electrical characteristics and dynamics of PV power plants under various meteorological conditions or for estimating the energy production and efficiency of a solar plant at specific locations. As a result, in this thesis, the main challenging problems of PV systems integration in different environmental conditions, especially in snowy climates, were investigated and categorized in the following topics:

1) Development of an optimized modeling method for characterizing the performance of PV modules under uniform snow coverage,

2) Development of a novel modeling technique for PV modules subjected to the nonuniform snow coverage,

3) Study of the effect of PV panels layout and snow patterns on their electrical characteristics, and

4) Development of a prediction model based on real field data coming from different PV technologies to estimate the maximum power production of snow-covered PV modules.

In response to the aforementioned needs, different approaches of modeling were proposed and validated through simulation and experimentation. To this end, the major findings of this project can be summarized as follows:

- A PV model was proposed to predict the behavior of PV modules covered with a uniform snow deposit. It capitalizes on the Giddings and LaChapelle theory to determine accurately the receiving solar radiation on the PV module surface because the albedo and the extinction of solar radiation are coupled based on this theory. The PSO algorithm was utilized in this model to update PV module parameters under different snow depths. The model was validated experimentally using PV modules based on different technologies, as well as using real data from a 12-MW PV farm. The results obtained by the proposed model are in a good agreement with those obtained experimentally. The model offers thus a great advantage in predicting electric characteristics of PV modules under different snow conditions, from light to heavy snowfall. The results obtained are of great importance as they can help to improve the electrical performance of PV systems under snow conditions. An empirical power loss equation has been proposed to calculate the snow-related power loss on the basis of climatic circumstances of PV panel exposure. The proposed PV model is capable of interfacing with power electronic converters and MPPT control techniques, allowing the simulation of whole PV plants and their interaction with other systems.

- A comprehensive method was introduced for modeling the behavior of PV system under various patterns of shading and partial snow accretion. The primary objectives were to evaluate the performance of PV systems in snowy climates and to propose an accurate multi-zone model for PV modules covered with nonuniform snow patterns. To this end, an experimental modeling approach based on the single-diode-five-parameter equivalent circuit incorporating the Giddings and LaChapelle theory was formulated to accurately determine the absorbed solar radiation on the PV module surface. In addition, a PSO optimization algorithm was used to extract the unknown parameters considering environmental conditions. Then, a series of systematic experimental tests under different

snow patterns were carried out using different PV technologies, typically used in cold regions. The results obtained from the proposed model are in good agreement with those obtained experimentally. In addition, an equation was derived to estimate the percentage of power losses of PV modules. The contributions of this research formulate the nonuniform shading pattern for characterizing the output of PV systems partially affected by the snow.

- A PV panel layout can play an important role in the productivity of a PV panel covered with nonuniform snow. For this purpose, a series of experiments were conducted using different scenarios of snow removal to emulate the partial shading coverage of snow on three different panels layout such as vertical, horizontal, and diagonal. The difference in energy generation is more obvious for bigger snow depths and smaller snow-covered areas. Based on the experimental results, it can be concluded that the vertical PV panels layout faces the greatest power loss due to nonuniform snow accretion in both PV module technologies. While the diagonal layouts can be a better choice than the vertical panels layout, the horizontal PV module layout is the most effective layout when subjected to the partial snow coverage. Hence, a proper layout can reduce the negative effects of nonuniform snow accretion on PV power production. Through the comparison in term of power losses for two different technologies, although the thin film technology demonstrates simpler characteristics, its efficiency is lower than that of monocrystalline technology. This study could provide a practical vision for investigating the impacts of snow/ice on the electrical characteristics of a PV array. The presented analysis forms the basis for designing large PV arrays, in order to mitigate the influence of snow/ice on the energy production of PV systems.

- The efficient and economic use of PV systems can be managed if the energy production for the period of time ahead is predicted. In the last part of research project, a prediction model of the PV system production was proposed by involving the combination of meteorological data and the historical output power data of the PV system under study during the cold months. Through the day-to-day data acquisition in the presence of different snow shading patterns for different technology of PV modules, the nonlinear effect different snow shading on the surface of panels was investigated and considered as

one of the input variables of the prediction model. Besides, the effective climatological parameters such as snow depth, humidity, pressure, UV index, and wind speed will also be considered in the training-based model that has not been formulated in the previous modeling methods. This learning-based prediction model is free of circuit-based modeling methods complexity and with appropriate training algorithm can predict the output energy production of the PV system accurately.

6.2 Future Work

Regarding the research work of this thesis, some prospective points for the future studies of this research are listed here:

- Development of an advanced PV model with a hybrid version of the PSO algorithm to reduce the simulation time especially for the large–scale PV arrays.
- Modeling of the tilt angle impact of PV modules on snow power losses.
- Investigating the appropriateness of bifacial PV modules as a candidate that utilizes additional sunlight of backside to improve the efficiency of snowy solar systems.
- Appropriate design of PV system to minimize snow and mismatch losses taking into consideration interconnection of PV panels, different arrangements of power electronics converters and optimal mounting angle.
- Evaluating the PV modules lifetime and payback period in the snowy regions.
- Developing a suitable snow removal method to alleviate the snow losses in PV sites.
- Implementing prediction model using the hybrid algorithms of machine learning to improve the accuracy of the model in snowy conditions.

APPENDICES

Appendix A **Modeling Codes Under Uniform Snow Coverage**

In this section, the software implementation is presented in greater detail for PSO-based algorithm of modeling for the first objective of thesis. This will entail a look at the general structure of modeling algorithm for the PV modules under uniform snow coverage based on the m-File codes in MATLAB environment to ensure everything operates in a controlled manner.

A.1 Objective Function

```
function f=ofun(x)

V=[0,0.264101968586330,0.528203937172660,…];
I=[7.12661538459698,7.12662441402581,…];
Vt=1.620068971992636;
 for s = 1 : size(V,2)
     og(s) = x(1)-x(2)*(exp((V(s)+I(s)*x(3))/Vt/x(4))-1)-
(V(s)+I(s)*x(3))/x(5)-I(s);
 end
% objective function (minimization)
f=sqrt((1/size(V,2))*sum(og.^2));
```

A.2 Run PSO Algorithm

```
tic
clc
clear all
close all
rng default

%%data sheet information of PV module

Iscn = 8.21;              %Nominal short-circuit voltage [A]
Vocn = 32.9;             %Nominal array open-circuit voltage
[V]
Impo = 7.61;               %Array current @ maximum power
point [A]
Vmpo = 26.3;              %Array voltage @ maximum power point
[V]
%Pmax_e = Vmp*Imp;        %Array maximum output peak power [W]
```

```
Kv = -0.123;            %Voltage/temperature coefficient
[V/K]
Ki = 0.0032;              %Current/temperature coefficient
[A/K]
Ns = 54;                %Nunber of series cells
a = 1.3;

Npp= 1 ; % Number of Modules in Parallel
Nss= 1; %Number of Modules is series

Rsn=0.221; %Series resistance obtained at STc
Rpn=415.405; %Parallel resistance obtained at STC

C0=1.006;
C1=-0.006;
C2=-0.117;
C3=-11.082;


%% PV model calculation

Gn = 1000;               %Nominal irradiance [W/m^2] @ 25oC
Tn = 25 + 273.15;        %Nominal operating temperature [K]

% Enter Arbitrary Insolation and Temperature
T = 75 + 273.15;
G = 851;

Geff = G/Gn;

k = 1.3806503e-23;   %Boltzmann [J/K]
q = 1.60217646e-19;  %Electron charge [C]

Vtn = Ns * k * Tn / q;           %Thermal junction voltage
(nominal)
Vt  = Ns * k * T  / q;           %Thermal junction voltage
(current temperature)


%Updating Vmp & Imp for different temperature and insolation
level

Imp = (C0*Geff+C1*Geff^2)*(Impo+Ki*(T-Tn));
Vmp = Vmpo + C2*a*Vt*log(Geff) + (C3*(a*Vt*log(Geff))^2)/Ns +
Kv*(T-Tn);
Pmax_e = Vmp*Imp
dT = T-Tn;
```

```
Voc = Vocn + a * Vt * log(Geff) + Kv * dT;
Isc = (Iscn + Ki*dT) *G/Gn;        % Actual short-circuit
current

%% PROGRAM STARTS HERE

% Modeling algorithm - here we are obtaining the PV model
parameters

% Reference values of Rs and Rp
% These values are not used in the modeling proces but they
will
% be displayed at the end.

dT = T-Tn;

Voc = Vocn + a * Vt * log(Geff) + Kv * dT;

Ion = ((Vocn-Rsn*Iscn)/Rpn-Iscn)/(exp(Rsn*Iscn/(Vtn*a))-
exp(Vocn/Vtn/a));
Ipvn = Iscn + Ion*(exp(Rsn*Iscn)/(a*Vtn)-1) + Rsn*Iscn/Rpn;

%Ipvn = (Rs+Rp)/Rp * Iscn;          % Nominal light-generated
current
Ipv = (Ipvn + Ki*dT) *G/Gn;        % Actual light-generated
current
Isc = (Iscn + Ki*dT) *G/Gn;        % Actual short-circuit
current
Io = (Ipv-Voc/Rp)/(exp(Voc/(a * Vt))-1); % Actual diode
saturation current

Rs_max = (Voc - Vmp)/ Imp;
Rp_min = Vmp/(Isc-Imp) - Rs_max;

% Initial guesses of Rp and Rs
Rs = 0;
Rp = Rp_min;


%% experimental I-V data

V=[0,0.264101968586330,0.528203937172660,…];
I=[7.12661538459698,7.12662441402581,…];
Vt=1.620068971992636;

% bounds of variables for PSO optimization
```

```
LB=[Ipv Ion 0 1 Rp_min];          %lower bounds of variables
UB=[Ipvn Io Rs_max 1.5 Rp];       %upper bounds of variables

% pso parameters values
m=5;              % number of variables
n=100;            % population size
wmax=0.9;         % inertia weight
wmin=0.4;         % inertia weight
c1=2;             % acceleration factor
c2=2;             % acceleration factor
%   constriction factor for inertia weight
% kappa = 1;
% phi1 = 2.05;
% phi2 = 2.05;
% phi = phi1 + phi2;
% chi = 2*kappa/abs(2-phi-sqrt(phi^2-4*phi));
% w = chi;              % Intertia Coefficient
% c1 = chi*phi1;        % Personal Acceleration Coefficient
% c2 = chi*phi2;        % Social Acceleration Coefficient
% wdamp=0.9;


% pso main program-----------------------------------------
---------start
maxite=10000;     % set maximum number of iteration
maxrun=20;        % set maximum number of runs need to be
for run=1:maxrun
    run
    % pso initialization---------------------------------
---------start
    for i=1:n
        for h=1:m
            x0(i,h)=round(LB(h)+rand()*(UB(h)-LB(h)));
        end
    end
    x=x0;         % initial population
    v=0.1*x0;     % initial velocity

% objective function (minimization)

    for i=1:n
        f0(i,1)=ofun(x0(i,:));
    end
    [fmin0,index0]=min(f0);
    pbest=x0;                 % initial pbest
    gbest=x0(index0,:);       % initial gbest
```

```
    % pso initialization-----------------------------------------
-----------end

    % pso algorithm-----------------------------------------------
---------start
    ite=1;
    tolerance=1;
    while ite<=maxite && tolerance>10^-12

        w=wmax-(wmax-wmin)*ite/maxite; % update inertial
weight

        % pso velocity updates
        for i=1:n
            for h=1:m
                v(i,h)=w*v(i,h)+c1*rand()*(pbest(i,h)-
x(i,h))...
                        +c2*rand()*(gbest(1,h)-x(i,h));
            end
        end

        % pso position update
        for i=1:n
            for h=1:m
                x(i,h)=x(i,h)+v(i,h);
            end
        end

        % handling boundary violations
        for i=1:n
            for h=1:m
                if x(i,h)<LB(h)
                    x(i,h)=LB(h);
                elseif x(i,h)>UB(h)
                    x(i,h)=UB(h);
                end
            end
        end

        % evaluating fitness
        for i=1:n
            f(i,1)=ofun(x(i,:));
        end

        % updating pbest and fitness
        for i=1:n
            if f(i,1)<f0(i,1)
```

```
                pbest(i,:)=x(i,:);
                f0(i,1)=f(i,1);
            end
        end

        [fmin,index]=min(f0);    % finding out the best
particle
        ffmin(ite,run)=fmin;     % storing best fitness
        ffite(run)=ite;          % storing iteration count

        % updating gbest and best fitness
        if fmin<fmin0
            gbest=pbest(index,:);
            fmin0=fmin;
        end

        % calculating tolerance
        if ite>100;
            tolerance=abs(ffmin(ite-100,run)-fmin0);
        end

        % displaying iterative results
        if ite==1
            disp(sprintf('Iteration    Best particle
Objective fun    inertia weight '));
        end
        disp(sprintf('%8g  %8g          %8.4f
%8.4f',ite,index,fmin0,w));
        ite=ite+1;
%         w = w * wdamp;

    end
    % pso algorithm-----------------------------------------
-----------end
    gbest;
    fvalue=ofun(gbest);
    fff(run)=fvalue;
    rgbest(run,:)=gbest;
    disp(sprintf('---------------------------------------'));
end
% pso main program--------------------------------------------
-----------end
disp(sprintf('\n'));
disp(sprintf('**********************************************
**********'));
disp(sprintf('Final Results-----------------------------'));
[bestfun,bestrun]=min(fff)
```

```
best_variables=rgbest(bestrun,:)
disp(sprintf('****-----<<<Extraction Of PV cell
Parameters>>>---<<one diode>>--***'));
 disp(sprintf('   Ipv    io     Rs     a      Rp '));
 disp(sprintf('-------------------------------------'));
 disp(sprintf('  %8.9f  %8.9f  %f   %f  %f
',rgbest(bestrun,:)))
disp(sprintf('**********************************************
**********'));
toc
Ipv=rgbest(bestrun,1);
Io=rgbest(bestrun,2);
Rs=rgbest(bestrun,3);
a=rgbest(bestrun,4);
Rp=rgbest(bestrun,5);

% Solving the I-V equation for several (V,I) pairs by
extracted PV parameters


Ix= zeros(1,size(V,2));     % Current vector

for h = 1 : size(V,2) %Calculates for all voltage values

% Solves g = I - f(I,V) = 0 with Newton-Raphson

g(h) = Ipv-Io*(exp((V(h)+Ix(h)*Rs)/Vt/a)-1)-
(V(h)+Ix(h)*Rs)/Rp-Ix(h);

while (abs(g(h)) > 0.0001)

g(h) = Ipv-Io*(exp((V(h)+Ix(h)*Rs)/Vt/a)-1)-
(V(h)+Ix(h)*Rs)/Rp-Ix(h);
glin(h) = -Io*Rs/Vt/a*exp((V(h)+Ix(h)*Rs)/Vt/a)-Rs/Rp-1;
I_(h) = Ix(h) - g(h)/glin(h);
Ix(h) = I_(h);

end

end % for h = 1 : size(V,2)


% Calculates power using the I-V equation
  P = (Ipv-Io*(exp((V+I.*Rs)/Vt/a)-1)-(V+I.*Rs)/Rp).*V;
%   P = I.*V;

  Px = (Ipv-Io*(exp((V+Ix.*Rs)/Vt/a)-1)-(V+Ix.*Rs)/Rp).*V;
```

```
  Pmax_m = max(P);


%% Outputs Curves

 % I-V curve
 figure(1)
 grid on
 hold on
 title('Adjusted I-V curve');
 xlabel('V [V]');
 ylabel('I [A]');
 xlim([0 max(V)*1.1]);
 ylim([0 max(I)*1.1]);
 plot(V,I,'LineWidth',3,'Color','r')

plot(V,Ix,'pentagram','LineWidth',2,'MarkerSize',7,'Color','b
')
 plot([0 Vmp Voc ],[Isc Imp 0
],'o','LineWidth',2,'MarkerSize',7,'Color','c')

% P-V curve
 figure(2)
 grid on
 hold on
 title('Adjusted P-V curve');
 xlabel('V [V]');
 ylabel('P [W]');
 xlim([0 Vocn*1.1]);
 ylim([0 Vmp*Imp*1.1]);
 plot(V,P,'LineWidth',3,'Color','r')

plot(V,Px,'diamond','LineWidth',2,'MarkerSize',7,'Color','b')
 plot([0 Vmp Voc ],[0 Pmax_e 0
],'o','LineWidth',2,'MarkerSize',7,'Color','c')



% PSO convergence characteristic
figure(3)
grid on
hold on
plot(ffmin(1:ffite(bestrun),bestrun),'LineWidth',2,'Color','r
');
xlabel('Iteration');
ylabel('Fitness function value');
```

```
title('PSO convergence characteristic')
%###########################################################
############## END
```

Appendix B **Modeling Codes Under Nonuniform Snow Coverage**

In this section, the software implementation is presented in greater detail for PSO-based algorithm of modeling for the second objective of thesis. This will entail a look at the general structure of modeling algorithm for the PV modules under nonuniform snow coverage based on the m-File codes in MATLAB environment to ensure everything operates in a controlled manner.

C.1 Multi-objective Function

```
function f=o1fun(x1)

V=[0    4.784671    4.784671    4.784671,…];
I=[4.984672 4.984672    4.984672    4.98467,…];
Vt=1.3635;
cp=97;
cp2=109;

  for s = 1 : cp
   og(s)= x1(1)-x1(2)*(exp((V(s)+I(s)*x1(3))/Vt/x1(4))-1)-
(V(s)+I(s)*x1(3))/x1(5)-I(s);

  end
 f=sqrt((1/cp)*sum(og.^2));
end


function f=o2fun(x2)
V=[0    4.784671    4.784671    4.784671,…];
I=[4.984672 4.984672    4.984672    4.98467,…];
Vt=1.3635;

cp=97;
cp2=109;
  for s = cp : cp2
   og(s)= x2(1)-x2(2)*(exp((V(s)+I(s)*x2(3))/Vt/x2(4))-1)-
(V(s)+I(s)*x2(3))/x2(5)-I(s);

  end
 f=sqrt((1/(size(V,2)-cp))*sum(og.^2));
end
```

```
function f=o3fun(x3)
V=[0    4.784671    4.784671    4.784671,…];
I=[4.984672 4.984672    4.984672    4.98467,…];
Vt=1.3635;

cp=97;
cp2=109;
  for s = cp2 : size(V,2)
   og(s)= x3(1)-x3(2)*(exp((V(s)+I(s)*x3(3))/Vt/x3(4))-1)-
(V(s)+I(s)*x3(3))/x3(5)-I(s);

  end
 f=sqrt((1/(size(V,2)-cp))*sum(og.^2));
end
```

C.2 Run PSO Algorithm

```
tic
clc
clear all
close all
rng default

%%data sheet information of PV module
Iscn = 9.12;              %Nominal short-circuit voltage [A]
Vocn = 37.5;             %Nominal array open-circuit voltage
[V]
Impo = 8.56;               %Array current @ maximum power
point [A]
Vmpo = 30.4;              %Array voltage @ maximum power point
[V]
%Pmax_e = Vmp*Imp;        %Array maximum output peak power [W]
Kv = -0.31e-2;             %Voltage/temperature coefficient
[V/K]
Ki = 0.41e-2;               %Current/temperature coefficient
[A/K]
Ns = 60;                  %Nunber of series cells
a = 1.5;

Npp= 1 ; % Number of Modules in Parallel
Nss= 1; %Number of Modules is series

Rsn=0.221; %Series resistance obtained at STc
Rpn=415.405; %Parallel resistance obtained at STC
```

```
C0=1.006;
C1=-0.006;
C2=-0.117;
C3=-11.082;


%% PV model calculation

Gn = 1000;               %Nominal irradiance [W/m^2] @ 25oC
Tn = 25 + 273.15;        %Nominal operating temperature [K]

% Enter Arbitrary Insolation and Temperature
T = -9.43388889 + 273.15;
G = 690.3;

Geff = G/Gn;

k = 1.3806503e-23;   %Boltzmann [J/K]
q = 1.60217646e-19;  %Electron charge [C]

Vtn = Ns * k * Tn / q;           %Thermal junction voltage
(nominal)
Vt  = Ns * k * T  / q;           %Thermal junction voltage
(current temperature)


%Updating Vmp & Imp for different temperature and insolation
level

Imp = (C0*Geff+C1*Geff^2)*(Impo+Ki*(T-Tn));
Vmp = Vmpo + C2*a*Vt*log(Geff) + (C3*(a*Vt*log(Geff))^2)/Ns +
Kv*(T-Tn);
Pmax_e = Vmp*Imp
dT = T-Tn;

Voc = Vocn + a * Vt * log(Geff) + Kv * dT;
Isc = (Iscn + Ki*dT) *G/Gn;       % Actual short-circuit
current

%% experimental I-V data
V=[0    4.784671    4.784671    4.784671,…];
I=[4.984672 4.984672    4.984672    4.98467,…];
Vt=1.3635;
```

```
% cp=size(V,2);
cp=97;
cp2=109;

LB1=[3 2.0114e-9 0.0260 0.3039 500];  %lower bounds of
variables
UB1=[5 11e-9 0.5 2 1000];             %upper bounds of
variables

LB2=[0.1 1.434e-16 0.099 0.5 100];   %lower bounds of
variables
UB2=[1 11e-16 1 2 500];              %upper bounds of
variables

LB3=[0.1 1.434e-16 0.099 0.5 100];  %lower bounds of
variables
UB3=[1 11e-16 1 2 500];             %upper bounds of
variables

% pso parameters values
m=5;             % number of variables
n=100;           % population size
wmax=0.9;        % inertia weight
wmin=0.4;        % inertia weight
c1=2;            % acceleration factor
c2=2;            % acceleration factor
%   constriction factor for inertia weight
% kappa = 1;
% phi1 = 2.05;
% phi2 = 2.05;
% phi = phi1 + phi2;
% chi = 2*kappa/abs(2-phi-sqrt(phi^2-4*phi));
% w = chi;              % Intertia Coefficient
% c1 = chi*phi1;        % Personal Acceleration Coefficient
% c2 = chi*phi2;        % Social Acceleration Coefficient
% wdamp=0.9;


% pso main program-----------------------------------------
---------start
maxite=10000;    % set maximum number of iteration
maxrun=50;      % set maximum number of runs need to be
for run=1:maxrun
    run
    % pso initialization---------------------------------
---------start
    for i=1:n
```

```
        for h=1:m
            x1_0(i,h)=round(LB1(h)+rand()*(UB1(h)-LB1(h)));
            x2_0(i,h)=round(LB2(h)+rand()*(UB2(h)-LB2(h)));
            x3_0(i,h)=round(LB3(h)+rand()*(UB3(h)-LB3(h)));
        end
    end
    x1=x1_0;        % initial population
    v1=0.1*x1_0;    % initial velocity
    x2=x2_0;        % initial population
    v2=0.1*x2_0;    % initial velocity
    x3=x3_0;        % initial population
    v3=0.1*x3_0;    % initial velocity
% objective function (minimization)

    for i=1:n
        f1_0(i,1)=o1fun(x1_0(i,:));
        f2_0(i,1)=o2fun(x2_0(i,:));
        f3_0(i,1)=o3fun(x3_0(i,:));
    end
    [f1min0,index1_0]=min(f1_0);
    p1best=x1_0;                % initial pbest
    g1best=x1_0(index1_0,:);     % initial gbest

    [f2min0,index2_0]=min(f2_0);
    p2best=x2_0;                % initial pbest
    g2best=x2_0(index2_0,:);     % initial gbest

    [f3min0,index3_0]=min(f3_0);
    p3best=x3_0;                % initial pbest
    g3best=x3_0(index3_0,:);     % initial gbest

    % pso initialization-------------------------------------
-----------end

    % pso algorithm-----------------------------------------
---------start
    ite=1;
    tolerance1=1;
     tolerance2=1;
     tolerance3=1;
    while ite<=maxite && tolerance1>10^-12 && tolerance2>10^-
12 && tolerance2>10^-12

        w=wmax-(wmax-wmin)*ite/maxite; % update inertial
weight

        % pso velocity updates
```

```
        for i=1:n
            for h=1:m
                v1(i,h)=w*v1(i,h)+c1*rand()*(p1best(i,h)-
x1(i,h))...
                        +c2*rand()*(g1best(1,h)-x1(i,h));

                v2(i,h)=w*v2(i,h)+c1*rand()*(p2best(i,h)-
x2(i,h))...
                        +c2*rand()*(g2best(1,h)-x2(i,h));

               v3(i,h)=w*v3(i,h)+c1*rand()*(p3best(i,h)-
x3(i,h))...
                        +c2*rand()*(g3best(1,h)-x3(i,h));

            end
        end

        % pso position update
        for i=1:n
            for h=1:m
                x1(i,h)=x1(i,h)+v1(i,h);
                x2(i,h)=x2(i,h)+v2(i,h);
                x3(i,h)=x3(i,h)+v3(i,h);
            end
        end

        % handling boundary violations
        for i=1:n
            for h=1:m
                if x1(i,h)<LB1(h)
                    x1(i,h)=LB1(h);
                elseif x1(i,h)>UB1(h)
                    x1(i,h)=UB1(h);
                end
            end
        end
        % handling boundary violations
        for i=1:n
            for h=1:m
                if x2(i,h)<LB2(h)
                    x2(i,h)=LB2(h);
                elseif x2(i,h)>UB2(h)
                    x2(i,h)=UB2(h);
                end
            end
        end
        % handling boundary violations
```

```
        for i=1:n
            for h=1:m
                if x3(i,h)<LB3(h)
                    x3(i,h)=LB3(h);
                elseif x3(i,h)>UB3(h)
                    x3(i,h)=UB3(h);
                end
            end
        end

        % evaluating fitness
        for i=1:n
            f1(i,1)=o1fun(x1(i,:));
            f2(i,1)=o2fun(x2(i,:));
            f3(i,1)=o3fun(x3(i,:));
        end

        % updating p1best and fitness
        for i=1:n
            if f1(i,1)<f1_0(i,1)
                p1best(i,:)=x1(i,:);
                f1_0(i,1)=f1(i,1);
            end
        end

         % updating p2best and fitness
        for i=1:n
            if f2(i,1)<f2_0(i,1)
                p2best(i,:)=x2(i,:);
                f2_0(i,1)=f2(i,1);
            end
        end

        % updating p2best and fitness
        for i=1:n
            if f3(i,1)<f3_0(i,1)
                p3best(i,:)=x3(i,:);
                f3_0(i,1)=f3(i,1);
            end
        end

        [f1min,index1]=min(f1_0);   % finding out the best
particle
        ff1min(ite,run)=f1min;    % storing best fitness
        ff1ite(run)=ite;          % storing iteration count
     %%%%%%%%%%%%%%
```

```
        [f2min,index2]=min(f2_0);   % finding out the best
particle
        ff2min(ite,run)=f2min;    % storing best fitness
        ff2ite(run)=ite;         % storing iteration count
     %%%%%%%%%%%%%%%%%%%%
        [f3min,index3]=min(f3_0);   % finding out the best
particle
        ff3min(ite,run)=f3min;    % storing best fitness
        ff3ite(run)=ite;         % storing iteration count

        % updating gbest and best fitness 1
        if f1min<f1min0
            g1best=p1best(index1,:);
            f1min0=f1min;
        end

        % updating gbest and best fitness 2
        if f2min<f2min0
            g2best=p2best(index2,:);
            f2min0=f2min;
        end
           % updating gbest and best fitness 2
        if f3min<f3min0
            g3best=p3best(index3,:);
            f3min0=f3min;
        end

        % calculating tolerance
        if ite>100;
            tolerance1=abs(ff1min(ite-100,run)-f1min0);
        end
        if ite>100;
            tolerance2=abs(ff2min(ite-100,run)-f2min0);
        end
        if ite>100;
            tolerance3=abs(ff3min(ite-100,run)-f3min0);
        end
        % displaying iterative results
        if ite==1
         disp(sprintf('Iteration  Best particle1
Objectivefun1  Best particle2   Objectivefun2  Best particle3
Objectivefun3  inertia weight '));
        end
 disp(sprintf('%8g  %8g  %8.4f     %8g     %8.4f     %8.4g
%8.4f   %8.4f'
,ite,index1,f1min0,index2,f2min0,index3,f3min0,w));
        ite=ite+1;
```

```
%          w = w * wdamp;

    end
    % pso algorithm-----------------------------------------
-----------end
    g1best;
    f1value=o1fun(g1best);
    fff1(run)=f1value;
    rg1best(run,:)=g1best;
    disp(sprintf('--------------------------------------'));

    g2best;
    f2value=o2fun(g2best);
    fff2(run)=f2value;
    rg2best(run,:)=g2best;
    disp(sprintf('--------------------------------------'));

    g3best;
    f3value=o3fun(g3best);
    fff3(run)=f3value;
    rg3best(run,:)=g3best;
    disp(sprintf('--------------------------------------'));
end
% pso main program--------------------------------------------
-----------end
disp(sprintf('\n'));
disp(sprintf('**************************************************
**********'));
disp(sprintf('Final Results1-----------------------------'));
[bestfun1,bestrun1]=min(fff1)
best_variables1=rg1best(bestrun1,:)
disp(sprintf('\n'));
disp(sprintf('**************************************************
**********'));
disp(sprintf('Final Results2-----------------------------'));
[bestfun2,bestrun2]=min(fff2)
best_variables2=rg2best(bestrun2,:)
disp(sprintf('\n'));
disp(sprintf('**************************************************
**********'));
disp(sprintf('Final Results3-----------------------------'));
[bestfun3,bestrun3]=min(fff3)
best_variables3=rg3best(bestrun3,:)
disp(sprintf('****-----<<<Extraction Of PV cell  Parameters
zone 1>>>---<<one diode>>--***'));
 disp(sprintf('     Ipv1         io1          Rs1          a1
Rp1 '));
```

```
 disp(sprintf('-----------------------------------------------
----------------'));
 disp(sprintf('  %8.4f  %6.11f  %8.4f   %8.3f  %8.2f
',rg1best(bestrun1,:)))
disp(sprintf('*************************************************
**********'));
disp(sprintf('****-----<<<Extraction Of PV cell  Parameters
zone 2>>>---<<one diode>>--***'));
 disp(sprintf('     Ipv2         io2          Rs2          a2
Rp2 '));
 disp(sprintf('-----------------------------------------------
----------------'));
 disp(sprintf('  %8.4f  %6.11f  %8.4f   %8.3f  %8.2f
',rg2best(bestrun2,:)))
disp(sprintf('*************************************************
**********'));
disp(sprintf('****-----<<<Extraction Of PV cell  Parameters
zone 3>>>---<<one diode>>--***'));
 disp(sprintf('     Ipv3         io3          Rs3          a3
Rp3 '));
 disp(sprintf('-----------------------------------------------
----------------'));
 disp(sprintf('  %8.4f  %6.11f  %8.4f   %8.3f  %8.2f
',rg3best(bestrun3,:)))
disp(sprintf('*************************************************
**********'));
toc
%%%%%%%%%%define parameters zone 1
Ipv1=rg1best(bestrun1,1);
Io1=rg1best(bestrun1,2);
Rs1=rg1best(bestrun1,3);
a1=rg1best(bestrun1,4);
Rp1=rg1best(bestrun1,5);
%%%%%%%%%%define parameters for zone 2
Ipv2=rg2best(bestrun2,1);
Io2=rg2best(bestrun2,2);
Rs2=rg2best(bestrun2,3);
a2=rg2best(bestrun2,4);
Rp2=rg2best(bestrun2,5);
%%%%%%%%%%define parameters for zone 2
Ipv3=rg3best(bestrun3,1);
Io3=rg3best(bestrun3,2);
Rs3=rg3best(bestrun3,3);
a3=rg3best(bestrun3,4);
Rp3=rg3best(bestrun3,5);
% Solving the I-V equation for several (V,I) pairs by
extracted PV parameters
```

```
%%%%curve 1

Ix1= zeros(1,cp);    % Current vector
Vx1= zeros(1,cp);     % voltage vector
for h = 1 : cp %Calculates for all voltage values

% Solves g = I - f(I,V) = 0

g1(h) = Ipv1-Io1*(exp((V(h)+Ix1(h)*Rs1)/Vt/a1)-1)-
(V(h)+Ix1(h)*Rs1)/Rp1-Ix1(h);

while (abs(g1(h)) > 0.0001)

g1(h) = Ipv1-Io1*(exp((V(h)+Ix1(h)*Rs1)/Vt/a1)-1)-
(V(h)+Ix1(h)*Rs1)/Rp1-Ix1(h);
g1lin(h) = -Io1*Rs1/Vt/a1*exp((V(h)+Ix1(h)*Rs1)/Vt/a1)-
Rs1/Rp1-1;
I_1(h) = Ix1(h) - g1(h)/g1lin(h);
Ix1(h) = I_1(h);
Vx1(h) = V(h);
end

end % for h = 1 : cp

% Solving the I-V equation for several (V,I) pairs by
extracted PV parameters
%%%%curve 2

Ix2= zeros(1,cp2-cp);    % Current vector
Vx2= zeros(1,cp2-cp);     % voltage vector
for h = cp+1 : cp2 %Calculates for all voltage values

% Solves g = I - f(I,V) = 0

g2(h) = Ipv2-Io2*(exp((V(h)+Ix2(h-cp)*Rs2)/Vt/a2)-1)-
(V(h)+Ix2(h-cp)*Rs2)/Rp2-Ix2(h-cp);

while (abs(g2(h)) > 0.0001)

g2(h) = Ipv2-Io2*(exp((V(h)+Ix2(h-cp)*Rs2)/Vt/a2)-1)-
(V(h)+Ix2(h-cp)*Rs2)/Rp2-Ix2(h-cp);
g2lin(h) = -Io2*Rs2/Vt/a2*exp((V(h)+Ix2(h-cp)*Rs2)/Vt/a2)-
Rs2/Rp2-1;
I_2(h) = Ix2(h-cp) - g2(h)/g2lin(h);
Ix2(h-cp) = I_2(h);
Vx2(h-cp) = V(h);
end
```

```
end % for h = cp : cp2
% Solving the I-V equation for several (V,I) pairs by
extracted PV parameters
%%%%curve 2

Ix3= zeros(1,size(V,2)-cp2);     % Current vector
Vx3= zeros(1,size(V,2)-cp2);      % voltage vector
for h = cp2+1 : size(V,2) %Calculates for all voltage values

% Solves g = I - f(I,V) = 0

g3(h) = Ipv3-Io3*(exp((V(h)+Ix3(h-cp2)*Rs3)/Vt/a3)-1)-
(V(h)+Ix3(h-cp2)*Rs3)/Rp3-Ix3(h-cp2);

while (abs(g3(h)) > 0.001)

g3(h) = Ipv3-Io3*(exp((V(h)+Ix3(h-cp2)*Rs3)/Vt/a3)-1)-
(V(h)+Ix3(h-cp2)*Rs3)/Rp3-Ix3(h-cp2);
g3lin(h) = -Io3*Rs3/Vt/a3*exp((V(h)+Ix3(h-cp2)*Rs3)/Vt/a3)-
Rs3/Rp3-1;
I_3(h) = Ix3(h-cp2) - g3(h)/g3lin(h);
Ix3(h-cp2) = I_3(h);
Vx3(h-cp2) = V(h);
end

end % for h = cp2 : size(V,2)

% Calculates power using the I-V equation
%   P = (Ipv-Io*(exp((V+I.*Rs)/Vt/a)-1)-(V+I.*Rs)/Rp).*V;
  P = I.*V;

  Px1 = (Ipv1-Io1*(exp((Vx1+Ix1.*Rs1)/Vt/a1)-1)-
(Vx1+Ix1.*Rs1)/Rp1).*Vx1;
  Px2 = (Ipv2-Io2*(exp((Vx2+Ix2.*Rs2)/Vt/a2)-1)-
(Vx2+Ix2.*Rs2)/Rp2).*Vx2;
  Px3 = (Ipv3-Io3*(exp((Vx3+Ix3.*Rs3)/Vt/a3)-1)-
(Vx3+Ix3.*Rs3)/Rp3).*Vx3;
  Pmax_m = max(P);



%% Outputs Curves

 % I-V curve
 figure(1)
 grid on
```

```
 hold on
 title('Adjusted I-V curve');
 xlabel('V [V]');
 ylabel('I [A]');
 xlim([0 max(V)*1.1]);
 ylim([0 max(I)*1.1]);
 plot(V,I,'LineWidth',3,'Color','r')

plot(Vx1,Ix1,'pentagram','LineWidth',2,'MarkerSize',7,'Color'
,'b')

plot(Vx2,Ix2,'pentagram','LineWidth',2,'MarkerSize',7,'Color'
,'k')

plot(Vx3,Ix3,'pentagram','LineWidth',2,'MarkerSize',7,'Color'
,'g')
%%%% dot line of each zone
 plot(Vx1,Ix1,':','LineWidth',2,'Color','b')
 plot(Vx2,Ix2,':','LineWidth',2,'Color','k')
 plot(Vx3,Ix3,':','LineWidth',2,'Color','g')
%  plot([0 Vmp Voc ],[Isc Imp 0
],'o','LineWidth',2,'MarkerSize',7,'Color','c')

% P-V curve
 figure(2)
 grid on
 hold on
 title('Adjusted P-V curve');
 xlabel('V [V]');
 ylabel('P [W]');
 xlim([0 Vocn*1.1]);
 ylim([0 Vmp*Imp*1.1]);
 plot(V,P,'LineWidth',3,'Color','r')

plot(Vx1,Px1,'diamond','LineWidth',2,'MarkerSize',7,'Color','
b')

plot(Vx2,Px2,'diamond','LineWidth',2,'MarkerSize',7,'Color','
k')

plot(Vx3,Px3,'diamond','LineWidth',2,'MarkerSize',7,'Color','
g')
%%%%% dot line of each zone
 plot(Vx1,Px1,':','LineWidth',2,'Color','b')
 plot(Vx2,Px2,':','LineWidth',2,'Color','k')
 plot(Vx3,Px3,':','LineWidth',2,'Color','g')
```

```
%  plot([0 Vmp Voc ],[0 Pmax_e 0
],'o','LineWidth',2,'MarkerSize',7,'Color','c')



% PSO convergence characteristic
figure(3)
grid on
subplot(311)
plot(ff1min(1:ff1ite(bestrun1),bestrun1),'LineWidth',2,'Color
','r');
grid on
ylabel('Fitness function zone1 value');
title('PSO convergence characteristic')
subplot(312)
plot(ff2min(1:ff2ite(bestrun2),bestrun2),'LineWidth',2,'Color
','b');
grid on
xlabel('Iteration');
ylabel('Fitness function zone2 value')
subplot(313)
plot(ff3min(1:ff3ite(bestrun3),bestrun3),'LineWidth',2,'Color
','m');
grid on
xlabel('Iteration');
ylabel('Fitness function zone3 value');

%##########################################################
############## END
```

Appendix C **Specification of PV Panels and Measurement Equipment**

C.1 **Canadian Solar's PV panel (CS6P-260P polycrystalline)**

Table C.1 Electrical data of CS6P-260P polycrystalline in STC.

Specification	Data
Nominal Max. Power (Pmax)	260 W
Opt. Operating Voltage (Vmp)	30.4 V
Opt. Operating Current (Imp)	8.56 A
Open Circuit Voltage (Voc)	37.5 V
Short Circuit Current (Isc)	9.12 A
Module Efficiency	16.16%
Operating Temperature	-40°C ~ +85°C
Max. System Voltage	1000 V (IEC) or 1000 V (UL)
Module Fire Performance	TYPE 1 (UL 1703) or CLASS C (IEC61730)
Max. Series Fuse Rating	15 A
Application Classification	Class A
Power Tolerance	0 ~ + 5 W

Table C.2 Mechanical data of CS6P-260P polycrystalline.

Specification	Data
Cell Type	Poly-crystalline, 6 inch
Cell Arrangement	60 (6 x 10)
Dimensions	1638 x 982 x 40 mm (64.5 x 38.7 x 1.57 in)
Weight	18 kg (39.7 lbs)
Front Cover	3.2 mm tempered glass
Frame Material	Anodized aluminium alloy
J-Box	IP67, 3 diodes
Cable	4 mm2 (IEC) or 4 mm2 & 12AWG 1000 V (UL) , 1000 mm (39.4 in) (650 mm (25.6 in) is optional)
Connectors Friends PV2a (IEC),	Friends PV2a (IEC), Friends PV2b (IEC / UL)
Standard Packaging	26 pieces, 515 kg (1135.4 lbs) (quantity & weight per pallet)
Module Pieces	per Container 728 pieces (40‘ HQ)

Table C.3 Temperature characteristics of CS6P-260P polycrystalline.

Specification	Data
Temperature Coefficient (Pmax)	-0.41% / °C
Temperature Coefficient (Voc)	-0.31% / °C
Temperature Coefficient (Isc)	0.053% / °C
Nominal Operating Cell Temperature	45±2°

C.2 **ET Solar‘s PV panel (ET-M53695 monocrystalline)**

Table C.4 Electrical data of ET-M53695 monocrystalline in STC.

Specification	Data
Peak Power (Pmax)	95W
Cell Efficiency	17.56%
Module Efficiency	14.47%
Maximum Power Voltage (Vmp)	18.52V
Maximum Power Current (Imp)	5.13A
Open Circuit Voltage (Voc)	22.5V
Short Circuit Current (Isc)	5.57A
Power Tolerance	0 to +5W
Maximum System Voltage	DC 1000V
Normal Operating Cell Temperature	44.4±2℃
Series Fuse Rating (A)	10A
Number of Bypass Diode	3

Table C.5 Mechanical data of ET-M53695 monocrystalline.

Specification	Data
Cell type	125mm x 125mm
Number of cells	36 cells in a series
Weight	8.23 kg (18.14lbs)
Dimensions	1205×545×35mm
Max Load	2400Pascals (50 lb/ft^2)

Table C.6 Temperature characteristics of ET-M53695 monocrystalline.

Specification	Data
Temperature Coefficient (Pmax)	-0.47 %/ ℃
Temperature Coefficient (Voc)	-0.336 %/ ℃
Temperature Coefficient (Isc)	0.042 %/ ℃

C.3 **First Solar‘s PV panel (FS-275 thin film)**

Table C.7 Electrical data of FS-275 thin film in STC.

Specification	Data
Nominal Power(+/-5%)	75 W
Voltage at PMAX	68.2 V
Current at PMAX	1.10 A
Open Circuit Voltage	89.6 V
Short Circuit Current ISC	1.23 A
Maximum System Voltage VSYS	1000 (600 UL2) V
Limiting Reverse Current IR(A)	2 A
Maximum Series Fuse	2

Table C.8 Mechanical data of FS-275 thin film.

Specification	Data
Length	1200mm
Width	600mm
Weight	12Kg
thickness	6.8mm
Area	0.78m2
Leadwire	4.0mm2, 610 mm
Connectors	Solarline 1 type connector
Bypass diode	None
Cell type	CdS/CdTe semiconductor, 116 active cells
Frame Material	None
Cover Type	3.2mm heat strengthened front glass laminated to 3.2mm tempered back glass
Encapsulation	Laminate material with edge seal

Table C.9 Temperature characteristics of FS-275 thin film.

Specification	Data
Temperature Coefficient (Pmax)	-0.25 %/ ℃
Temperature Coefficient (Voc)	-0.20 %/ ℃
Temperature Coefficient (Isc)	0.04 %/ ℃

C.4 **HT Instruments I-V 400 PV Panel Analyzer**

Table C.10 Electrical specification of HT Instruments I-V 400 at STC.

Specification	Range of Data
V_{DC} voltage	5.0−999.9 V
I_{DC} Current	0.10−15.00 A
P_{MAX} Maximum Power	50−9999 W
Irradiance	1.0−100 mV
Temperature	-20−100 °C

Table C.11 General specification of HT Instruments I-V 400 at STC.

Specification	Data
Features	128x128pxl custom LCD with backlight
Memory capacity	256kbytes
Saved data	249 curves (I-V curve test)
internal power supply	6x1.5V alkaline batteries type LR6, AA, AM3, MN 1500
PC communication port	optical/USB
Dimensions (L x W x H)	235 x 165 x 75mm
Weight (batteries included)	1.2kg
Reference temperature	23°C - 5°C
Working temperature	0° - 40°C
Working humidity	<80%HR
Storage temperature (batt. not included)	-10 to 60°C
Storage humidity	<80%HR
Safety	IEC/EN61010-1
Safety of measurement accessories	IEC/EN61010-031
	I-V curve measurement: IEC/EN60891 (I-V curve test)
Insulation	double insulation
Pollution degree	2
Overvoltage category	CAT II 1000V DC, CAT III 300V AC to ground
	Max 1000V among inputs P1, P2, C1, c2
Max altitude of use	2000m

REFERENCES

[1] H. E. Murdock *et al.*, "Renewables 2019 Global Status Report," 2019.

[2] J. Bai, Y. Cao, Y. Hao, Z. Zhang, S. Liu, and F. Cao, "Characteristic output of PV systems under partial shading or mismatch conditions," *J. Sol. Energy*, vol. 112, pp. 41-54, Feb 2015.

[3] K. Branker, M. Pathak, and J. M. Pearce, "A review of solar photovoltaic levelized cost of electricity," *Renewable and sustainable energy reviews*, vol. 15, no. 9, pp. 4470-4482, 2011.

[4] M. Bazilian *et al.*, "Re-considering the economics of photovoltaic power," *Renew. Energy*, vol. 53, pp. 329-338, May 2013.

[5] IEA. (2016) World Energy Outlook 2016 Part B: Special focus on renewable energy. Available: https://www.iea.org

[6] R. W. Andrews, A. Pollard, and J. M. Pearce, "The effects of snowfall on solar photovoltaic performance," *Sol.Energy*, vol. 92, pp. 84-97, 2013.

[7] CanSIA. Roadmap 2020: powering Canada's future with solar electricity. Canadian Solar Industries Association. Available: www.cansia.ca

[8] D. Kobayashi, "Snow accumulation on a narrow board," *Cold Regions Science and Technology*, vol. 13, no. 3, pp. 239-245, 1987.

[9] M. Ross, "Snow and ice accumulation on photovoltaic arrays: An assessment of the TN conseil passive melting technology, report# EDRL 95-68 (TR), energy diversification research laboratory, CANMET," *Natural Resources Canada, Varennes*, 1995.

[10] M. Brennan, A. Abramase, R. W. Andrews, and J. M. Pearce, "Effects of spectral albedo on solar photovoltaic devices," *Sol. Energy Mater Sol. Cells.*, vol. 124, pp. 111-116, 2014.

[11] A. Asgharzadeh, B. Marion, C. Deline, C. Hansen, J. S. Stein, and F. Toor, "A sensitivity study of the impact of installation parameters and system configuration on the performance of bifacial PV arrays," *IEEE Journal of Photovoltaics*, vol. 8, no. 3, pp. 798-805, 2018.

[12] E. Molin, B. Stridh, A. Molin, and E. Wäckelgård, "Experimental yield study of bifacial PV modules in nordic conditions," *IEEE Journal of Photovoltaics*, vol. 8, no. 6, pp. 1457-1463, 2018.

[13] B. L. Brench. (1979) Snow-covering effects on the power output of solar photovoltaic arrays. *The U.S. Department of Energy, Agreement No. DE-AC02-76ET20279, Massachusetts Institute of Technology*. Available: https://www.osti.gov/

[14] M. M. D. Ross. (1995) Snow and ice accumulation on photovoltaic arrays: An assessment of the TN conseil passive melting technology, report# EDRL 95-68 (TR), energy diversification research laboratory, CANMET. *Natural Resources Canada, Varennes*. Available: http://www.rerinfo.ca/

[15] B. Marion *et al.*, "Performance parameters for grid-connected PV systems," in *Photovoltaic Specialists Conference, 2005. Conference Record of the Thirty-first IEEE*, 2005, pp. 1601-1606: IEEE.

[16] G. Becker, B. Schiebelsberger, W. Weber, C. Vodermayer, M. Zehner, and G. Kummerle. (2006) An approach to the impact of snow on the yield of grid connected PV systems. *Bavarian Association for the Promotion of Solar Energy, Munich, Germany*. Available: https://www.sev-bayern.de/

[17] L. Powers, J. Newmiller, and T. Townsend, "Measuring and modeling the effect of snow on photovoltaic system performance," in *Photovoltaic Specialists Conference (PVSC), 2010 35th IEEE*, 2010, pp. 000973-000978: IEEE.

[18] T. Townsend and L. Powers, "Photovoltaics and snow: An update from two winters of measurements in the sierra," in *Photovoltaic Specialists Conference (PVSC), 2011 37th IEEE*, 2011, pp. 003231-003236: IEEE.
[19] B. Marion, R. Schaefer, H. Caine, and G. Sanchez, "Measured and modeled photovoltaic system energy losses from snow for Colorado and Wisconsin locations," *Sol. Energ.*, vol. 97, pp. 112-121, 2013.
[20] N. Heidari, J. Gwamuri, T. Townsend, and J. M. Pearce, "Impact of Snow and ground interference on photovoltaic electric system performance," *IEEE J. Photovolt*, vol. 5, no. 6, pp. 1680-1685, 2015.
[21] S. Pisklak, "Commercial implementation of a snow impact model for PV performance prediction," in *2016 IEEE 43rd Photovoltaic Specialists Conference (PVSC)*, 2016, pp. 1002-1006: IEEE.
[22] S. Hosseini, S. Taheri, M. Farzaneh, and H. Taheri, "Modeling of snow-covered photovoltaic modules," *IEEE Transactions on Industrial Electronics*, vol. 65, no. 10, pp. 7975-7983, 2018.
[23] S. G. Warren, "Optical properties of snow," *Rev. Geophys.*, vol. 20, no. 1, pp. 67-89, 1982.
[24] L. Wang, F. Liu, S. Yu, P. Quan, and Z. Zhang, "The Study on Micromismatch Losses of the Bifacial PV Modules Due to the Irradiance Nonuniformity on Its Backside Surface," *IEEE Journal of Photovoltaics*, vol. 10, no. 1, pp. 135-143, 2019.
[25] A. Askarzadeh and A. Rezazadeh, "Parameter identification for solar cell models using harmony search-based algorithms," *Solar Energy*, vol. 86, no. 11, pp. 3241-3249, 2012.
[26] A. Askarzadeh and A. Rezazadeh, "Artificial bee swarm optimization algorithm for parameters identification of solar cell models," *Applied Energy*, vol. 102, pp. 943-949, 2013.
[27] F. Dkhichi, B. Oukarfi, A. Fakkar, and N. Belbounaguia, "Parameter identification of solar cell model using Levenberg–Marquardt algorithm combined with simulated annealing," *Solar Energy*, vol. 110, pp. 781-788, 2014.
[28] D. Oliva, E. Cuevas, and G. Pajares, "Parameter identification of solar cells using artificial bee colony optimization," *Energy*, vol. 72, pp. 93-102, 2014.
[29] A. Askarzadeh and L. dos Santos Coelho, "Determination of photovoltaic modules parameters at different operating conditions using a novel bird mating optimizer approach," *Energy Conversion and Management*, vol. 89, pp. 608-614, 2015.
[30] S.-x. Lun, C.-j. Du, T.-t. Guo, S. Wang, J.-s. Sang, and J.-p. Li, "A new explicit I–V model of a solar cell based on Taylor's series expansion," *Solar Energy*, vol. 94, pp. 221-232, 2013.
[31] K. Ishaque, Z. Salam, S. Mekhilef, and A. Shamsudin, "Parameter extraction of solar photovoltaic modules using penalty-based differential evolution," *Applied Energy*, vol. 99, pp. 297-308, 2012.
[32] T. Ma, H. Yang, and L. Lu, "Development of a model to simulate the performance characteristics of crystalline silicon photovoltaic modules/strings/arrays," *Solar Energy*, vol. 100, pp. 31-41, 2014.
[33] M. Chegaar, Z. Ouennoughi, and A. Hoffmann, "A new method for evaluating illuminated solar cell parameters," *Solid-state electronics*, vol. 45, no. 2, pp. 293-296, 2001.
[34] J. A. Jervase, H. Bourdoucen, and A. Al-Lawati, "Solar cell parameter extraction using genetic algorithms," *Measurement science and technology*, vol. 12, no. 11, p. 1922, 2001.
[35] M. Zagrouba, A. Sellami, M. Bouaïcha, and M. Ksouri, "Identification of PV solar cells and modules parameters using the genetic algorithms: Application to maximum power extraction," *Solar energy*, vol. 84, no. 5, pp. 860-866, 2010.
[36] M. Ye, X. Wang, and Y. Xu, "Parameter extraction of solar cells using particle swarm optimization," *J. Appl. Phys.*, vol. 105, no. 9, p. 094502, 2009.

[37] H. Wei, J. Cong, X. Lingyun, and S. Deyun, "Extracting solar cell model parameters based on chaos particle swarm algorithm," in *2011 International conference on electric information and control engineering*, 2011, pp. 398-402: IEEE.
[38] K. M. El-Naggar, M. AlRashidi, M. AlHajri, and A. Al-Othman, "Simulated annealing algorithm for photovoltaic parameters identification," *Solar Energy*, vol. 86, no. 1, pp. 266-274, 2012.
[39] M. AlHajri, K. El-Naggar, M. AlRashidi, and A. Al-Othman, "Optimal extraction of solar cell parameters using pattern search," *Renewable Energy*, vol. 44, pp. 238-245, 2012.
[40] J. Ma, T. Ting, K. L. Man, N. Zhang, S.-U. Guan, and P. W. Wong, "Parameter estimation of photovoltaic models via cuckoo search," *Journal of applied mathematics*, vol. 2013, 2013.
[41] K. Ishaque and Z. Salam, "An improved modeling method to determine the model parameters of photovoltaic (PV) modules using differential evolution (DE)," *Solar energy*, vol. 85, no. 9, pp. 2349-2359, 2011.
[42] W. Gong and Z. Cai, "Parameter extraction of solar cell models using repaired adaptive differential evolution," *Solar Energy*, vol. 94, pp. 209-220, 2013.
[43] A. Askarzadeh and A. Rezazadeh, "A new heuristic optimization algorithm for modeling of proton exchange membrane fuel cell: bird mating optimizer," *International journal of energy research*, vol. 37, no. 10, pp. 1196-1204, 2013.
[44] R. Sirjani and H. Shareef, "Parameter extraction of solar cell models using the lightning search algorithm in different weather conditions," *Journal of Solar Energy Engineering*, vol. 138, no. 4, 2016.
[45] A. Ratnaweera, S. K. Halgamuge, and H. C. Watson, "Self-organizing hierarchical particle swarm optimizer with time-varying acceleration coefficients," *IEEE Transactions on evolutionary computation*, vol. 8, no. 3, pp. 240-255, 2004.
[46] C.-m. Yan, B.-l. Guo, and X.-x. Wu, "Empirical study of the inertia weight particle swarm optimization with constrained factor," *International Journal of Soft Computing and Software engineer-Ing*, vol. 2, no. 2, 2012.
[47] X. Liang, Z. Yin, Y. Wang, and Q. Sun, "Impulse engine ignition algorithm based on genetic particle swarm optimization," in *International Conference in Swarm Intelligence*, 2013, pp. 35-43: Springer.
[48] N. F. A. Hamid, N. A. Rahim, and J. Selvaraj, "Solar cell parameters extraction using particle swarm optimization algorithm," in *2013 IEEE conference on clean energy and technology (CEAT)*, 2013, pp. 461-465: IEEE.
[49] T. Wei, F. Yu, G. Huang, and C. Xu, "A Particle-Swarm-Optimization-Based parameter extraction routine for three-diode lumped parameter model of organic solar cells," *IEEE Electron Device Letters*, vol. 40, no. 9, pp. 1511-1514, 2019.
[50] A. Harrag and S. Messalti, "Three, five and seven pv model parameters extraction using pso," *Energy Procedia*, vol. 119, pp. 767-774, 2017.
[51] M. Joisher, D. Singh, S. Taheri, D. R. Espinoza-Trejo, E. Pouresmaeil, and H. Taheri, "A Hybrid Evolutionary-Based MPPT for Photovoltaic Systems Under Partial Shading Conditions," *IEEE Access*, vol. 8, pp. 38481-38492, 2020.
[52] S. Obukhov, A. Ibrahim, A. A. Z. Diab, A. S. Al-Sumaiti, and R. Aboelsaud, "Optimal Performance of Dynamic Particle Swarm Optimization Based Maximum Power Trackers for Stand-Alone PV System Under Partial Shading Conditions," *IEEE Access*, vol. 8, pp. 20770-20785, 2020.
[53] K. Ishaque, Z. Salam, M. Amjad, and S. Mekhilef, "An improved particle swarm optimization (PSO)–based MPPT for PV with reduced steady-state oscillation," *IEEE transactions on Power Electronics*, vol. 27, no. 8, pp. 3627-3638, 2012.

[54] R. Subha and S. Himavathi, "Accelerated particle swarm optimization algorithm for maximum power point tracking in partially shaded PV systems," in *2016 3rd International Conference on Electrical Energy Systems (ICEES)*, 2016, pp. 232-236: IEEE.

[55] A. Botchkarev, "Evaluating performance of regression machine learning models using multiple error metrics in Azure Machine Learning Studio," *Available at SSRN 3177507*, 2018.

[56] H. S. Moreira *et al.*, "Experimental Analysis of Photovoltaic Modeling for Partially Shading Conditions," in *2018 13th IEEE International Conference on Industry Applications (INDUSCON)*, 2018, pp. 242-248: IEEE.

[57] N. Kaushika and A. K. Rai, "An investigation of mismatch losses in solar photovoltaic cell networks," *Energy J.*, vol. 32, no. 5, pp. 755-759, May 2007.

[58] R. S. Magdaleno, P. Sánchez-Pérez, J. R. Cruz, D. M. Escobar, and A. Sánchez-Juárez, "Influence of partial shading on the power output of a solar cell and a PV module," in *2018 IEEE 7th World conference on photovoltaic energy conversion (WCPEC)(A joint conference of 45th IEEE PVSC, 28th PVSEC & 34th EU PVSEC)*, 2018, pp. 1324-1327: IEEE.

[59] K. S. Faldu and P. Kulkarni, "Maximization of The Output Power from Photovoltaic Array Under Partial Shading Conditions," in *2020 IEEE International Students' Conference on Electrical, Electronics and Computer Science (SCEECS)*, 2020, pp. 1-6: IEEE.

[60] A. Kovach and J. Schmid, "Determination of energy output losses due to shading of building-integrated photovoltaic arrays using a raytracing technique," *J. Sol. Energy*, vol. 57, no. 2, pp. 117-124, 1996.

[61] B. Meyers and M. Mikofski, "Accurate modeling of partially shaded PV arrays," in *2017 IEEE 44th Photovoltaic Specialist Conference (PVSC)*, 2017, pp. 3354-3359: IEEE.

[62] V. Quaschning and R. Hanitsch, "Numerical simulation of current-voltage characteristics of photovoltaic systems with shaded solar cells," *J. Sol. Energy*, vol. 56, no. 6, pp. 513-520, Jun 1996.

[63] K. Ishaque and Z. Salam, "A comprehensive MATLAB Simulink PV system simulator with partial shading capability based on two-diode model," *Solar energy*, vol. 85, no. 9, pp. 2217-2227, 2011.

[64] K. Ishaque, Z. Salam, and H. Taheri, "Modeling and simulation of photovoltaic (PV) system during partial shading based on a two-diode model," *Simulation Modelling Practice and Theory*, vol. 19, no. 7, pp. 1613-1626, 2011.

[65] S. Moballegh and J. Jiang, "Modeling, prediction, and experimental validations of power peaks of PV arrays under partial shading conditions," *IEEE Trans.Sustain. Energy*, vol. 5, no. 1, pp. 293-300, Jan 2013.

[66] M. Seyedmahmoudian, S. Mekhilef, R. Rahmani, R. Yusof, and E. T. Renani, "Analytical modeling of partially shaded photovoltaic systems," *Energies*, vol. 6, no. 1, pp. 128-144, 2013.

[67] Y.-J. Wang and P.-C. Hsu, "Analytical modelling of partial shading and different orientation of photovoltaic modules," *IET Renewable Power Generation*, vol. 4, no. 3, pp. 272-282, 2010.

[68] P. Bharadwaj and V. John, "Subcell Modeling of Partially Shaded Photovoltaic Modules," *IEEE Transactions on Industry Applications*, vol. 55, no. 3, pp. 3046-3054, 2019.

[69] N. D. Kaushika and N. K. Gautam, "Energy yield simulations of interconnected solar PV arrays," *IEEE Trans. Energy Convers*, vol. 18, no. 1, pp. 127-134, Mar 2003.

[70] Y.-H. Ji, J.-G. Kim, S.-H. Park, J.-H. Kim, and C.-Y. Won, "C-language based PV array simulation technique considering effects of partial shading," in *2009 IEEE international conference on industrial technology*, 2009, pp. 1-6: IEEE.

[71] H. Kawamura *et al.*, "Simulation of I–V characteristics of a PV module with shaded PV cells," *Solar Energy Materials and Solar Cells*, vol. 75, no. 3-4, pp. 613-621, 2003.

[72] Y. Mahmoud and E. F. El-Saadany, "A photovoltaic model with reduced computational time," *IEEE transactions on industrial electronics*, vol. 62, no. 6, pp. 3534-3544, 2014.
[73] A. G. Peter and A. Saha, "Electrical Characteristics Improvement of Photovoltaic Modules Using Two-Diode Model and its Application Under Mismatch Conditions," in *2019 Southern African Universities Power Engineering Conference/Robotics and Mechatronics/Pattern Recognition Association of South Africa (SAUPEC/RobMech/PRASA)*, 2019, pp. 328-333: IEEE.
[74] C.-T. Hsu, R. Korimara, L.-J. Tsai, and T.-J. Cheng, "Photovoltaic power generation system modeling using an artificial neural network," in *Proceedings of the 3rd International Conference on Intelligent Technologies and Engineering Systems (ICITES2014)*, 2016, pp. 365-371: Springer.
[75] H. Mekki, A. Mellit, and H. Salhi, "Artificial neural network-based modelling and fault detection of partial shaded photovoltaic modules," *Simulation Modelling Practice and Theory*, vol. 67, pp. 1-13, 2016.
[76] E. I. Batzelis, P. S. Georgilakis, and S. A. Papathanassiou, "Energy models for photovoltaic systems under partial shading conditions: a comprehensive review," *IET Renewable Power Generation*, vol. 9, no. 4, pp. 340-349, 2014.
[77] V. Quaschning and R. Hanitsch, "Numerical simulation of current-voltage characteristics of photovoltaic systems with shaded solar cells," *Solar energy*, vol. 56, no. 6, pp. 513-520, 1996.
[78] S. Moballegh and J. Jiang, "Modeling, prediction, and experimental validations of power peaks of PV arrays under partial shading conditions," *IEEE Transactions on Sustainable Energy*, vol. 5, no. 1, pp. 293-300, 2013.
[79] M. Khenar, S. Hosseini, S. Taheri, A.-M. Cretu, E. Pouresmaeil, and H. Taheri, "Particle swarm optimisation-based model and analysis of photovoltaic module characteristics in snowy conditions," *IET Renew. Power Gener.*, vol. 13, no. 11, pp. 1950-1957, Aug 2019.
[80] *How Do Solar Panels Work*. Available: https://www.mrsolar.com/what-is-a-solar-panel/
[81] *Common Roof Solar Panel Problems*. Available: https://www.feldcoroofing.com/common-roof-solar-panel-problems/
[82] C. A. Fernandes, J. P. N. Torres, P. C. Branco, J. Fernandes, and J. Gomes, "Cell string layout in solar photovoltaic collectors," *Energy Conversion and Management*, vol. 149, pp. 997-1009, 2017.
[83] M. Bischoff, O. Hennig, K.-H. Kufer, K. Plociennik, I. Schule, and J. Weber, "Method for designing a physical layout of a photovoltaic system," ed: Google Patents, 2016.
[84] R. Luthander, "Photovoltaic System Layout for Optimized Self-Consumption," ed, 2013.
[85] S. Hosseini, S. Taheri, E. Pouresmaeil, and H. Taheri, "Analysis of electrical behaviour of PV arrays covered with non-uniform snow," *Electronics Letters*, 2019.
[86] P. Bacher, H. Madsen, and H. A. Nielsen, "Online short-term solar power forecasting," *Solar energy*, vol. 83, no. 10, pp. 1772-1783, 2009.
[87] T. Bien and H. Musikowski, "Forecasting photovoltaic energy using a fourier series based method," in *23rd European Photovoltaic Solar Energy Conference*, 2008, pp. 3088-3091.
[88] J. Aznarte, R. Girard, B. Espinar, A. Moussa, and G. Kariniotakis, "Forecasting functions with focus to PV prediction for microgrids," *Short term forecasting of photovoltaic power production*, 2009.
[89] M. Cococcioni, E. D'Andrea, and B. Lazzerini, "One day-ahead forecasting of energy production in solar photovoltaic installations: An empirical study," *Intelligent Decision Technologies*, vol. 6, no. 3, pp. 197-210, 2012.
[90] J. G. da Silva Fonseca, T. Oozeki, T. Takashima, G. Koshimizu, Y. Uchida, and K. Ogimoto, "Photovoltaic power production forecasts with support vector regression: A study on the forecast horizon," in *2011 37th IEEE Photovoltaic Specialists Conference*, 2011, pp. 002579-002583: IEEE.

[91] J. DA S FONSECA Jr, "Forecast of power production of a photovoltaic power plant in Japan with multilayer precipitation artificial neural networks and support vector machines," *26^< th> EU-PVSEC, 2011*, 2011.
[92] E. Ogliari, F. Grimaccia, S. Leva, and M. Mussetta, "Hybrid predictive models for accurate forecasting in PV systems," *Energies*, vol. 6, no. 4, pp. 1918-1929, 2013.
[93] E. Karatepe and T. Hiyama, "Artificial neural network-polar coordinated fuzzy controller based maximum power point tracking control under partially shaded conditions," *IET Renewable Power Generation*, vol. 3, no. 2, pp. 239-253, 2009.
[94] J. A. Dolan *et al.*, "Neural network estimation of photovoltaic I–V curves under partially shaded conditions," in *The 2011 International Joint Conference on Neural Networks*, 2011, pp. 1358-1365: IEEE.
[95] E. Karatepe, M. Boztepe, and M. Colak, "Development of a suitable model for characterizing photovoltaic arrays with shaded solar cells," *Solar energy*, vol. 81, no. 8, pp. 977-992, 2007.
[96] R. De Leone, M. Pietrini, and A. Giovannelli, "Photovoltaic energy production forecast using support vector regression," *Neural Computing and Applications*, vol. 26, no. 8, pp. 1955-1962, 2015.
[97] M. Ceci, R. Corizzo, F. Fumarola, D. Malerba, and A. Rashkovska, "Predictive modeling of pv energy production: How to set up the learning task for a better prediction?," *IEEE Transactions on Industrial Informatics*, vol. 13, no. 3, pp. 956-966, 2016.
[98] J. Wang, P. Li, R. Ran, Y. Che, and Y. Zhou, "A short-term photovoltaic power prediction model based on the gradient boost decision tree," *Applied Sciences*, vol. 8, no. 5, p. 689, 2018.
[99] I. A. Ibrahim, M. Hossain, and B. C. Duck, "An optimized offline random forests-based model for ultra-short-term prediction of PV characteristics," *IEEE Transactions on Industrial Informatics*, vol. 16, no. 1, pp. 202-214, 2019.
[100] M. Q. Raza, N. Mithulananthan, J. Li, K. Y. Lee, and H. B. Gooi, "An Ensemble Framework For Day-Ahead Forecast of PV Output Power in Smart Grids," *IEEE Transactions on Industrial Informatics*, vol. 15, no. 8, pp. 4624-4634, 2018.
[101] H. Zang *et al.*, "Hybrid method for short-term photovoltaic power forecasting based on deep convolutional neural network," *IET Generation, Transmission & Distribution*, vol. 12, no. 20, pp. 4557-4567, 2018.
[102] T. Yang, B. Li, and Q. Xun, "LSTM-Attention-Embedding Model-Based Day-Ahead Prediction of Photovoltaic Power Output Using Bayesian Optimization," *IEEE Access*, vol. 7, pp. 171471-171484, 2019.
[103] U. K. Das *et al.*, "SVR-based model to forecast PV power generation under different weather conditions," *Energies*, vol. 10, no. 7, p. 876, 2017.
[104] G. Perveen, M. Rizwan, and N. Goel, "Comparison of intelligent modelling techniques for forecasting solar energy and its application in solar PV based energy system," *Energy Systems Integration*, vol. 1, no. 1, pp. 34-51, 2019.
[105] W. VanDeventer *et al.*, "Short-term PV power forecasting using hybrid GASVM technique," *Renewable energy*, vol. 140, pp. 367-379, 2019.
[106] J. Ospina, A. Newaz, and M. O. Faruque, "Forecasting of PV plant output using hybrid wavelet-based LSTM-DNN structure model," *IET Renewable Power Generation*, vol. 13, no. 7, pp. 1087-1095, 2019.
[107] R. W. Andrews and J. M. Pearce, "Prediction of energy effects on photovoltaic systems due to snowfall events," in *2012 38th IEEE Photovoltaic Specialists Conference*, 2012, pp. 003386-003391: IEEE.
[108] A. A. Shishavan, E. C. Foresman, and F. Toor, "Performance analysis of crystalline silicon and amorphous silicon photovoltaic systems in Iowa: 2011 to 2014," in *2016 IEEE 43rd Photovoltaic Specialists Conference (PVSC)*, 2016, pp. 2625-2630: IEEE.

[109] E. Lorenz, D. Heinemann, and C. Kurz, "Local and regional photovoltaic power prediction for large scale grid integration: Assessment of a new algorithm for snow detection," *Progress in Photovoltaics: Research and Applications*, vol. 20, no. 6, pp. 760-769, 2012.
[110] T. Hong, C. Koo, and M. Lee, "Estimating the loss ratio of solar photovoltaic electricity generation through stochastic analysis," *Growth*, vol. 1, p. 2, 2013.
[111] B. Hashemi, A.-M. Cretu, and S. Taheri, "Snow Loss Prediction for Photovoltaic Farms Using Computational Intelligence Techniques," *IEEE Journal of Photovoltaics*, 2020.
[112] J. Giddings and E. LaChapelle, "Diffusion theory applied to radiant energy distribution and albedo of snow," *J. Geophys Res.*, vol. 66, no. 1, pp. 181-189, 1961.
[113] Y. Mahmoud and E. El-Saadany, "Accuracy improvement of the ideal PV model," *IEEE Trans. Sustain. Energy*, vol. 6, no. 3, pp. 909-911, 2015.
[114] K. Nishioka, N. Sakitani, Y. Uraoka, and T. Fuyuki, "Analysis of multicrystalline silicon solar cells by modified 3-diode equivalent circuit model taking leakage current through periphery into consideration," *Sol. Energy Mater Sol. Cells.*, vol. 91, no. 13, pp. 1222-1227, 2007.
[115] E. I. Batzelis and S. A. Papathanassiou, "A method for the analytical extraction of the single-diode PV model parameters," *IEEE Trans. Sustain. Energy*, vol. 7, no. 2, pp. 504-512, 2016.
[116] L. E. Trainor, "The special reflection and absorption of radiation by snow," M.A. thesis, Dept. Physics., Sask Univ., Saskatchewan, Canada,1947.
[117] R. Dunkle and J. Gier. (1953) Radiation in a diffusing medium with application to snow. *Inst Eng. Res., Univ. Berkeley, CA, USA* Available: http://www.dtic.mil/dtic/tr/fulltext/u2/023217.pdf
[118] F. Domine *et al.*, "Snow physics as relevant to snow photochemistry," *Atmospheric Chem. Phys.*, vol. 8, no. 2, pp. 171-208, 2008.
[119] D. Sera, R. Teodorescu, and P. Rodriguez, "PV panel model based on datasheet values," in *Ind. Electron, 2007. ISIE 2007. IEEE International Symposium on*, 2007, pp. 2392-2396: IEEE.
[120] M. G. Villalva, J. R. Gazoli, and E. Ruppert Filho, "Comprehensive approach to modeling and simulation of photovoltaic arrays," *IEEE Trans. Power Electron.*, vol. 24, no. 5, pp. 1198-1208, 2009.
[121] Y. Mahmoud and E. F. El-Saadany, "A photovoltaic model with reduced computational time," *IEEE Trans. Ind. Electron.*, vol. 62, no. 6, pp. 3534-3544, Jun. 2015.
[122] R. Eberhart and J. Kennedy, "A new optimizer using particle swarm theory," in *Micro Machine and Human Science, 1995. MHS'95., Proceedings of the Sixth International Symposium on*, 1995, pp. 39-43: IEEE.
[123] M. A. Rodriguez-Guerrero, A. Y. Jaen-Cuellar, R. D. Carranza-Lopez-Padilla, R. A. Osornio-Rios, G. Herrera-Ruiz, and R. d. J. Romero-Troncoso, "Hybrid Approach Based on GA and PSO for Parameter Estimation of a Full Power Quality Disturbance Parameterized Model," *IEEE Trans. Ind. Informat.*, vol. 14, no. 3, pp. 1016-1028, 2018.
[124] BIPM, "Evaluation of measurement data—Guide to the expression of uncertainty in measurement," *JCGM 100:2008*, available at the website of Bureau International des Poids et Mesures (BIPM) https://www.bipm.org/en/publications/guides/gum.html.
[125] S.Hosseini, "Integration of photovoltaic systems in cold regions," Ph.D. Thesis, Département d'informatique et d'ingénierie, Université du Québec en Outaouais,Gatineau, Dec, 2018.
[126] J. Accarino, G. Petrone, C. Ramos-Paja, and G. Spagnuolo, "Symbolic algebra for the calculation of the series and parallel resistances in PV module model," in *Proc. Int. Conf. Clean Electr.*, 2013, pp. 62-66: IEEE.
[127] Y.-J. Wang and S.-S. Lin, "Analysis of a partially shaded PV array considering different module connection schemes and effects of bypass diodes," in *2011 International*

Conference & Utility Exhibition on Power and Energy Systems: Issues and Prospects for Asia (ICUE), 2011, pp. 1-7: IEEE.

[128] M. C. Di Vincenzo and D. Infield, "Detailed PV array model for non-uniform irradiance and its validation against experimental data," *J. Sol. Energy*, vol. 97, pp. 314-331, Nov 2013.

[129] R. Rathee, V. Khanna, and B. Das, "Comparative Analysis To Study The Effects Of Partial Shading On PV Array Withlt-Spice And Matlab/Simulink Environment," *International Journal of Engineering Research & Technology (IJERT)*, vol. 2, no. 5, pp. 1501-1508, 2013.

[130] M. C. Di Piazza, M. Luna, G. Petrone, and G. Spagnuolo, "Translation of the single-diode PV model parameters identified by using explicit formulas," *IEEE J. Photovolt.*, vol. 7, no. 4, pp. 1009-1016, 2017.

[131] G. Petrone, C. A. Ramos-Paja, G. Spagnuolo, and W. Xiao, *Photovoltaic sources modeling*. Wiley Online Library, 2017.

[132] C.-T. Sah, R. N. Noyce, and W. Shockley, "Carrier generation and recombination in pn junctions and pn junction characteristics," *Proceedings of the IRE*, vol. 45, no. 9, pp. 1228-1243, 1957.

[133] K. Ding, X. Bian, H. Liu, and T. Peng, "A MATLAB-simulink-based PV module model and its application under conditions of nonuniform irradiance," *IEEE Trans. Energy Convers*, vol. 27, no. 4, pp. 864-872, Dec 2012.

[134] H. Zheng, S. Li, R. Challoo, and J. Proano, "Shading and bypass diode impacts to energy extraction of PV arrays under different converter configurations," *Renew.Energy*, vol. 68, pp. 58-66, Aug 2014.

[135] A. Dolara, G. C. Lazaroiu, S. Leva, and G. Manzolini, "Experimental investigation of partial shading scenarios on PV (photovoltaic) modules," *Energy*, vol. 55, pp. 466-475, 2013.

[136] E. V. Paraskevadaki and S. A. Papathanassiou, "Evaluation of MPP voltage and power of mc-Si PV modules in partial shading conditions," *IEEE Transactions on Energy Conversion*, vol. 26, no. 3, pp. 923-932, 2011.

[137] A. Jones and C. Underwood, "A thermal model for photovoltaic systems," *Solar energy*, vol. 70, no. 4, pp. 349-359, 2001.

[138] H. Patel and V. Agarwal, "Maximum power point tracking scheme for PV systems operating under partially shaded conditions," *IEEE transactions on industrial electronics*, vol. 55, no. 4, pp. 1689-1698, 2008.

[139] *Environment and Climate Change Canada, "Canadian climate normals 1981–2020," Winter. 2020.[Online]*. Available: https://climate.weather.gc.ca/historical_data/search_historic_data_e.html

[140] I. Tsamardinos, A. Rakhshani, and V. Lagani, "Performance-estimation properties of cross-validation-based protocols with simultaneous hyper-parameter optimization," *International Journal on Artificial Intelligence Tools*, vol. 24, no. 05, p. 1540023, 2015.

[141] N. Ye, *Data mining: theories, algorithms, and examples*. CRC press, 2013.

[142] B. Lambert, D. Tcheng, and S. C. Lu, "Generalized recursive splitting algorithms for learning hybrid concepts," in *Proceedings of the sixth international workshop on Machine learning*, 1989, pp. 496-498: Elsevier.

[143] B. Boehmke and B. M. Greenwell, *Hands-on machine learning with R*. CRC Press, 2019.

[144] S. Hochreiter and J. Schmidhuber, "Long short-term memory," *Neural computation*, vol. 9, no. 8, pp. 1735-1780, 1997.